EFFECT OF BEDDING PLANES ON CERCHAR ABRASIVITY INDEX

THITI PATCHARAARPAKUL

A Thesis Submitted in Partial Fulfillment of the Requirements for the
Degree of Master of Engineering in Civil, Transportation
and Geo-resources Engineering
Suranaree University of Technology
Academic Year 2024

ผลกระทบการวางตัวของชั้นหินต่อดัชนีการสึกกร่อนเซอคาร์

นายฐิติ พัชรอาภากุล

วิทยานิพนธ์นี้เป็นส่วนหนึ่งของการศึกษาตามหลักสูตรปริญญาวิศวกรรมศาสตรมหาบัณฑิต
สาขาวิชาวิศวกรรมโยธา ขนส่ง และทรัพยากรธรณี
มหาวิทยาลัยเทคโนโลยีสุรนารี
ปีการศึกษา 2567

EFFECT OF BEDDING PLANES ON CERCHAR ABRASIVITY INDEX

Suranaree University of Technology has approved this thesis submitted in partial fulfillment of the requirements for a Master's Degree.

Thesis Examining Committee

.....

(Assoc. Prof. Dr. Pornkasem Jongpradist)

Chairperson

.....

(Dr. Thanittha Thongprapha)

Member (Thesis Advisor)

.....

(Asst. Prof. Dr. Prachya Tepnarong)

Member

.....

(Assoc. Prof. Dr. Yupaporn Ruksakulpiwat)

Vice Rector for Academic Affairs

and Quality Assurance

.....

(Assoc. Prof. Dr. Pornsiri Jongkol)

Dean of Institute of Engineering

ฐิติ พัชรอาภากุล : ผลกระทบการวางตัวของชั้นหินต่อดัชนีการสึกกร่อนเซอคาร์ (EFFECT OF BEDDING PLANES ON CERCHAR ABRASIVITY INDEX) อาจารย์ที่ปรึกษา : ดร.ธนิษฐา ทองประภา, 112 หน้า.

คำสำคัญ: ความทนทานต่อการขัดสี/ แอนไอโซโทปี/ พลังงานจำเพาะเซอคาร์

การศึกษานี้ได้ทำการตรวจสอบผลกระทบของทิศทางระนาบชั้นหิน (α) และทิศทางการขูด (θ) ต่อดัชนีการสึกกร่อนของเซอคาร์ ปริมาตรร่องขูด พลังงาน และพลังงานจำเพาะเซอคาร์ ในหิน 5 ชนิด ได้แก่ หินปูนดินดานเขาขาด หินปูนเป็นชั้นเขาขาด หินทรายภูกระดึง หินทรายภูพาน และหินยิปซัมตากฟ้า ผลการทดสอบระบุว่า หินแข็ง เช่น หินปูนและหินทราย แสดงค่าดัชนีการสึกกร่อน แรงขูดและพลังงานจำเพาะเซอคาร์ที่สูงในขณะที่ค่าปริมาตรร่องมีค่าลดลงเมื่อเทียบกับหินยิปซัมเนื้ออ่อน การขูดในทิศทางที่สวนทางกับการเทเอียงหรือตั้งฉากกับระนาบชั้นหิน ส่งผลให้ค่าดัชนีการสึกร่อนและพลังงานจำเพาะเซอคาร์เพิ่มขึ้น โดยเฉพาะในหินแข็ง เนื่องจากแท่งเหล็กขูดสามารถสัมผัสกับชั้นหินที่วางตัวสลับชั้นได้มากขึ้น ในทางกลับกัน การขูดขนานกับระนาบชั้นหินส่งผลให้ค่าดัชนีการสึกร่อนและแรงขูดมีค่าลดลง แต่ปริมาตรร่องขูดเพิ่มขึ้น แม้ว่าพลังงานมีความสอดคล้องโดยตรงกับแรงขูด แต่ค่าพลังงานจำเพาะเซอคาร์ไม่มีความสอดคล้องกับค่าดัชนีการสึกกร่อนหรือการสึกหรอของหัวเหล็กขูด ซึ่งเป็นข้อจำกัดของพลังงานจำเพาะเซอคาร์ เป็นตัวบ่งชี้ของการสึกกร่อน ผลการศึกษาเหล่านี้ทำให้เข้าใจเกี่ยวกับกลไกการสึกกร่อนในหินที่มีสมบัติต่างกันในแต่ละทิศทางและได้นำเสนอแนวทางที่สามารถคาดการณ์ประสิทธิภาพของเครื่องมือการขุดเจาะในชั้นหินที่วางตัวสลับชั้นได้

สาขาวิชา เทคโนโลยีธรณี ลายมือชื่อนักศึกษา ฐิติ พัชรอาภากุล

ปีการศึกษา 2567 ลายมือชื่ออาจารย์ที่ปรึกษา

THITI PATCHARAARPAKUL: EFFECT OF BEDDING PLANES ON CERCHAR ABRASIVITY INDEXS. THESIS ADVISOR: DR. THANITTHA THONGPRAPHA, 112 PP.

Keyword: Abrasiveness/ Anisotropy / CERCHAR scratch energy

This study investigates the effects of bedding plane orientations (α) and scratching directions (θ) on the CERCHAR abrasivity index (CAI), groove volume (V), work energy (W), and CERCHAR scratch energy (CSE) in five rock types, including Khao Khad argillaceous limestone, Khao Khad bedded limestone, Phu Kadueng sandstone, Phu Phan sandstone, and Tak Fa gypsum. The results indicate that strong rocks such as limestones and sandstones show higher CAI, ploughing forces (F), and CSE values, while producing smaller groove volumes compared to the softer gypsum. Scratching opposite to the bedding dip or perpendicular to the bedding plane leads to an increase of CAI and CSE, particularly in strong rocks, due to enhanced stylus interaction with alternating layers. In contrast, scratching along the bedding plane dip results in lower CAI and F but larger groove volumes. Although the energy correlates directly with F, CSE does not consistently align with CAI or stylus wear, suggesting limitations in using CSE as a reliable wear indicator. These findings provide a better understanding of wear mechanisms in anisotropic rocks and offer practical implications for predicting tool performance in stratified geological formations.

School of Geotechnology
Academic Year 2024

Student's Signature .....
Advisor's Signature .....

ACKNOWLEDGEMENT

I wish to acknowledge the funding support from Suranaree University of Technology (SUT).

I would like to express thanks to Dr. Thanittha Thongprapha, thesis advisor, who gave a critical review. I appreciate his encouragement, suggestions, and comments during the research period. I would like to express thanks to Assoc. Prof. Dr. Pornkasem Jongpradist, Asst. Prof. Dr. Prachya Tepnarong, and Emeritus Prof. Dr. Kittitep Fuenkajorn for their valuable suggestions and comments on my research works as thesis committee members. Grateful thanks are given to all staffs of Geomechanics Research Unit, Institute of Engineering who supported my work.

Finally, I most gratefully acknowledge my parents for all their support and encouragement throughout the period of this study.

Thiti Patcharaarpakul

TABLE OF CONTENTS

Page

ABSTRACT (THAI) I
ABSTRACT (ENGLIST) II
ACKNOWLEDGEMENT III
TABLE OF CONTENTS IV
LIST OF TABLES VIII
LIST OF FIGURES IX
SYMBOLS AND ABBREVIATIONS XII
CHAPTER
I INTRODUCTION 1
1.1 Background and Rationale 1
1.2 Research Objective 1
1.3 Scope and Limitations 2
1.4 Research Methodology 2
1.4.1 Literature Reviews 3
1.4.2 Samples Collection and Preparation 3
1.4.3 CERCHAR abrasivity testing 3
1.4.4 X-ray Diffraction analysis 4
1.4.5 Analysis 4
1.4.6 Discussions and Conclusions 4
1.4.7 Thesis Writing 4
1.5 Thesis Contents 4
II LITERATURE REVIEW 6

TABLE OF CONTENTS (Continued)

Page

2.1 Rock abrasiveness 6
2.2 Factors affecting CERCHAR abrasivity index 7
2.2.1 Surface conditions 7
2.2.2 Stylus hardness 8
2.2.3 Scratching rate 8
2.2.4 Grain size 9
2.2.5 Moisture content 9
2.3.6 Temperature 10
2.3.7 Mineral compositions 10
2.3.8 Rock properties 11
2.3 CERCHAR specific energy 15

III SAMPLE PREPARATION 17

3.1 Introduction 17
3.2 Rock Description 18
3.2.1 Khao Khad argillaceous limestone 18
3.2.2 Khao Khad bedded limestone 18
3.2.3 Phu Kradueng sandstone 18
3.2.4 Phu Phan sandstone 18
3.2.5 Tak Fa gypsum 18
3.3 Rock specimens preparation 18

IV TEST APPARATUS AND METHODS 22

4.1 Introduction 22

TABLE OF CONTENTS (Continued)

Page

4.2 CERCHAR test 22
4.3 X-ray diffraction (XRD) analysis 26
V TEST RESULTS 27
5.1 Introduction 27
5.2 CERCHAR abrasivity index 27
5.3 Lateral force 30
5.4 Groove volumes 33
VI ANALYSIS OF TEST RESULTS 36
6.1 Introduction 36
6.2 CERCHAR abrasivity index 36
6.3 Groove volume 39
6.4 Lateral force 42
6.4 Work and energy 48
6.5 CERCHAR Specific Energy 54
VII DISCUSSIONS AND CONCLUSIONS 59
7.1 Discussions 59
7.2 Conclusions 60
7.3 Recommendations for future studies 61
REFERENCES 62
APPENDIX A 67
APPENDIX B 83
APPENDIX C 89

TABLE OF CONTENTS (Continued)

Page

APPENDIX D 95

APPENDIX E 101

BIOGRAPHY 112

LIST OF TABLES

Table **Page**

2.1 Classification of CAI (ASTM D7625-22)..... 7

3.1 Mineral composition for all rock types..... 19

3.2 Rock dimensions and density for all rock types..... 21

5.1 Average CAI and standard deviation 28

5.2 Mean groove volumes for different angle α and θ..... 34

6.1 Numerical values from empirical constants l_1, l_2 and l_3 of equation 6.1..... 37

6.2 Numerical values from empirical constants m_1 and η_1 of equation 6.2..... 38

6.3 Numerical values from empirical constants k_1, k_2 and k_3 of equation 6.3..... 40

6.4 M Numerical values from empirical constants m_2 and η_2 of equation 6.4..... 41

6.5 Empirical constants a and b for F-d_s relation and R^2..... 45

6.6 Empirical constants a (α) and b (α) for F-d_s relation and R^2 47

6.7 Empirical constants a (θ) and b (θ) for F-d_s relation and R^2 48

6.8 Work done for all rock tests 50

6.9 Numerical values from empirical constants e_1, e_2 and e_3 of equation 6.9..... 52

6.10 Numerical values from empirical constants m_5 and η_5 of equation 6.10..... 53

6.11 CERCHAR specific energy for all rock tests 56

6.12 Numerical values from empirical constants ɡ1, ɡ2 and ɡ3 of equation 6.12 ... 57

6.13 Numerical values from empirical constants m_6 and η_6 of equation 6.13..... 58

LIST OF FIGURES

Figure **Page**

1.1 Research methodology 3

1.2 Scratching direction as compound to bedding plane angles (a), and as compared to trends of bedding planes (b) 3

2.1 Relationship between CAI values of rough surface and saw-cut surface (Yaralı and Duru, 2016) 8

2.2 CAI testing, where black solid line represents mean CAI derived from single test, and red dashed line represents mean CAI value obtained from all individual tests (Kathancharoen and Fuenkajorn, 2023) 11

2.3 P-wave velocity in relation to the anisotropy angle (Jin et al., 2018) 12

2.4 Correlation between (a) compressive modulus and (b) Uniaxial compressive strength (UCS) concerning the anisotropy angle (Jin et al., 2018) 12

2.5 Correlation between strength anisotropy curves of Arkansas, Ranyah, and fractured sandstones (Al-Harthi, 1998) 13

2.6 Relationship between CAI and basic mechanical tests a) UCS b) E c) BTS d) Is50 (Teymen, 2020) 14

2.7 CAI versus testing orientations, where black solid line represents mean CAI derived from single test, and red dashed line represents mean CAI value obtained from all individual tests (Zhang, Konietzky, and Frühwirt, 2020) 15

3.1 Samples obtained from various locations in Thailand 17

3.2 Specimens with various bedding plane orientations and scratching directions prepared for CERCHAR tests 20

4.1 Device based on West CERCHAR apparatus with additional torque and vertical displacement measurements (Kathancharoen and Fuenkajorn, 2023) 24

LIST OF FIGURES (Continued)

Figure **Page**

4.2 Schematic drawing of CERCHAR device (Kathancharoen and Fuenkajorn, 2023) 24

4.3 Stylus pins (HRC 55) are used in this study..... 25

4.4 Steel stylus test variables, N is normal load (N), F is horizontal force (N), dn is vertical displacement (mm), ds is scratching distance (mm), and d is wear flat width of stylus tip 25

4.5 X-ray diffraction Bruker, D8 advance (Center for Scientific and Technology Equipment University of Technology)..... 26

5.1 CAI as a function of bedding plane angle (a), and scratching direction (b) 29

5.2 Scratching forces (F) as a function of scratching distance (d_s) of Khao Khad argillaceous limestone, bedding plane orientations (a) and scratching directions (b) 30

5.3 Scratching forces (F) as a function of scratching distance (d_s) of Khao Khad bedded limestone, bedding plane orientations (a) and scratching directions (b) 31

5.4 Scratching forces (F) as a function of scratching distance (d_s) of Phu Kadueng sandstone, bedding plane orientations (a) and scratching directions (b)..... 31

5.5 Scratching forces (F) as a function of scratching distance (d_s) of Phu Phan sandstone, bedding plane orientations (a) and scratching directions (b)..... 32

5.6 Scratching forces (F) as a function of scratching distance (d_s) of Tak Fa gypsum, bedding plane orientations (a) and scratching directions (b)..... 32

5.7 Mean groove volumes as a function of bedding plane orientations (a), and scratching directions (b) 35

6.1 CERCHAR abrasivity index (CAI) as functions of α, with polynomial equations 37

6.2 CERCHAR abrasivity index (CAI) as functions of θ, with linear equations..... 38

LIST OF FIGURES (Continued)

Figure **Page**

6.3 Groove volumes as functions of α, with polynomial equations 39

6.4 Groove volumes as functions of θ, with linear equations 41

6.5 Lateral force as a function of bedding plane orientations (α) 43

6.6 Lateral force as a function of bedding plane orientations (θ) 44

6.7 Empirical constants a (α) and b (α) for F-d_s with R^2 values by rock type 46

6.8 Empirical constants a (θ) and b (θ) for F-d_s with R^2 values by rock type 47

6.9 Work done as a function of bedding plane orientations (α) 49

6.10 Work done as a function of scratching directions (θ) 49

6.11 Work done as functions of α, with polynomial equations 51

6.12 Work done as functions of θ, with linear equations 53

6.13 CSE as a function of bedding plane orientations (α) 55

6.14 CSE as a function of scratching directions (θ) 55

6.15 CSE as a function of bedding plane orientations (α), with polynomial equations 57

6.16 CSE as a function of scratching directions (θ), with linear equations 58

SYMBOLS AND ABBREVIATIONS

θ	=	Scratching direction
α	=	Bedding plane orientations
β	=	the angle between normal bedding planes and major principal stress
CAI	=	CERCHAR abrasivity index
HRC	=	Rockwell hardness
XRD	=	X-ray diffraction analysis
EQC	=	Equivalent quartz content
SE	=	Specific energy
SSE	=	Scratching specific energy
CSE	=	CERCHAR specific energy
W	=	Work done
V	=	Material removed volume or mean groove volume
d	=	Diameter of wear flat area of stylus tip
d_{sc}	=	Wear flat of stylus tip for saw cut surface specimen
N	=	Normal load
F	=	Horizontal force or ploughing force
d_s	=	Scratching distance
d	=	Wear flat width of stylus tip
T	=	Torque
P	=	Screw pitch

CHAPTER I
INTRODUCTION

1.1 Background and Rationale

Assessing rock properties and steel durability are important for determining the lifespan of cutting tools in construction and excavation industries. Abrasivity testing evaluates tool durability against wear from rock surfaces. CERCHAR abrasivity index (CAI) is one of the methods that have been widely used. Several researchers have identified various factors affecting the CAI, such as stylus hardness, scratching rate, scratching distance, surface condition, moisture content, temperature, and rock properties. Bedding planes, which are inherent stratifications within sedimentary rocks, may also considerably affect their abrasivity. Numerous tests on anisotropic rock properties have demonstrated that anisotropic characteristics significantly affecting rock strength results, with maximum rock strengths typically observed at bedding plane orientations of 0° and 90°, and minimum values between 45° and 60°. The effect of bedding planes and their orientations on the abrasiveness of cutting tools has rarely been investigated.

1.2 Research Objective

The objective of this study is to laboratory investigate the effect of bedding planes and their orientation on CERCHAR abrasivity index. Khao Khad argillaceous limestone, Khao Khad bedded limestone, Phu Kadueng sandstone, Phu Phan sandstone, and Tak Fa gypsum are used as test specimens. The nominal angles (α) between the test surface and bedding plane vary from 0°, 45°, 90° to 135°. The scratching directions of the stylus pin with respect to the bedding trends vary from 0° to 90°. Scratching forces and ploughing volumes are measured and compared between

different rock types, scratching directions, and mineral compositions. CERCHAR specific energy for all test conditions will be evaluated.

1.3 Scope and Limitations

The research scope and limitations are outlined as follows.

1) Five types of rock specimens are prepared and tested including Khao Khad argillaceous limestone, Khao Khad bedded limestone, Phu Kadueng sandstone, Phu Phan sandstone, and Tak Fa gypsum.

2) CERCHAR abrasivity tests are performed on saw-cut surfaces.

3) Different angles of bedding planes at 0, 45, 90 and 135 degrees and scratching directions at 0, 45 and 90 degrees are performed.

4) CERCHAR abrasivity test procedure follows ASTM D7625-22 standard practice.

5) Mineral compositions are analyzed by XRD.

6) Ploughing forces and groove volumes on specimens are measured.

1.4 Research Methodology

The research methodology shown in Figure 1.1 consists of eight steps: literature review, sample collection and preparation, CERCHAR abrasivity testing, X-ray diffractometer analysis, result interpretation, mathematical correlations, discussions and conclusions, and thesis composition.

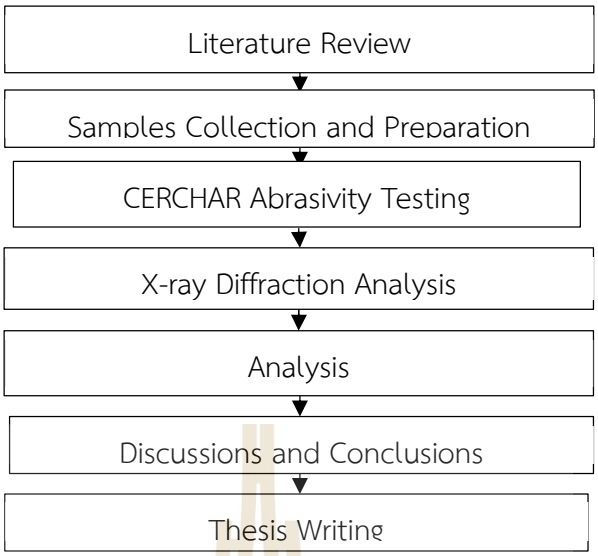

Figure 1.1 Research methodology.

1.4.1 Literature Reviews

Previous research investigation on rock abrasion, CERCHAR abrasivity test, factors influencing CERCHAR abrasivity index will be reviewed.

1.4.2 Samples Collection and Preparation

Preparation takes place at the Geomechanics Research Unit (GMR), Suranaree University of Technology. A total of five types of rock are drilled to obtain core specimens with a diameter of 63.5 mm at various bedding plane angles and scratching directions as shown in Figure 1.2.

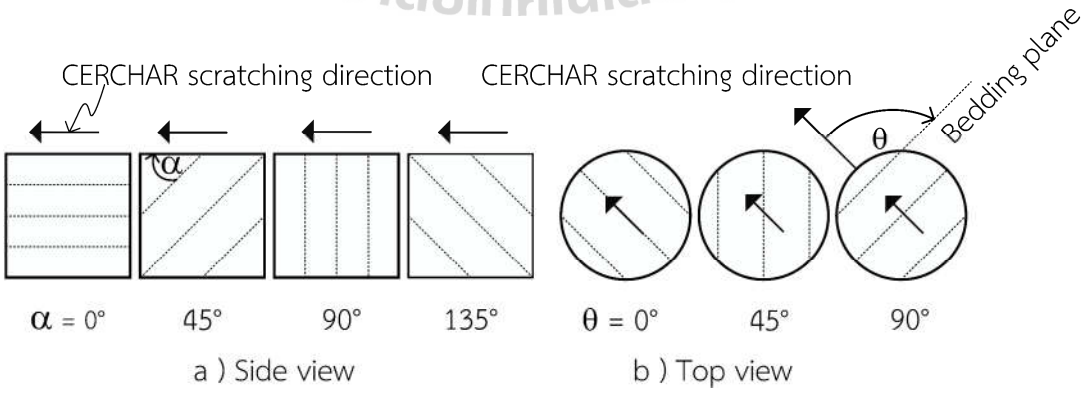

Figure 1.2 Scratching direction as compound to bedding plane angles (a), and as compared to trends of bedding planes (b).

1.4.3 CERCHAR abrasivity testing

The CERCHAR abrasivity testing is conducted on saw-cut surfaces using the west apparatus, as depicted in Figure 1.3. This test objective is to determine the CERCHAR abrasivity index (CAI) of rock specimens. The testing procedure follows ASTM D7625-22 standard practice. There will be additional measurements beyond standard method, including crank rotation torque throughout the entire scratching process.

1.4.4 X-ray Diffraction analysis

The XRD analysis is conducted on finely ground rock powder. The results can be utilized to determine the influence of mineral compositions on the CAI value.

1.4.5 Analysis

Mathematical relations are established based on the correlation between scratching force (F) and scratching distance (ds) to determine the energy utilized by the drilling head at various angles of the bedding planes and scratching directions. They are used to estimate the drill bit's wear and its operational lifespan.

1.4.6 Discussions and Conclusion

All research activities, methodologies, and results are documented and compiled in thesis. The contents and findings will be published in a conference.

1.4.7 Thesis Writing

All research activities, methods, and results are documented and complied in the thesis.

1.5 Thesis Contents

Chapter I describes the background of problems and significance of the study. The research objectives, methodology, scope and limitations are identified. Chapter II summarizes the results of the literature review. Chapter III describes the sample preparations. Chapter IV describes the testing. Chapter V gives the test results. Chapter

VI calculates CERCHAR specific energy. Chapter VII discusses and concludes the research results and provides recommendations for future research studies.

CHAPTER II
LITERATURE REVIEW

This section gives a summary of the literature review to improve an understanding of the impact of bedding planes on CERCHAR abrasivity index (CAI) test and the influencing factors related to CAI.

2.1 Rock abrasiveness

Rock abrasiveness is understood as the ability of a rock or minerals to cause wear, erosion, or damage to cutting or grinding tools upon contact. It is considered a vital characteristic in several industries, such as mining, construction, and geology. The performance of mine excavation machinery is significantly influenced by it. The expenses and delays incurred in replacing worn-out parts directly impact the overall machinery performance (Atkinson, Cassapi, and Singh, 1986). Mucha (2023) emphasizes the widespread and aggressive nature of abrasive wear, particularly in the processes concerning the extraction, transportation, and utilization of hard-rock-type mineral substances.

Commonly used testing methods for assessing the abrasiveness of geological materials are developed in France, including CERCHAR abrasivity test for rocks and LCPC abrasivity test for soils or grain materials (Janc, Jovicic, and Vukelić, 2020). Test procedure follows the International Society for Rock Mechanics (ISRM) in Alber et al. (2014) suggested method. The test procedure is also given by ASTM D7625-22 standard practice as presented in Table 2.1.

Table 2.1 Classification of CAI (ASTM D7625-22).

Mean CAI	Classifications
0.30 – 0.50	Very low abrasiveness
0.50 – 1.00	Low abrasiveness
1.00 – 2.00	Medium abrasiveness
2.00 – 4.00	High abrasiveness
4.00 – 6.00	Extreme abrasiveness
6.00 – 7.00	Quartzite

2.2 Factors affecting CERCHAR abrasivity index

2.2.1 Surface conditions

Several researchers investigate the effects of rough and smooth surfaces on the CERCHAR abrasivity index (CAI). Their results show that rough surfaces tend to yield higher CAI values compared to smooth surfaces due to increased friction and resistance. Al Ameen and Waller (1994) highlight that rough surface, with their asperities and irregularities, cause greater tool wear, resulting in higher abrasivity readings. Käsling and Thuro (2010) confirm that rough surfaces generate higher CAI values because of increased friction, while smooth surfaces produce lower values due to reduced friction. Aydın, Yaralı, and Duru (2016) find similar results, emphasizing the importance of standardizing surface texture to improve test accuracy and repeatability, Yaralı and Duru (2016) perform tests on both rough and saw-cut rock samples, resulting in a total of 27,000 scratches (Figure 2.1). CAI on the rough surface is approximately 18% higher than that on the saw-cut surface (Hamzaban, Rostami, Dahl, Macias, and Jakobsen, 2022) reinforced these findings in a critical review, noting that rough surfaces lead to higher CAI values and greater tool wear, while smooth surfaces result in lower CAI values. Together, these studies underscore the necessity of consistent surface preparation in CAI testing to ensure reliable and comparable results.

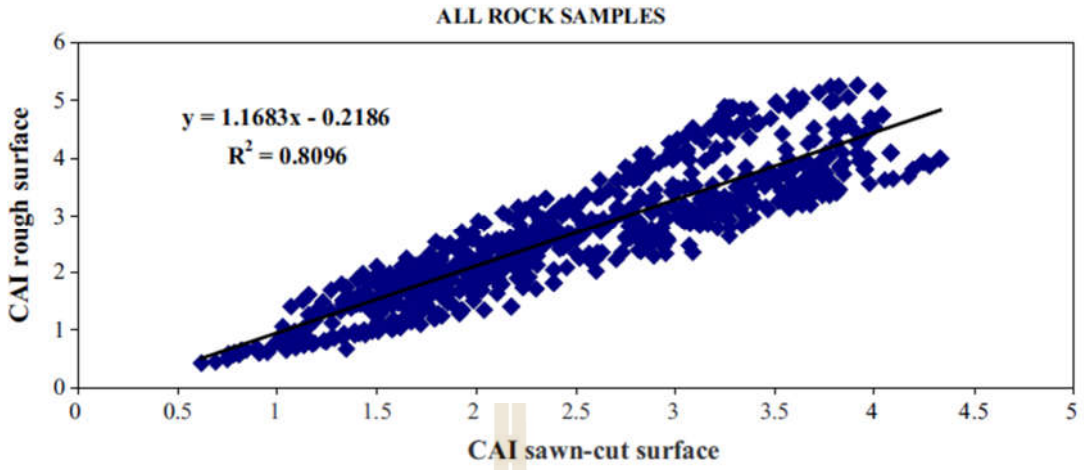

Figure 2.1 Relationship between CAI values of rough surface and saw-cut surface (Yaralı and Duru, 2016).

2.2.2 Stylus hardness

Sanford and Hagan (2009) assess the impact of stylus metallurgy on CAI measurements, finding that using harder materials like tungsten carbide for the stylus results in more reliable and accurate CAI values compared to steel. Specifically, the hardness of the stylus, such as those with a Rockwell Hardness (HRC) of 55, plays a critical role in the accuracy and consistency of CAI measurements. Yaralı and Duru (2016) investigate the effect of mechanical properties of rocks on CAI, revealing that higher rock strength and hardness positively correlate with higher CAI values. Teymen (2020) demonstrates the usability of CAI for estimating mechanical rock properties, showing a strong correlation between CAI and rock strength and hardness. The research underscores that a stylus with HRC 55 hardness provides a reliable standard for measuring CAI, ensuring consistent and reproducible results.

2.2.3 Scratching rate

Aydın (2019) investigates the effects of various testing parameters on CAI and its repeatability, finding that pin speed is a crucial factor affecting CAI results. Hamzaban, Karami, and Rostami (2019) examine the impact of pin speed on CAI test

results and discovere that higher pin speeds lead to reduced CAI values. Supporting this, Kotsombat, Thongprapha, and Fuenkajorn (2020) study the effects of scratching rate on CAI of sandstones, finding that lower scratching rates result in lower CAI values. Zhang, Konietzky, Song, and Huang (2020) also highlight the importance of controlling testing conditions, including pin speed, to improve the reliability of CAI measurements.

2.2.4 Grain size

Research spanning from Al Ameen and Waller (1994) to Zhang et al. (2021) consistently emphasizes the significant impact of abrasive minerals, particularly quartz, on the CERCHAR Abrasivity Index (CAI). Al Ameen and Waller (1994) demonstrate that rocks with high quartz content exhibit higher CAI values. Building on this, Er and Tuğrul (2016) confirm a positive correlation between rock density, quartz content, and CAI. Similarly, Torrijo, Garzón-Roca, Company, and Cobos (2019) find that higher quartz content directly increases CAI. Zhang et al. (2021) further reinforced these findings, showing a positive relationship between rock hardness, quartz content, and CAI. Across these studies, the presence of abrasive minerals like quartz consistently correlates with the increased CAI, indicating their crucial role in determining rock abrasivity.

2.2.5 Moisture content

Plinninger, Käsling, Thuro, and Spaun (2003) find that moisture conditions significantly influence CERCHAR abrasiveness index (CAI) values. Supporting this, Aydın (2019) investigates the effects of various testing parameters on CAI and its repeatability, finding that moisture is a crucial factor affecting CAI results. Kotsombat et al. (2020) further find that saturated sandstones exhibit lower CAI values compared to dry sandstones under the same scratching rate. Zhang, Konietzky, Song, et al. (2020) also highlight the importance of controlling moisture conditions during CAI testing, noting that variations in moisture can lead to significant discrepancies in CAI values. Comakli and Aldalahali (2024) explore the effect of water saturation on CAI in clay-rich

rocks at different scratch lengths, finding that increasing water saturation reduces CAI values.

2.3.6 Temperature

Plinninger et al. (2003) suggest that testing temperature conditions significantly influence CAI values. Aydın (2019) investigates the effects of various testing parameters on CAI and its repeatability, showing that temperature is a crucial factor affecting CAI results. Rossi, Saar, and Rudolf von Rohr (2020) demonstrate that combining thermal and mechanical drilling reduces CAI values. Similarly, Ji, Wang, Zheng and Wu (2021) show that higher temperatures reduce CAI values of Bukit Timah granite, providing clear evidence that thermal treatment supports more efficient and durable drilling operations. Wang, Guo, and Wu (2023) find that thermal treatment reduces CAI of brittle rock. Zhang, Konietzky, Song, et al. (2020) further analyse the impact of various testing conditions, including temperature, on CAI values.

2.3.7 Mineral compositions

Numerous studies have investigated parameters influencing CAI test outcomes. West (1989) underscores the pivotal role of quartz content (QC) in affecting CAI results. Plinninger et al. (2003) highlight the insufficiency of solely relying on equivalent quartz content (EQC) for interpreting CAI values. Conversely, Lee, Jeong and Jeon (2013) show the significant impact of EQC on CAI values compared to quartz content. However, Lassnig, Latal and Klima (2008) observe no direct correlation between CAI values and grain size. Yaralı, Yaşar, Bacak and Ranjith (2008) test sedimentary rocks, proposing a robust linear relationship between CAI values, quartz content, degree of cementing, equivalent quartz content, and quartz grain size. Er and Tuğrul (2016) investigate the correlation between CAI and physico-mechanical characteristics of granitic rock samples. The study's findings suggest a substantial influence of quartz size and content on CAI. An escalation in quartz content and size within granitic rocks leads to higher CAI values. Kathancharoen and Fuenkajorn (2023)

highlight importance of not solely considering EQC but rather focusing on volume metric hardness as a more relevant factor as shown in Figure 2.2.

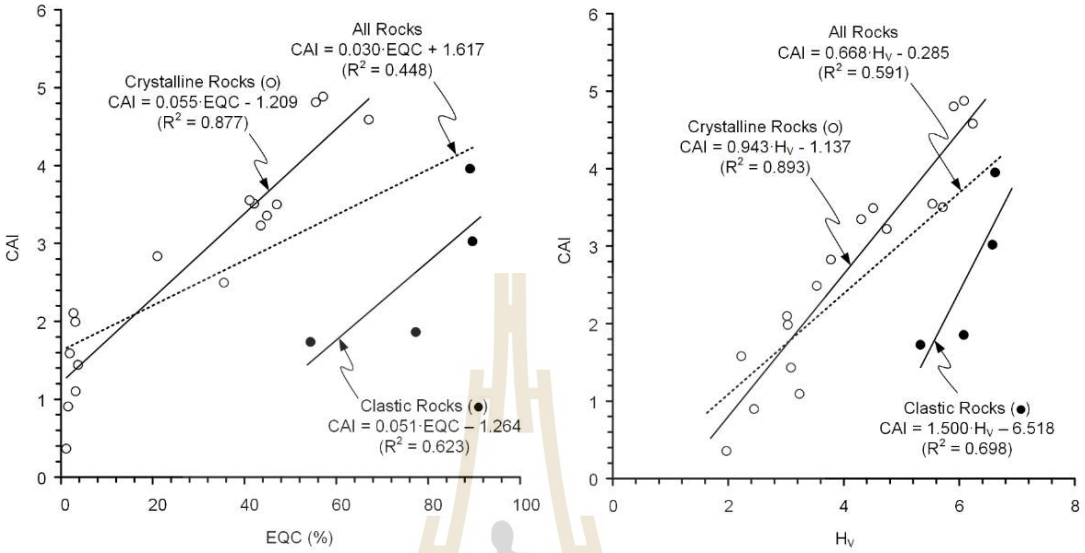

Figure 2.2 CAI testing, where black solid line represents mean CAI derived from single test, and red dashed line represents mean CAI value obtained from all individual tests (Kathancharoen and Fuenkajorn, 2023).

2.3.8 Rock properties

Bedding plane anisotropy characterizes specific rock formations, notably prevalent in sedimentary rocks like sandstone, siltstone, mudstone, and shale (Ramamurthy, 1993). Jin, Li, Jin, Hambleton and Cusatis (2018) perform a study on the relationship between the calculated P-wave velocities for individual specimens and their anisotropy angle (Figure 2.3). The highest velocities are observed when the direction of longitudinal wave propagation aligns parallel to the isotropy or bedding plane, as notably seen in the specimen with θ = 90°. In contrast, the lowest velocity occurs at an anisotropy angle of 0°, where the direction of longitudinal wave propagation is perpendicular to the isotropy plane. In uniaxial compression test, specimens are prepared with five different bedding plane orientations: 0°, 30°, 45°, 60°, and 90° with respect to the applied loading direction. As for the Brazilian test, the

samples were shaped into dice-like forms with orientations consistent with the UCS test in Figure 2.4.

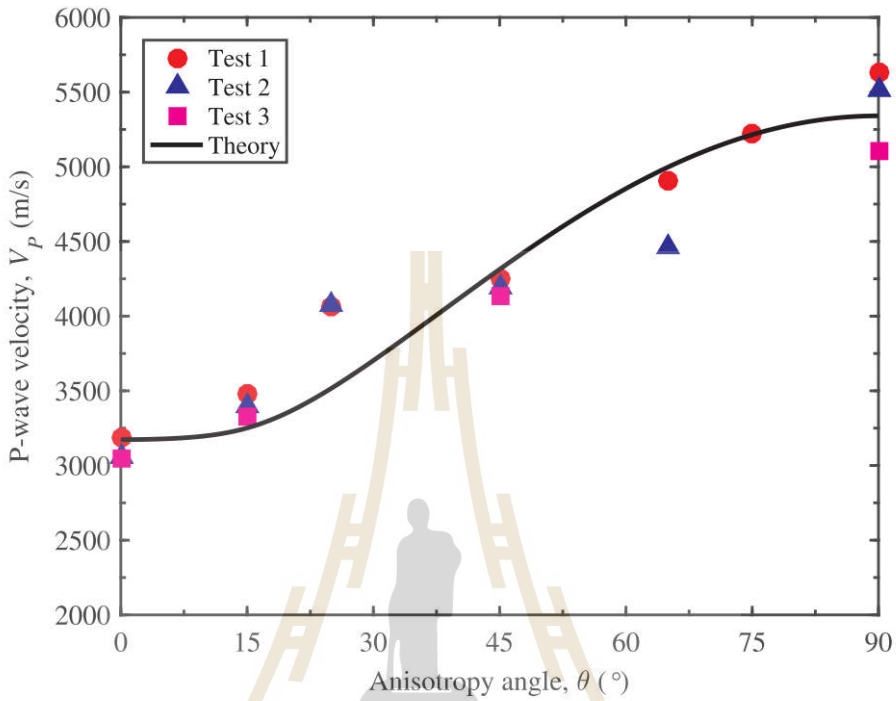

Figure 2.3 P-wave velocity in relation to the anisotropy angle (Jin et al., 2018).

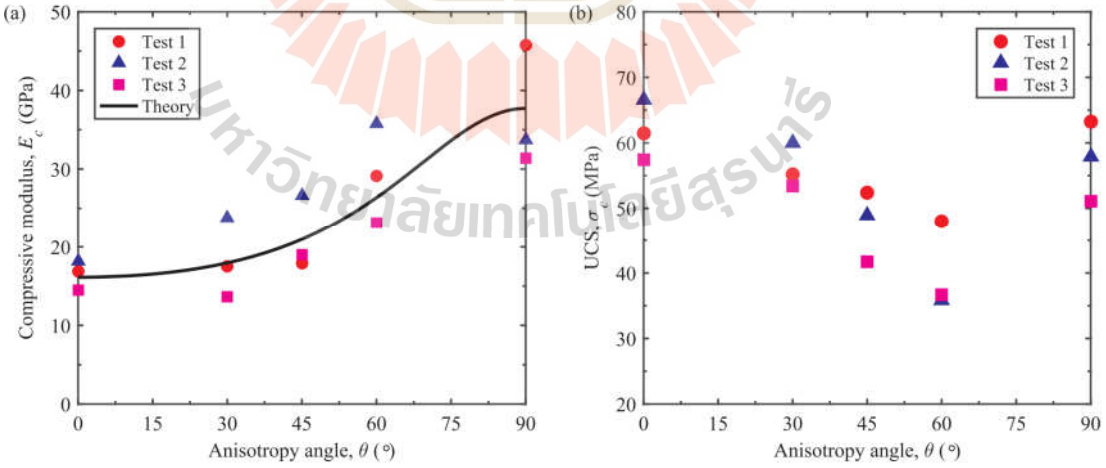

Figure 2.4 Correlation between (a) compressive modulus and (b) Uniaxial compressive strength (UCS) concerning the anisotropy angle (Jin et al., 2018).

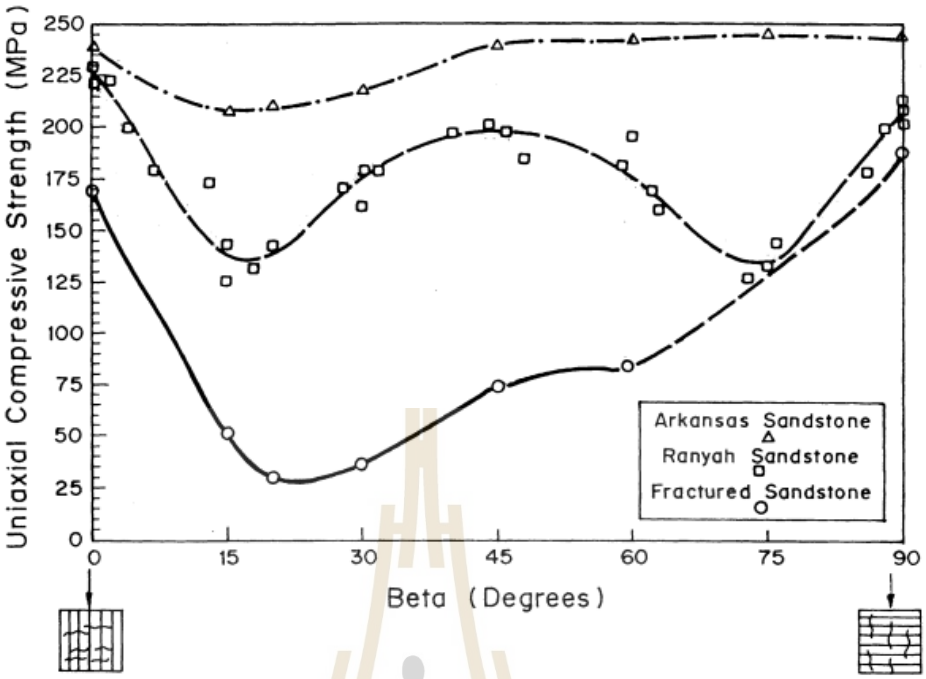

Figure 2.5 Correlation between strength anisotropy curves of Arkansas, Ranyah, and fractured sandstones (Al-Harthi, 1998).

Al-Harthi (1998) establishes a correlation between the strength anisotropy curves of Arkansas, Ranyah, and fractured sandstones (Figure 2.5). Correlation is obtained between the strength anisotropy curves of Arkansas, Ranyah, and fractured sandstones (Chenevert and Gatlin, 1965) and another fractured sandstone (Horino and Ellickson, 1970) Arkansas sandstone exhibits light banding and features as a single set of discontinuities. The highest compressive strength is observed at orientations of both $\beta = 0°$ and $\beta > 45°$. The anisotropy curve for Arkansas sandstone follows the typical U-shaped pattern, with the lowest compressive strength at $\beta = 15°$ and a relatively flat region between $\beta = 45°$ and 90°.

Sukjaroen, Thongprapha, Liabkrathok, and Fuenkajorn (2021) study the impact of bedding planes at various angles of gypsum by conducting compressive strength tests. The strengths are found to be highest at $\beta = 0°$ and lowest at $\beta = 60°$.

Additionally, Fuenkajorn and Singkhiaw (2022), who tested sandstone, observed that the compressive strengths are highest at β = 0° and lowest at β = 75°.

Teymen (2020) performs a series of statistical analyses to estimate the fundamental rock mechanics test results performed on specimens of specific sizes using the CAI test, commonly applied in rock abrasion assessments. The study reveals a significant relationship between the basic rock mechanics properties, such as Young's modulus and uniaxial compressive strength, and CAI (Figure 2.6). The multiple regression models are found to be more reliable than simple regression equations, displaying correlation coefficients ranging from 0.72 to 0.96.

Li et al. (2021) find a substantial impact of the bedding angle on the strength of layered rocks. Typically, the maximum failure strength is observed at 0° or 90°, while the minimum failure strength tends to occur within the range of 30°–45° bedding angles.

Zhang, Konietzky, and Frühwirt (2020) find that CAI test may not offer a dependable indication for anisotropic rocks like phyllite, owing to their distinctive characteristics (Figure 2.7).

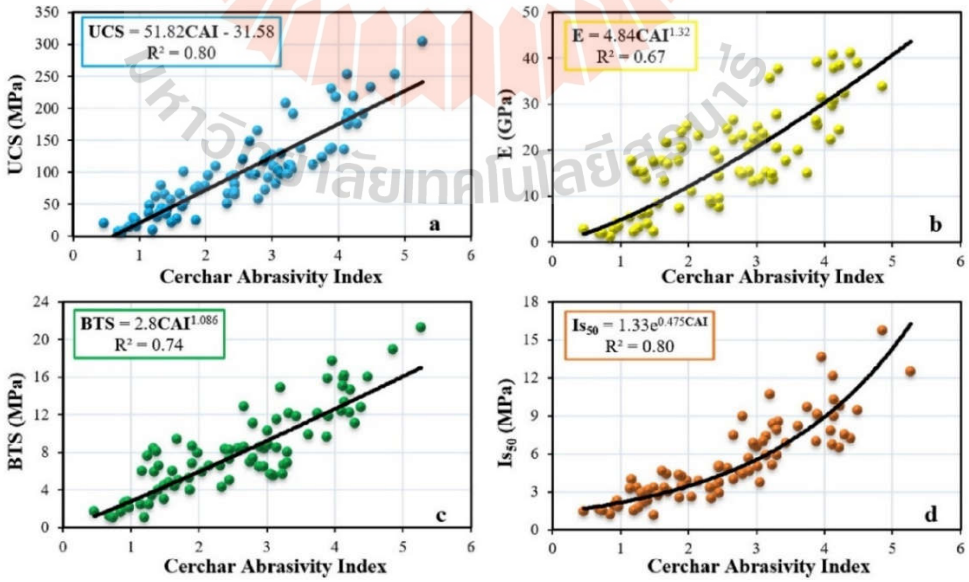

Figure 2.6 Relationship between CAI and basic mechanical tests a) UCS b) E c) BTS d) Is_{50} (Teymen, 2020).

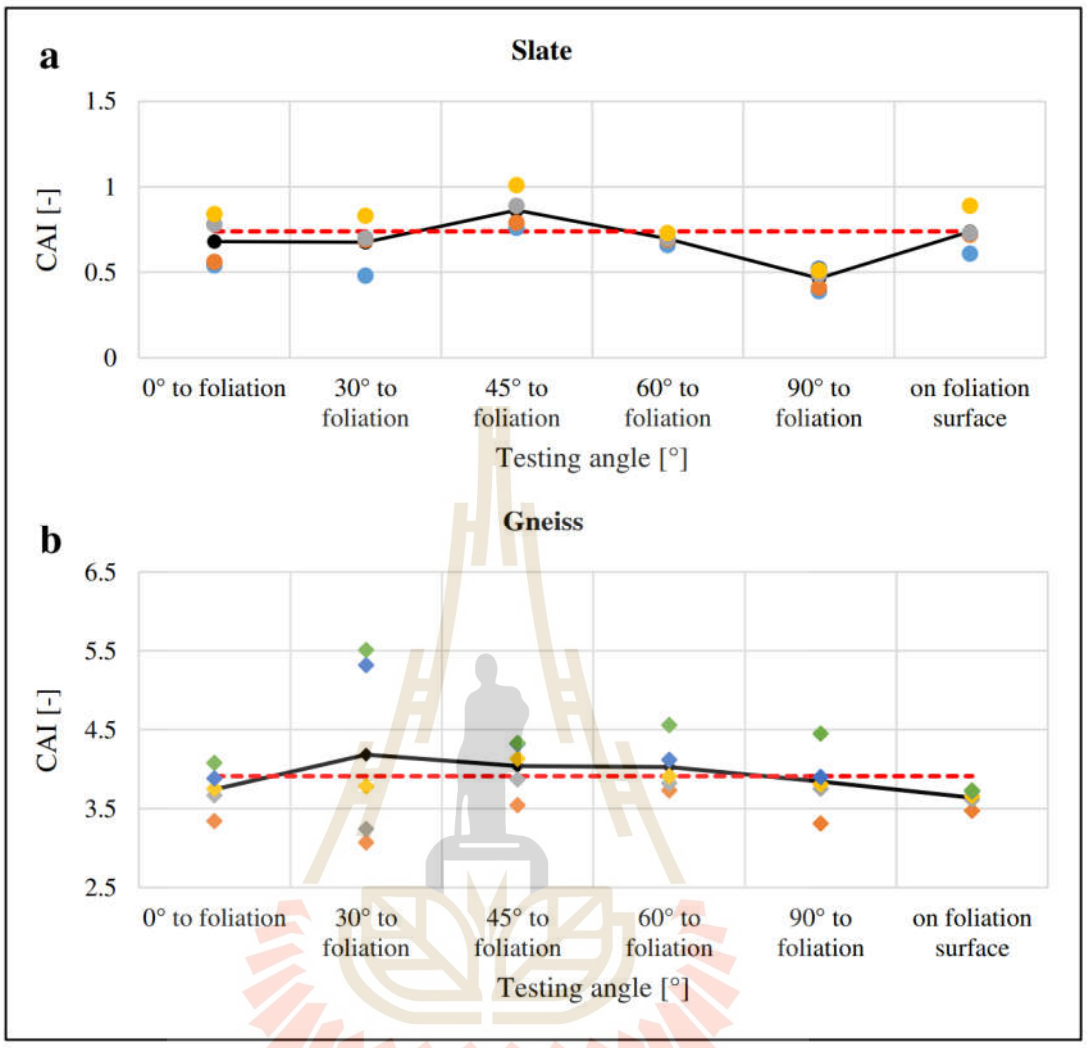

Figure 2.7 CAI versus testing orientations, where black solid line represents mean CAI derived from single test, and red dashed line represents mean CAI value obtained from all individual tests (Zhang, Konietzky, and Frühwirt, 2020).

2.3 CERCHAR specific energy

The concept of specific energy (SE) in the context of the CERCHAR test revolves around the energy derived from the action of a stylus scratching across a rock surface, as introduced by Hamzaban, Memarian, and Rostami (2018). This energy, crucial in assessing rock material properties, is further elaborated upon by Zhang, Konietzky, and Frühwirt (2020). In their work, they introduce additional terms for this parameter,

referring to it interchangeably as scratching specific energy (SSE) or CERCHAR specific energy (CSE). The energy in question can be quantified by determining the work done (W) during the movement of the pin stylus. This is accomplished by integrating the scratching force exerted on the stylus over a predetermined scratching distance, conventionally set at 10 mm. The scratching force, measured throughout the scratching process, encapsulates the resistance encountered by the stylus as it traverses the rock surface. Upon obtaining the total work done (W), it is then divided by the excavated or removed volume (V) of the specimen. This volume measurement encompasses the entirety of the material displaced or removed by the scratching action along the entire length of the scratch.

CHAPTER III

SAMPLE PREPARATION

3.1 Introduction

This chapter describes test specimens' preparation with different bedding plane orientations and scratching directions, description of specimens, and their mineral compositions obtained from X-ray diffraction analysis (XRD). The rock samples include Khao Khad argillaceous limestone, Khao Khad bedded limestone, Phu Kradueng sandstone, Phu Phan sandstone, and Tak Fa gypsum. The location of these rocks is shown in Figure 3.1.

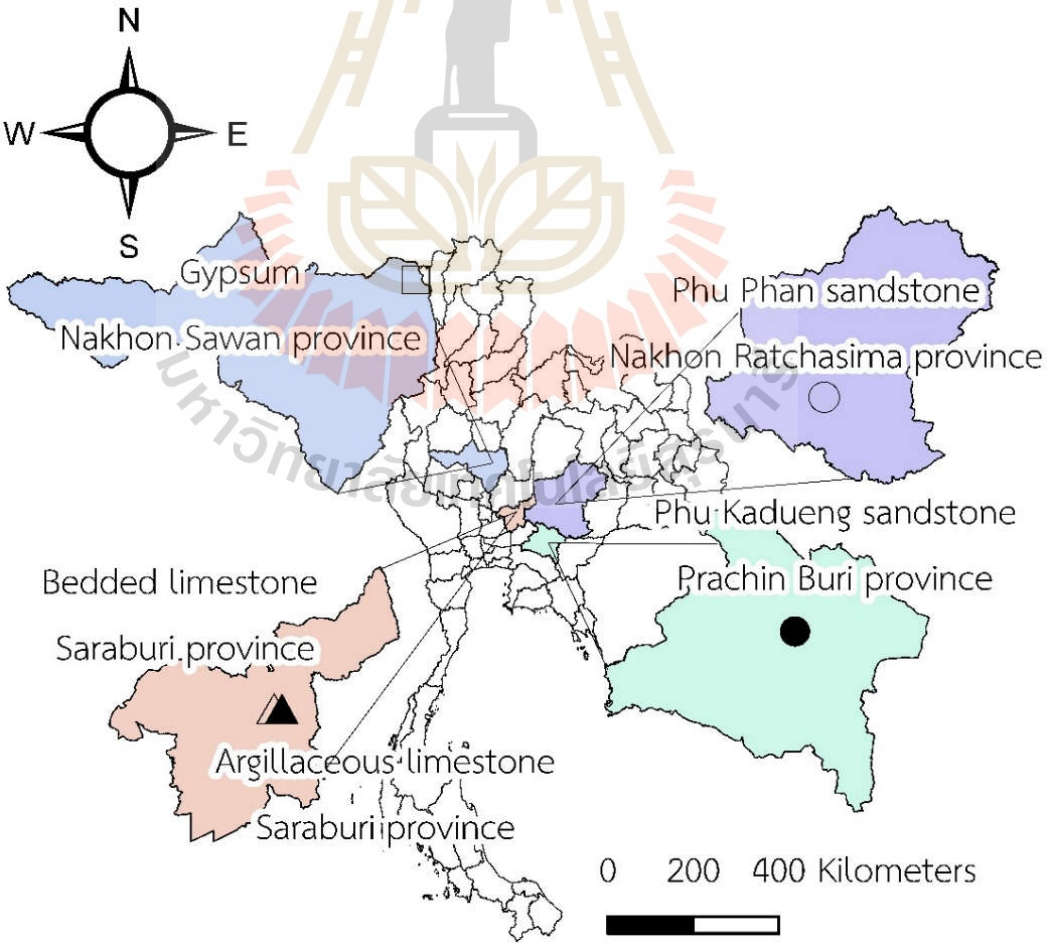

Figure 3.1 Samples obtained from various locations in Thailand.

3.2 Rock Description

3.2.1 Khao Khad argillaceous limestone

Rock samples obtained from Khao Khad formation, located on Saraburi Province, have bedding planes which can be observed by the alternation of gray limestone and pale brown clay bands, with average thickness of 1 mm.

3.2.2 Khao Khad bedded limestone

The bedded limestone is obtained from Khao Khad formation, located on Saraburi Province. Their bedding planes can be observed by the alternation of gray limestone and white calcite bands, with average thickness of 0.5 mm.

3.2.3 Phu Kradueng sandstone

Phu Kradueng sandstone is a member of the Korat Group, found in the Korat Plateau region. Their bedding planes can be observed by the alternation of pale green quartz and black biotite bands, with average thickness of 1.5 mm.

3.2.4 Phu Phan sandstone

Rock samples obtained from Phu Phan formation, located on the Korat Plateau in northeastern Thailand have bedding planes that can be observed by the alternation of pale red quartz and red microcline bands, with average thickness of 1 mm.

3.2.5 Tak Fa gypsum

Gypsum samples are collected from Nakhon Sawan Province. Their bedding planes can be observed by the alternation of white gypsum and gray anhydrite bands, with average thickness of 2 mm.

3.3 Rock specimens preparation

Cylindrical specimens with diameter is 63.5 mm are prepared from all rock types (Figure 3.2). Test specimens contain different bedding plane orientations and scratching directions. The α angle is measured between scratching direction on the

horizontal plane and dip angle of bedding planes varying from 0, 45, 90 and 135 degrees. The θ angle is between strike line and scratching directions varying from 0, 45 and 90 degrees. A total of 30 specimens have been prepared. Table 3.2 shows rock dimensions and their density.

The specimens after CERCHAR test are finely ground to obtain a powder with less than 0.25 mm particle size (pass through mesh #60) as following the ASTM E1426-14e1 standard practice. The representative specimens, maximum and minimum density values, are used to determine the average weight percentage of mineral compositions by using the X-ray diffraction method (XRD). The results are shown in Tables 3.1. The X-ray diffraction (Bruker, D2 Phaser) is used.

Table 3.1 Mineral composition for all rock types.

Rock type	Mineral compositions (%)
Khao Khad argillaceous limestone	Quartz 2.80, Feldspar, 0.86, Calcite 94.90, Montmorillonite 1.33, Pyrite 0.04, Illite 0.06
Khao Khad bedded limestone	Quartz 0.58, Calcite 99.42
Phu Kadueng sandstone	Quartz 79.72, Feldspar 0.33, Biotite 0.76, Anorthite 1.14, Muscovite 0.28, Kaolinite 4.98, Andesine 0.18, Oligoclase 1.91, Calcite 6.78, Illite 3.55, Montmorillonite 0.25, Orthorhombic kalsilite 0.11
Phu Phan sandstone	Quartz 67.69, Oligoclase 11.50, Albite 8.26, Chlorite 5.58, Microcline 3.35, Anorthite 2.00, Calcite 1.11, Kaolinite 0.25, Muscovite 0.25
Tak Fa gypsum	Chlorite 3.00, Calcite 7.98, Gypsum 88.90, Anhydrite 0.12

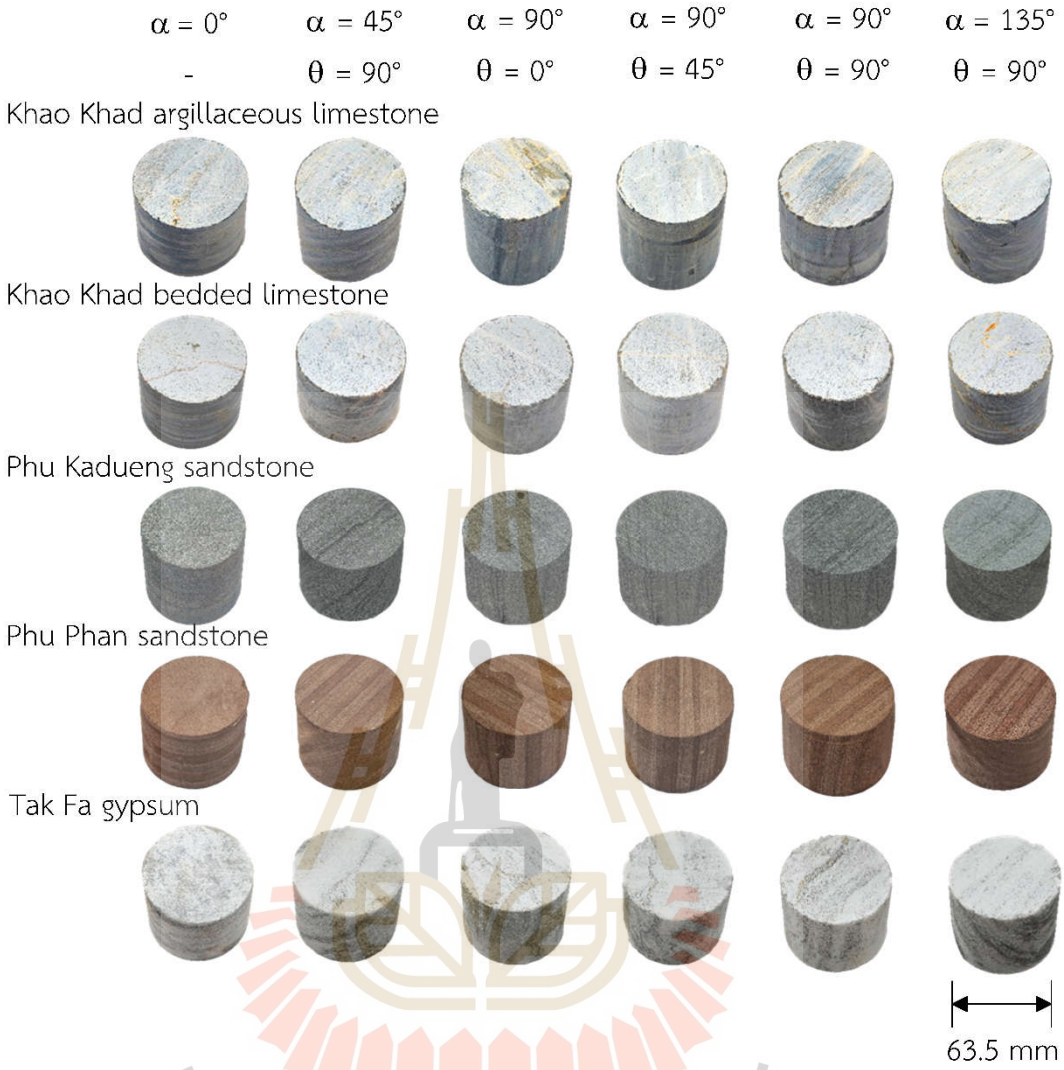

Figure 3.2 Specimens with various bedding plane orientations and scratching directions prepared for CERCHAR tests.

.

Table 3.2 Rock dimensions and density for all rock types.

Rock type	α (degrees)	θ (degrees)	Length (mm)	Weight (g)	Density (g/cc)
Khao Khad argillaceous limestone	0	-	40.42	343.65	2.68
	45	90	39.42	334.32	2.68
	90	0	41.28	352.45	2.70
	90	45	42.58	364.12	2.70
	90	90	41.74	355.38	2.69
	135	90	41.58	355.14	2.70
Khao Khad bedded limestone	0	-	40.24	342.58	2.69
	45	90	38.58	330.12	2.70
	90	0	40.46	344.25	2.69
	90	45	40.98	349.58	2.69
	90	90	40.44	346.25	2.70
	135	90	38.62	330.25	2.70
Phu Kadueng sandstone	0	-	40.22	334.58	2.63
	45	90	38.58	321.28	2.63
	90	0	40.24	334.25	2.62
	90	45	40.3	333.45	2.61
	90	90	41.28	342.48	2.62
	135	90	38.78	320.54	2.61
Phu Phan sandstone	0	-	40.18	299.88	2.36
	45	90	40.32	299.84	2.35
	90	0	40.18	298.98	2.35
	90	45	40.24	298.55	2.34
	90	90	40.22	298.95	2.35
	135	90	40.22	299.58	2.35
Tak Fa Gypsum	0	-	40.02	293.65	2.32
	45	90	40.18	294.68	2.32
	90	0	40.04	293.45	2.31
	90	45	39.88	292.58	2.32
	90	90	40.12	294.36	2.32
	135	90	40.08	294.68	2.32

CHAPTER IV
TEST APPARATUS AND METHODS

4.1 Introduction

This chapter presents test apparatus and methods used to determine the CERCHAR abrasivity index (CAI) and the parameters required for calculating the CERCHAR specific energy (CSE). These parameters encompass ploughing force, vertical displacement, and mean groove volume. Additionally, the chapter describes the test apparatus and methods employed to ascertain the physical and mechanical properties, as well as the mineral compositions of the rock specimens.

4.2 CERCHAR test

CERCHAR testing is conducted on saw-cut surfaces of rock specimens with varying bedding plane angles using a device based on West apparatus, as depicted in Figure 4.1. The apparatus comprises a vice for holding the rock specimen, a pin chuck or casing for the stylus pin, a static load of 70 N, and a hand crank. During testing, the specimen is moved beneath the stylus at a constant scratching rate of 1 mm/s, achieved by rotating the hand crank ten times over a duration of ten seconds, given the 1 mm pitch of the screw connecting the hand crank and the vice holding. This ensures adherence to the test procedure recommended by the International Society for Rock Mechanics (ISRM) and American Society for Testing and Materials (ASTM).

The stylus pin, with a Rockwell hardness (HRC) of 55 ± 1, is subjected to scratching over a standardized length of 10 mm for each test. Following scratching, the wear flat of the stylus tip is meticulously measured under a microscope with 50x magnification, with measurements taken at four angles (0°, 90°, 180°, and 270°) around its axis. Results from these measurements are averaged for each pin, with five pins

used for testing each rock type. The CERCHAR abrasiveness index (CAI) values are then determined using the formula: CAI = d × 10, where d represents diameter of the scratch flat area of the stylus tip resulting from smooth surface testing. The diameter d can be correlated with smooth surfaces testing (d_s) by (eq .2):

$$d = 1.14 \cdot d_{sc} \tag{4.1}$$

where d_{sc} is the wear flat of stylus tip for the saw cut surface specimen performed in this study.

It is recognized that smooth surface testing is an option for CAI test methods of ASTM and ISRM. To meet the objective of determining the effects of bedding planes on CERCHAR abrasivity index, the effect of surface roughness is excluded here. It is noted that surface roughness of rock is difficult to control, as the same rock type may yield different surface roughness values. This adds an uncontrollable variable to our test plan. Some investigations that perform CAI tests on both rough and smooth rock surfaces find that CAI obtained from rough surfaces shows higher variation than those from smooth rock surfaces. As a result, they recommend using smooth rock surfaces for CAI testing. In addition, mathematical representations of rock surface roughness require relatively long surface profiles, while CAI testing uses only 10 mm. This may pose difficulty when such CAI is correlated with a roughness parameter, particularly when the roughness profile is not uniform along the entire length.

Additional parameters have been incorporated beyond those suggested by the ISRM. The vertical displacement of the stylus is currently being measured along the scratching length using digital displacement gauges with a precision of 0.001 mm, allowing us to determine the groove depth produced by scratching. Moreover, the lateral force exerted on the stylus is calculated based on the torque applied to the crank. A torque meter with a precision of 0.01 N·m is utilized for this purpose. The lateral force can be determined using the equation:

$$F = 2 \cdot \pi \cdot T / P \tag{4.2}$$

where F represents the ploughing force (N), T denotes the torque (N·m) applied on the crank, and P signifies the screw pitch of 0.001 mm.

Furthermore, volume of the scratching groove is obtained through laser-scanning profiles along the 10 mm scratching length. Both the groove width and depth are meticulously measured to the nearest 0.001 mm, ensuring precise characterization of the scratching morphology.

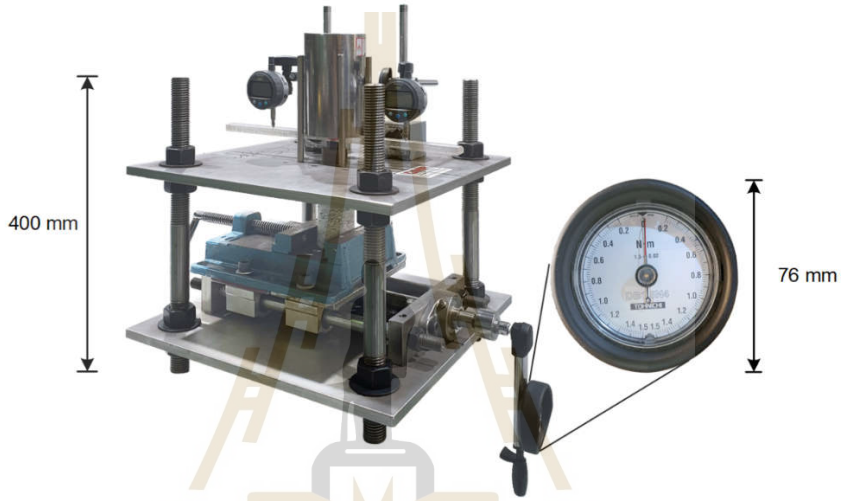

Figure 4.1 Device based on West CERCHAR apparatus with additional torque and vertical displacement measurements (Kathancharoen and Fuenkajorn, 2023).

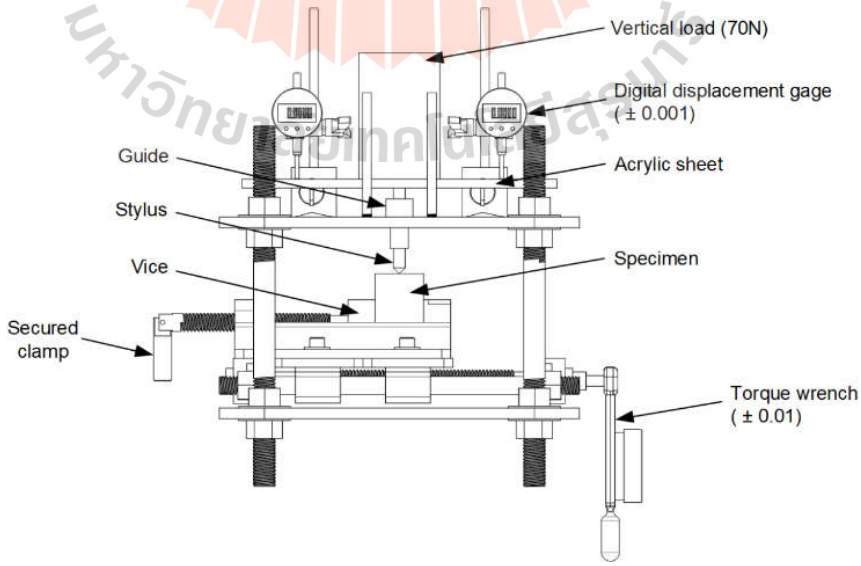

Figure 4.2 Schematic drawing of CERCHAR device (Kathancharoen and Fuenkajorn, 2023).

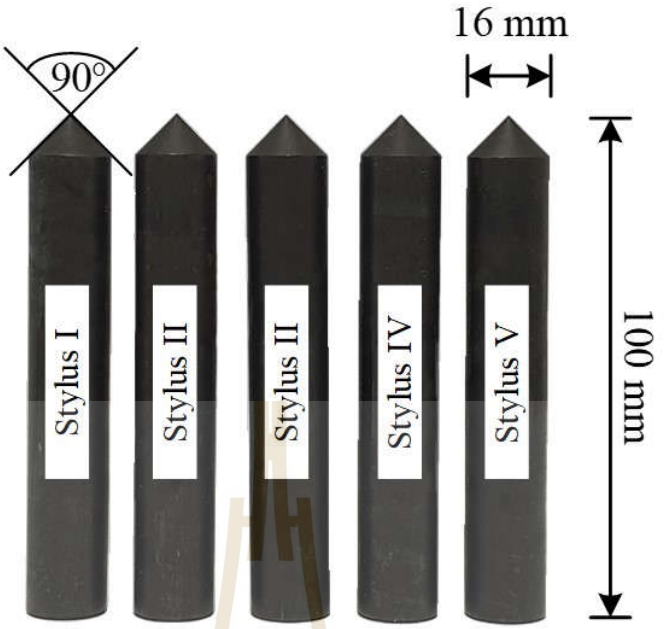

Figure 4.3 Stylus pins (HRC 55) are used in this study.

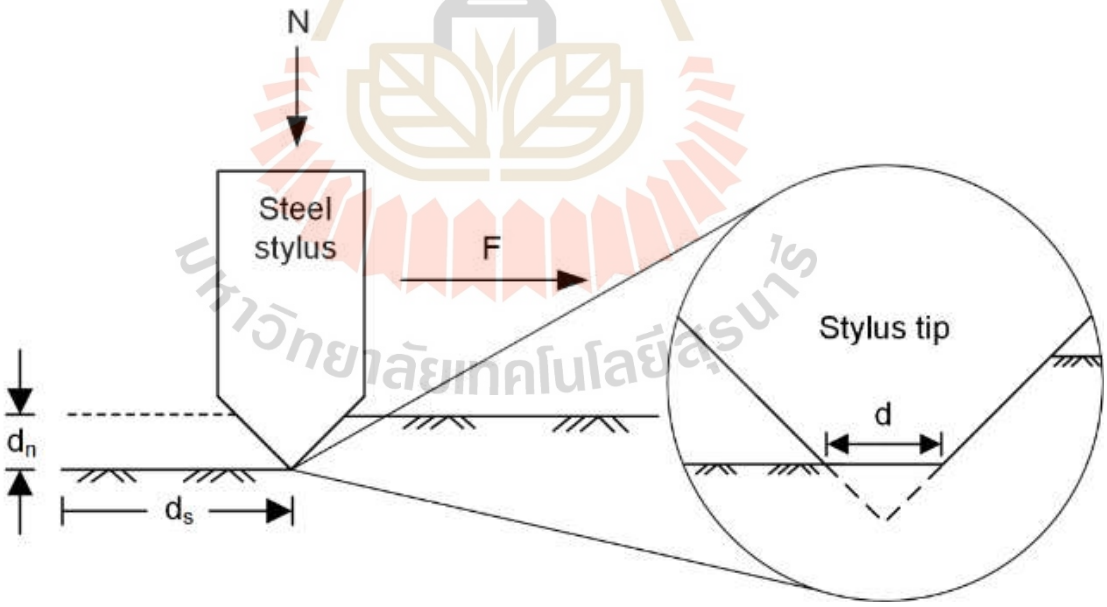

Figure 4.4 Steel stylus test variables, N is normal load (N), F is horizontal force (N), d_n is vertical displacement (mm), d_s is scratching distance (mm), and d is wear flat width of stylus tip.

4.3 X-ray diffraction (XRD) analysis

After CERCHAR test, certain specimens undergo preparation for X-ray diffraction analysis, conducted using the Bruker D8 Advance, as depicted in Figure 4.8. The testing methodology adheres to the ASTM D5357-19 (2019) standard practice. These specimens are ground to produce powder with particle sizes smaller than 0.25 mm (able to pass through mesh #60). Approximately 5 to 10 grams of this powder are utilized. The DIFFRAC.EVA software is employed to ascertain the weight percentage of mineral compositions within the specimens. These mineral compositions serve to elucidate the results of the CAI testing.

Figure 4.5 X-ray diffraction Bruker, D8 advance (Center for Scientific and Technology Equipment University of Technology).

CHAPTER V
TEST RESULTS

5.1 Introduction

This chapter presents CERCHAR test results, scratching forces, and the groove volume observed on the specimen surfaces. These measurements contribute to a more comprehensive understanding of rock abrasivity and the relationship between bedding plane orientation, scratching direction, and the resulting wear characteristics.

5.2 CERCHAR abrasivity index

For each rock type CERCHAR test is performed on five specimens with different bedding plane orientations (α) and scratching directions (θ). Five scratching tests are performed under each bedding plane condition. The average wear width served as the input for determining the CERCHAR Abrasivity Index (CAI), as presented in Appendix B, which is computed using Equation (4.1) given in Chapter 4. The resulting CAI values are then categorized into abrasivity classifications according to the ASTM D7625-22 CERCHAR method, as presented in Table 5.1. Regarding of bedding plane orientation, stronger rocks (i.e. limestone) tend to show higher CAI values than the softer ones (i.e. gypsum).

The CAI results for all tested rock types, are plotted in Figure 5.1. They reveal clear effects of bedding plane orientations (α) and scratching directions (θ). In general CAI tends to increase with α angle. Argillaceous limestone and the two sandstones, however, show the highest CAI value at α = 0° and the lowest at α = 45°. This behavior does not show for bedded limestone and gypsum (Figure 5.1a). All rocks show similar effect of scratching directions with respect to bedding plane direction (Figure 5.1b). The lowest CAI value are obtained under θ = 0°. The abrasivity gradually increases to

the maximum at θ = 90°. Scratching parallel to bedding trends gives low abrasivity than that perpendicular to the beds.

Table 5.1 Average CAI and standard deviation.

Rock type	α (degrees)	θ (degrees)	CAI ± SD	Abrasiveness (ASTM D7625-22)
Khao Khad argillaceous limestone	0	-	2.54 ± 0.11	High
	45	90	1.86 ± 0.02	Medium
	90	0	1.61 ± 0.01	Medium
	90	45	1.76 ± 0.02	Medium
	90	90	1.99 ± 0.04	Medium
	135	90	2.20 ± 0.00	High
Khao Khad bedded limestone	0	-	1.17 ± 0.01	Medium
	45	90	1.20 ± 0.01	Medium
	90	0	1.07 ± 0.01	Medium
	90	45	1.10 ± 0.00	Medium
	90	90	1.26 ± 0.01	Medium
	135	90	1.28 ± 0.01	Medium
Phu Kadueng sandstone	0	-	1.90 ± 0.01	Medium
	45	90	1.39 ± 0.01	Medium
	90	0	1.16 ± 0.01	Medium
	90	45	1.32 ± 0.02	Medium
	90	90	1.55 ± 0.01	Medium
	135	90	1.63 ± 0.01	Medium
Phu Phan sandstone	0	-	1.63 ± 0.01	Medium
	45	90	1.13 ± 0.01	Medium
	90	0	0.93 ± 0.01	Low
	90	45	1.03 ± 0.01	Medium
	90	90	1.19 ± 0.01	Medium
	135	90	1.24 ± 0.01	Medium
Tak Fa gypsum	0	-	0.40 ± 0.00	Very low
	45	90	0.43 ± 0.01	Very low
	90	0	0.29 ± 0.01	Very low
	90	45	0.36 ± 0.02	Very low
	90	90	0.45 ± 0.00	Very low
	135	90	0.50 ± 0.03	Very low

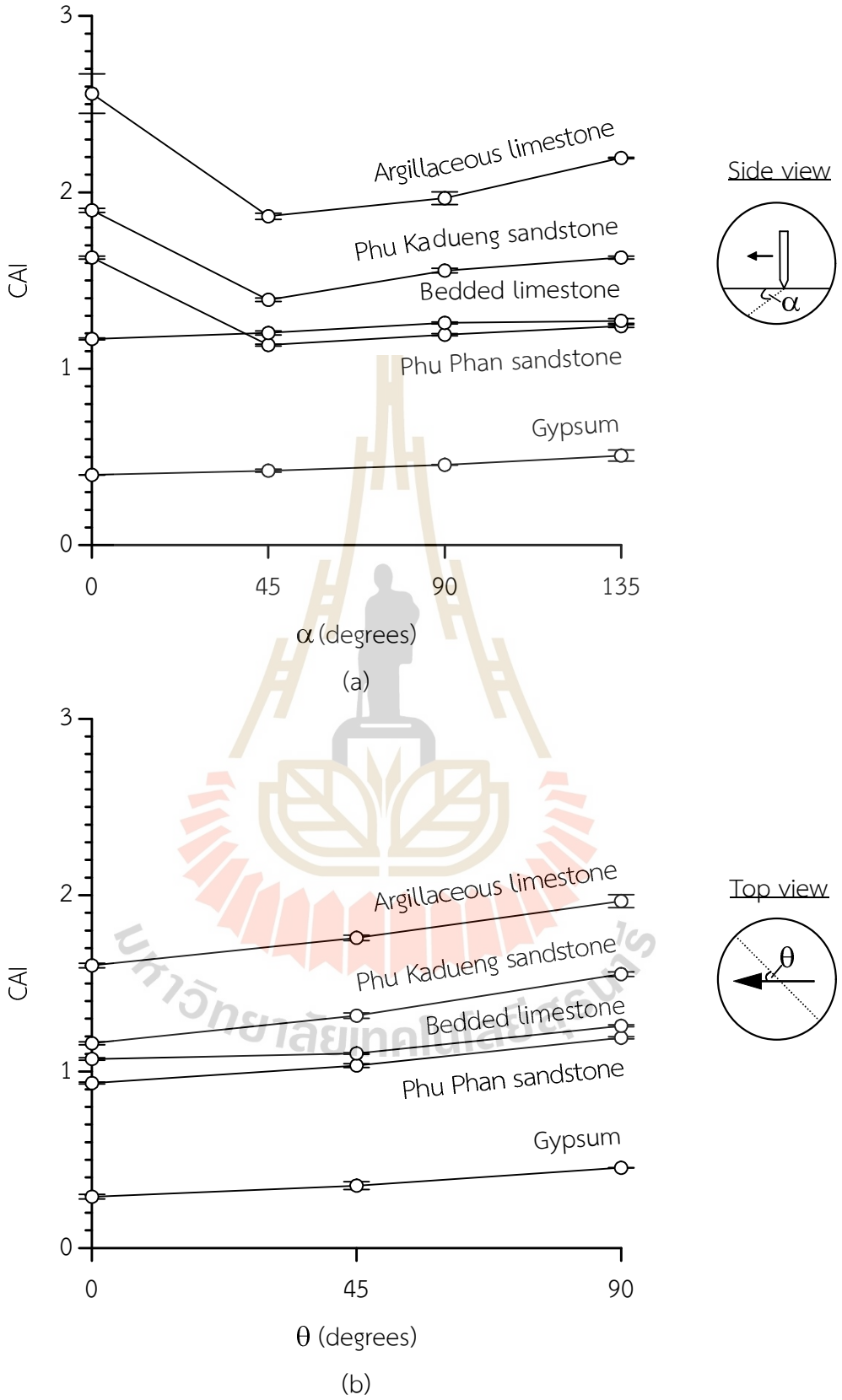

Figure 5.1 CAI as a function of bedding plane angle (a), and scratching direction (b).

5.3 Lateral force

Before obtaining the average lateral force, individual lateral force measurements for the five scratches have been recorded. These forces, derived from the rotational torque of the stylus pin, represent an additional parameter beyond those specified in the ASTM D7625-22 standard method. The lateral force values for each bedding plane condition are shown in Appendix C. The average lateral forces (F) as a function of scratching distance (d_s) for all test rocks are shown in Figures 5.2 through 5.6. For all rock types the scratching forces increase rapidly within the first 2-4 mm of scratching. Then they tend to remain constant with the distance. Stronger rocks (i.e. limestone and sandstone) show higher scratching force than the softer ones (i.e. gypsum). The effect of angle α on the scratching force is similar to those on the CAI value. The force generally increase with angle α. Scratching the stylus pin perpendicular to bedding plane trend (θ = 90°) show the largest force, as compared to those under θ = 0°. This holds trend for all rock types.

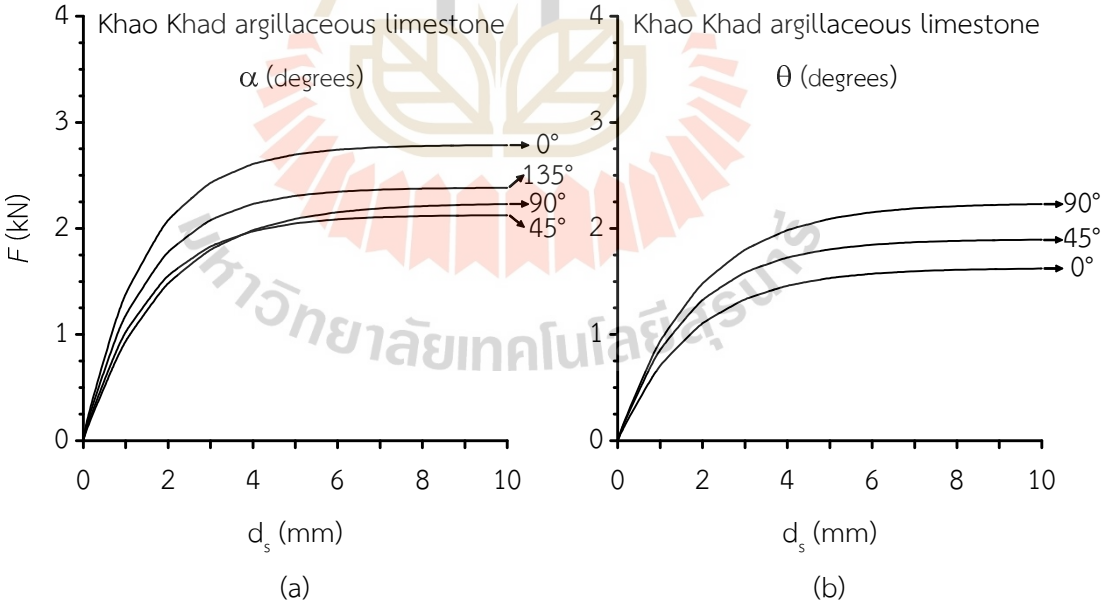

Figure 5.2 Scratching forces (F) as a function of scratching distance (d_s) of Khao Khad argillaceous limestone, bedding plane orientations (a) and scratching directions (b).

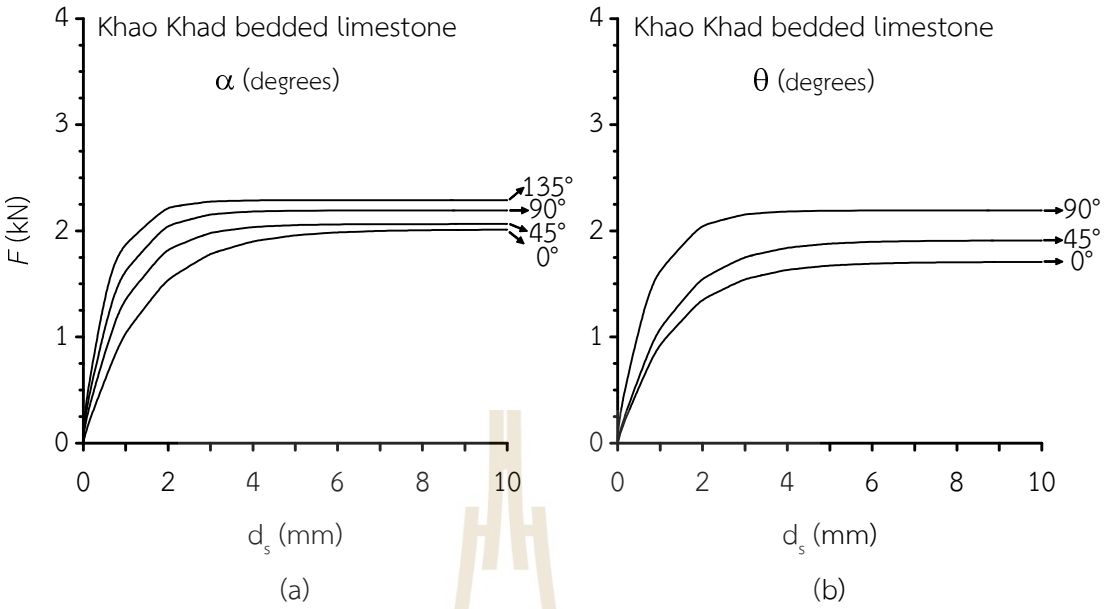

Figure 5.3 Scratching forces (F) as a function of scratching distance (d_s) of Khao Khad bedded limestone, bedding plane orientations (a) and scratching directions (b).

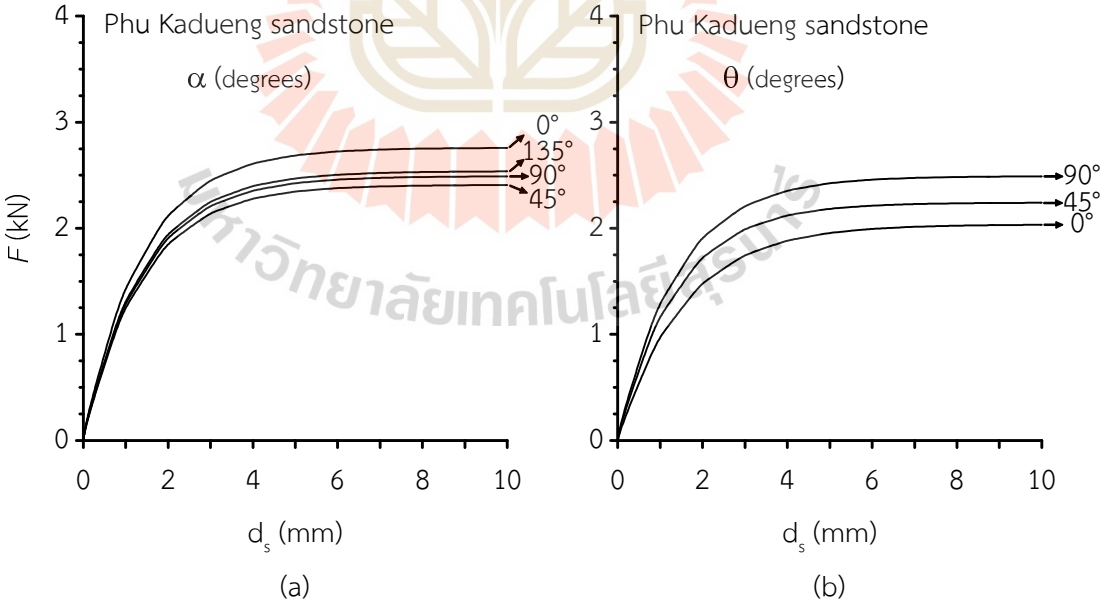

Figure 5.4 Scratching forces (F) as a function of scratching distance (d_s) of Phu Kadueng sandstone, bedding plane orientations (a) and scratching directions (b).

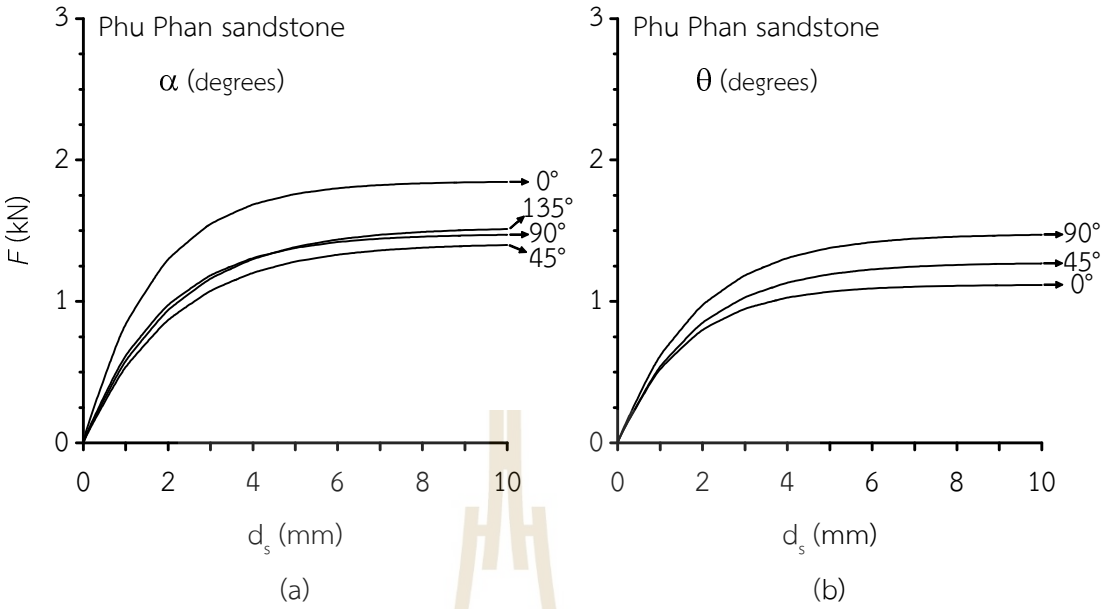

Figure 5.5 Scratching forces (F) as a function of scratching distance (d_s) of Phu Phan sandstone, bedding plane orientations (a) and scratching directions (b).

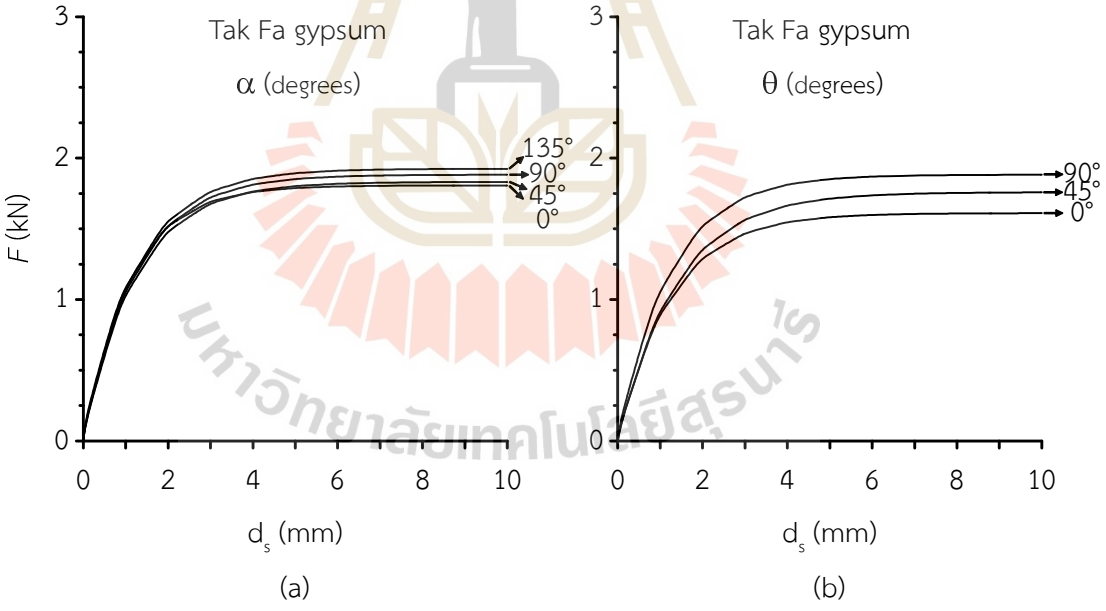

Figure 5.6 Scratching forces (F) as a function of scratching distance (d_s) of Tak Fa gypsum, bedding plane orientations (a) and scratching directions (b).

5.4 Groove volumes

The groove volumes for all tested rocks are averaged to obtain the mean groove volume (V) along with the corresponding standard deviation, Reflecting the results of rock's abrasivity characteristics. These results are summarized in Table 5.2, which provides a detailed comparison of the groove volumes across different rock types, highlighting variations with their bedding planes orientations and scratching directions.

As shown in Figure 5.7, higher groove volumes correspond to lower CAI values, as observed in Tak Fa gypsum (very low abrasiveness). However, a direct correlation between groove volume and CAI is not always evident, such as in the case of Phu Phan sandstone (medium abrasiveness), which shows groove volumes similar to those of Tak Fa gypsum. These discrepancies can be attributed to the mineralogical resistance to scratching, where bedding plane orientations and scratching directions align more consistently with the trends in CAI and lateral force for all test rocks. The groove images obtained from different bedding plane conditions are shown in Appendix C. Their corresponding values calculated form the method of laser scanning techniques explained in chapter IV are given in Figures D.1 – D.5 in Appendix D. Figure 5.7a shows the effect of bedding plane angle α on the groove volume. The maximum volumes are obtained with α = 45° for all rock types. Whereas softer rocks (i.e. gypsum and Phu Phan sandstone) show the largest scratching volumes, as compared to the stronger ones (such as limestone). Scratching the stylus pin parallel to bedding plane (θ = 0°) trend yields the largest volume. The lowest volumes are obtained when the stylus pin moves normal to the bedding plane trend (θ = 90°).

Table 5.2 Mean groove volumes for different angle α and θ.

Rock type	α (degrees)	θ (degrees)	Volume ± SD (mm^3)
Khao Khad argillaceous limestone	0	-	0.314 ± 0.03
	45	90	0.819 ± 0.06
	90	0	0.969 ± 0.04
	90	45	0.859 ± 0.05
	90	90	0.679 ± 0.05
	135	90	0.584 ± 0.04
Khao Khad bedded limestone	0	-	0.717 ± 0.02
	45	90	0.632 ± 0.04
	90	0	0.973 ± 0.06
	90	45	0.755 ± 0.03
	90	90	0.452 ± 0.02
	135	90	0.407 ± 0.07
Phu Kadueng Sandstone	0	-	0.536 ± 0.03
	45	90	0.846 ± 0.10
	90	0	1.097 ± 0.05
	90	45	0.900 ± 0.05
	90	90	0.768 ± 0.08
	135	90	0.635 ± 0.04
Phu Phan Sandstone	0	-	1.489 ± 0.10
	45	90	2.051 ± 0.04
	90	0	2.630 ± 0.12
	90	45	2.307 ± 0.05
	90	90	1.898 ± 0.03
	135	90	1.732 ± 0.08
Tak Fa Gypsum	0	-	1.899 ± 0.06
	45	90	1.931 ± 0.05
	90	0	2.501 ± 0.04
	90	45	2.243 ± 0.03
	90	90	1.889 ± 0.07
	135	90	1.706 ± 0.06

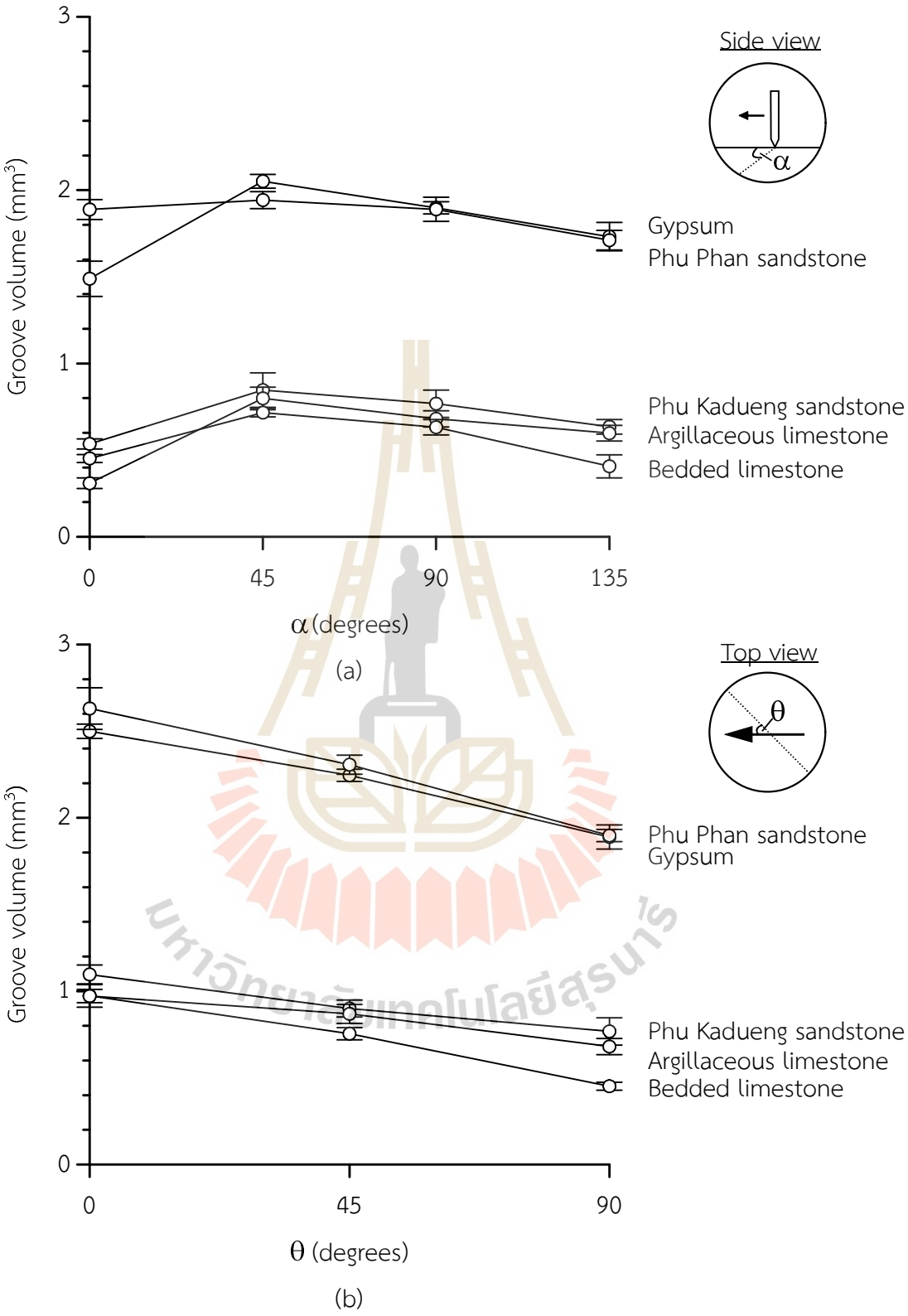

Figure 5.7 Mean groove volumes as a function of bedding plane orientations (a), and scratching directions (b).

CHAPTER VI

ANALYSIS OF TEST RESULTS

6.1 Introduction

This chapter analyzes the CERCHAR abrasivity index (CAI) results and its variations due to bedding plane orientations and scratching directions. The investigation focuses on the anisotropic nature of rock abrasiveness and its implications for rock cutting and excavation processes. The concept of work and energy associated with scratching forces and groove volumes is derived to assess the energy required by the steel stylus pin during the test.

6.2 CERCHAR abrasivity index

The specimens are tested under varying bedding plane orientations (α) and scratching directions (θ) to evaluate their effects on the CERCHAR abrasivity index (CAI). The results show that the CAI values show variations depending on α and θ. Figure 6.1 plots CAI as a function of α, showing different effects of bedding plane orientations for different rock types. For the well-defined bedding plane rocks (e.g. argillaceous limestone and sandstones), CAI shows the maximum value at α = 90°, where at α = 0° and 135° CAI's are highest. For the poorly defined bedding planes (bedded limestone and gypsum) CAI's slightly increases form α = 0° toward 135°. A polynomial equation is proposed to represent these relationships as:

$$CAI = l_1 \cdot \alpha^2 + l_2 \cdot \alpha + l_3 \quad (6.1)$$

where l_1, l_2 and l_3 are empirical constants. Good correlations are obtained (R^2>0.8). Table 6.1 gives their numerical values.

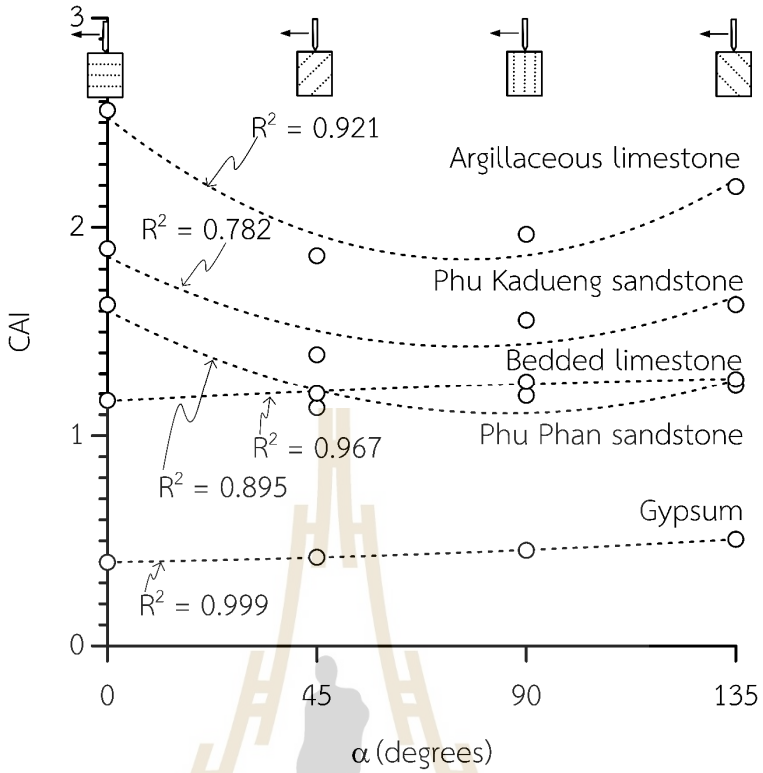

Figure 6.1 CERCHAR abrasivity index (CAI) vs functions of α, with polynomial equations.

Table 6.1 Numerical values from empirical constants l_1, l_2 and l_3 of equation 6.1.

Type	Polynomial regression equations	R^2
Khao Khad argillaceous limestone	$CAI = 1.1400 \cdot 10^{-4}\alpha^2 - 0.0176\alpha + 2.5257$	0.921
Khao Khad bedded limestone	$CAI = -2.8148 \cdot 10^{-6}\alpha^2 - 0.0012\alpha + 1.1651$	0.967
Phu Kadueng sandstone	$CAI = 7.1778 \cdot 10^{-5}\alpha^2 - 0.1111\alpha + 1.8599$	0.782
Phu Phan sandstone	$CAI = 6.7204 \cdot 10^{-5}\alpha^2 - 0.1154\alpha + 1.6020$	0.895
Tak Fa gypsum	$CAI = 3.5185 \cdot 10^{-6}\alpha^2 - 0.0033\alpha + 0.3984$	0.999

Figure 6.2 shows CAI as a function of angle θ. For all rock types, CAI slightly increases with θ where they can be represented by a linear equation:

$$CAI = m_1 \cdot \theta + \eta_1 \qquad (6.2)$$

where m_1 and η_1 are empirical constants. Good correlations are obtained ($R^2>0.9$). Their numerical values are given in Table 6.2.

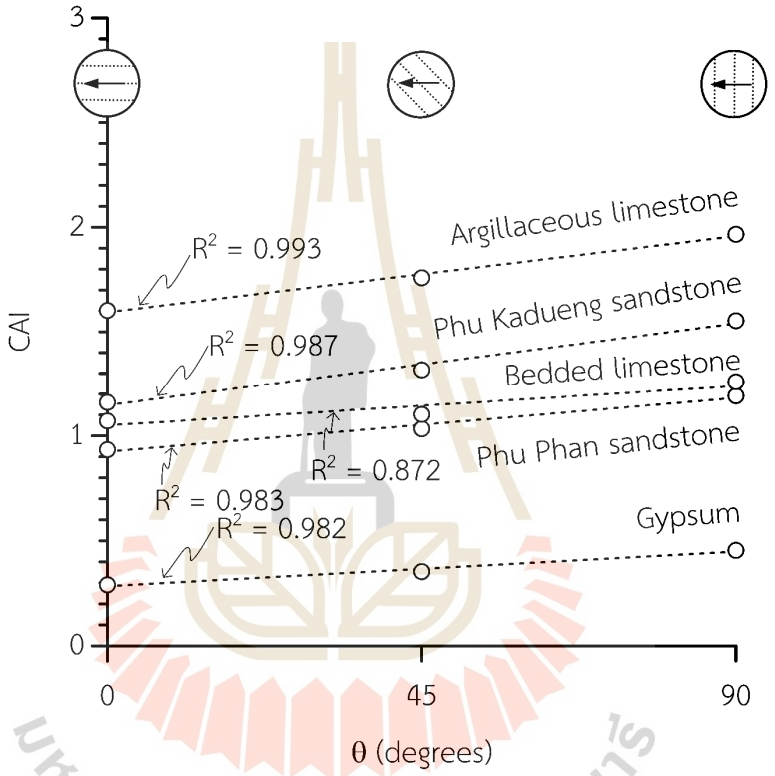

Figure 6.2 CERCHAR abrasivity index (CAI) as functions of θ, with linear equations.

Table 6.2 Numerical values from empirical constants m_1 and η_1 of equation 6.2.

Type	Linear regression equations	R^2
Khao Khad argillaceous limestone	CAI = 0.0040 · θ + 1.5931	0.972
Khao Khad bedded limestone	CAI = 0.0020 · θ + 1.0508	0.991
Phu Kadueng sandstone	CAI = 0.0043 · θ + 1.1473	0.994
Phu Phan sandstone	CAI = 0.0029 · θ + 0.9253	0.996
Tak Fa gypsum	CAI = 0.0018 · θ + 0.2842	0.991

6.3 Groove volume

The groove volume occurs during CERCHAR testing reflects the material removal characteristics as influenced by bedding plane orientations (α) and scratching directions (θ), Figures 6.3 plots groove volumes as functions of α, showing different effects of bedding plane orientations for different rock types. For all rock types, groove volume shows the maximum value at α about 90°, where at α = 0° and 135°, groove volume is smallest. The relationship can be described using a polynomial equation.

$$V = k_1 \cdot \alpha^2 + k_2 \cdot \alpha + k_3 \quad (6.3)$$

where k_1, k_2 and k_3 are empirical constants. Good correlations are obtained (R^2>0.8) and their numerical values are presented in Table 6.3.

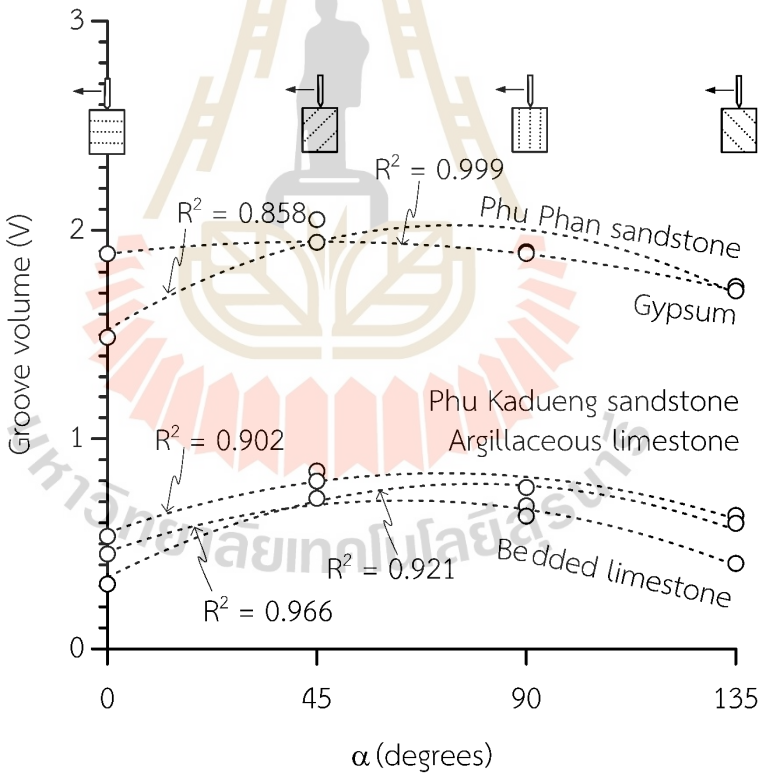

Figure 6.3 Groove volumes as functions of α, with polynomial equations.

Table 6.3 Numerical values from empirical constants k_1, k_2 and k_3 of equation 6.3.

Type rock	Polynomial regression equations	R^2
Khao Khad argillaceous limestone	$V = -7.0755 \cdot 10^{-5}\alpha^2 - 0.0112\alpha + 0.3407$	0.842
Khao Khad bedded limestone	$V = -6.0501 \cdot 10^{-5}\alpha^2 - 0.0077\alpha + 0.4624$	0.966
Phu Kadueng sandstone	$V = -5.4777 \cdot 10^{-5}\alpha^2 - 0.0079\alpha + 0.5524$	0.902
Phu Phan sandstone	$V = -8.9941 \cdot 10^{-5}\alpha^2 - 0.0134\alpha + 1.5238$	0.858
Tak Fa gypsum	$V = -2.8778 \cdot 10^{-5}\alpha^2 - 0.0026\alpha + 1.8872$	0.999

Figure 6.4 shows groove volume as a function of θ. The results show a slight increase in groove volume with θ for all rock types, which can be represented by a linear equation:

$$V = m_2 \cdot \theta + \eta_2 \qquad (6.4)$$

where m_2 and η_2 are empirical constants. Good correlations are obtained ($R^2>0.9$). Their numerical values are given in Table 6.4.

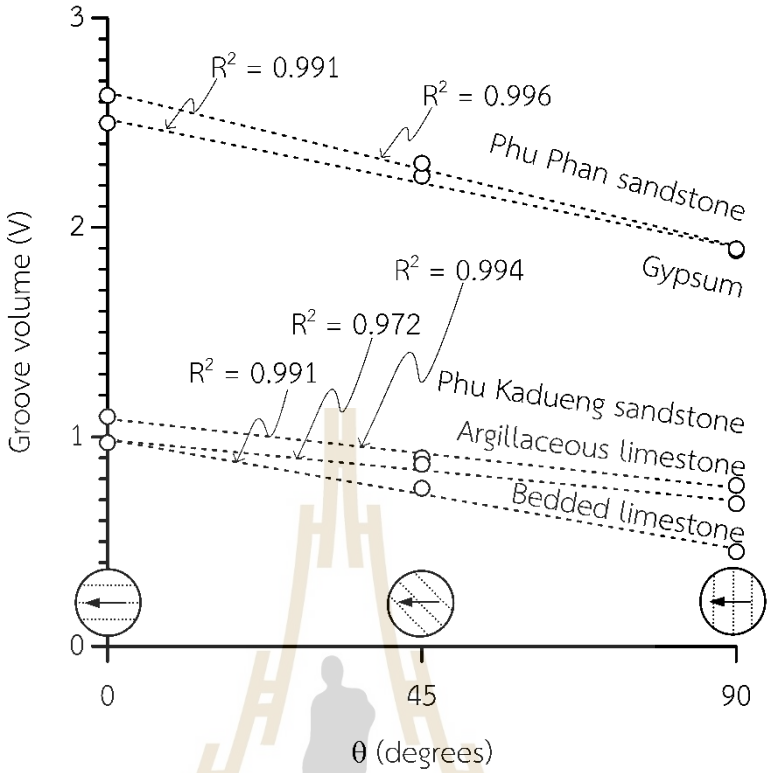

Figure 6.4 Groove volumes as functions of θ, with linear equations.

Table 6.4 Numerical values from empirical constants m_2 and η_2 of equation 6.4.

Type rock	Linear regression equations	R^2
Khao Khad argillaceous limestone	V = - 0.0032 · θ + 0.9863	0.972
Khao Khad bedded limestone	V = - 0.0058 · θ + 0.9872	0.991
Phu Kadueng sandstone	V = - 0.0029 · θ + 0.9253	0.994
Phu Phan sandstone	V = - 0.0081 · θ + 2.6446	0.996
Tak Fa gypsum	V = - 0.0068 · θ + 2.5159	0.991

6.4 Lateral force

The lateral force occurs during scratching provides insight into the resistance of different rock types under varying bedding plane orientations and scratching directions. Figure 6.5 and 6.6 plot lateral forces as a function of bedding plane orientations (α) and scratching directions (θ), showing different effects of bedding plane orientations for different rock types. In stronger rocks (e.g. Khao Khad argillaceous limestone), lateral force varies significantly with orientation. Softer rock (e.g. Tak Fa gypsum) shows relatively stable values across different orientations. The best-fit equations describing the force-distance F–d_s relationships for bedding plane orientations and scratching directions are presented in Equation (6.5) and summarized in Table 6.5. To describe the relationship between lateral force (F) and scratching distance (d_s) is described using an empirical model:

$$F = a \cdot (1 - \exp \cdot (- b \cdot d_s)) \quad (6.5)$$

where a and b are empirical constants specific to each rock type. Good correlations are obtained (R^2>0.9). The numerical values of the empirical constants are provided in Table 6.5.

The lateral force is influenced by both the scratching distance and bedding plane orientations and scathing directions, the empirical constants a and b are not fixed values but instead vary as functions of α or θ. This variation accounts for directional anisotropy in rock strength and abrasiveness, allowing a more comprehensive representation of force behavior.

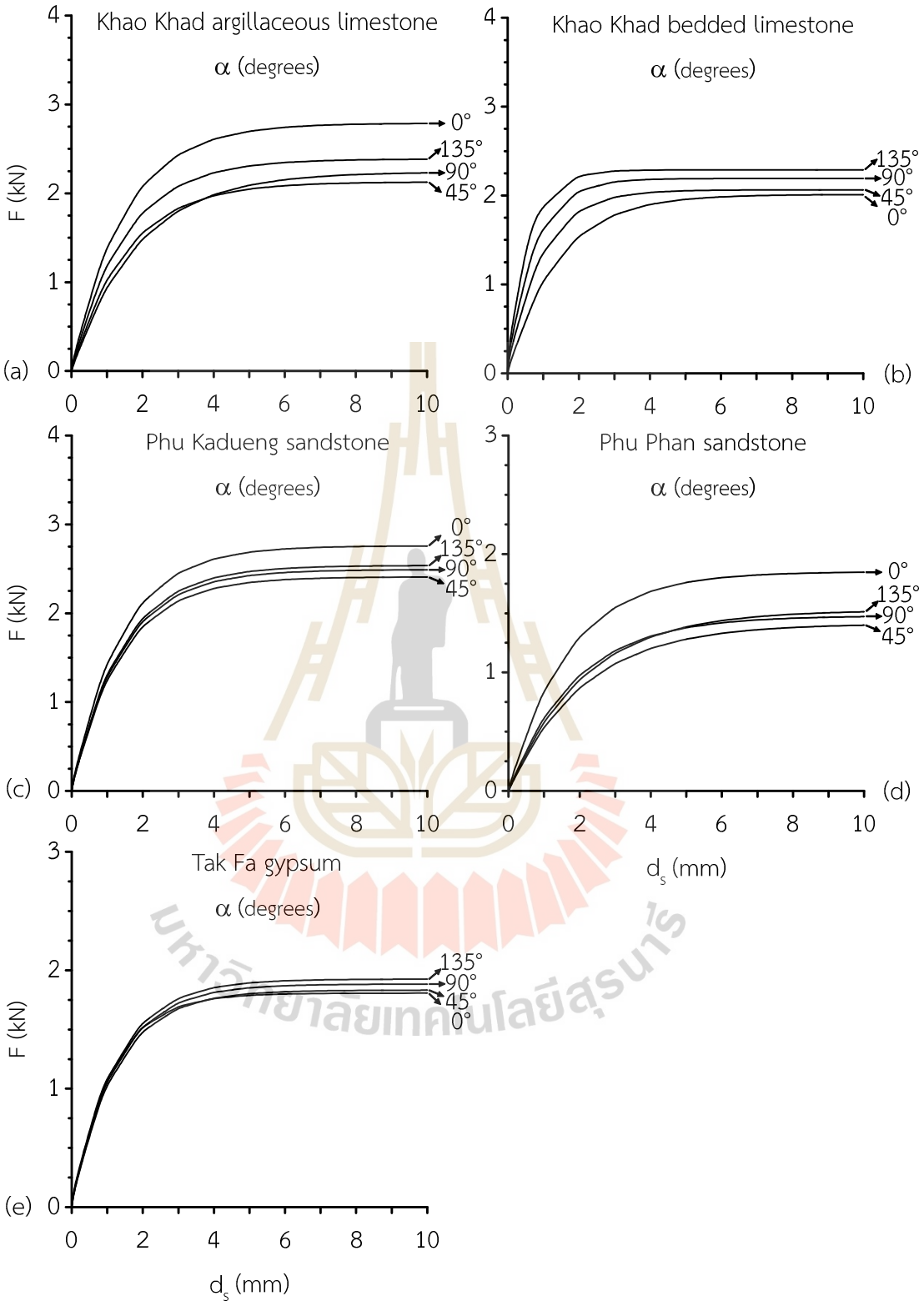

Figure 6.5 Lateral force as a function of bedding plane orientations (α).

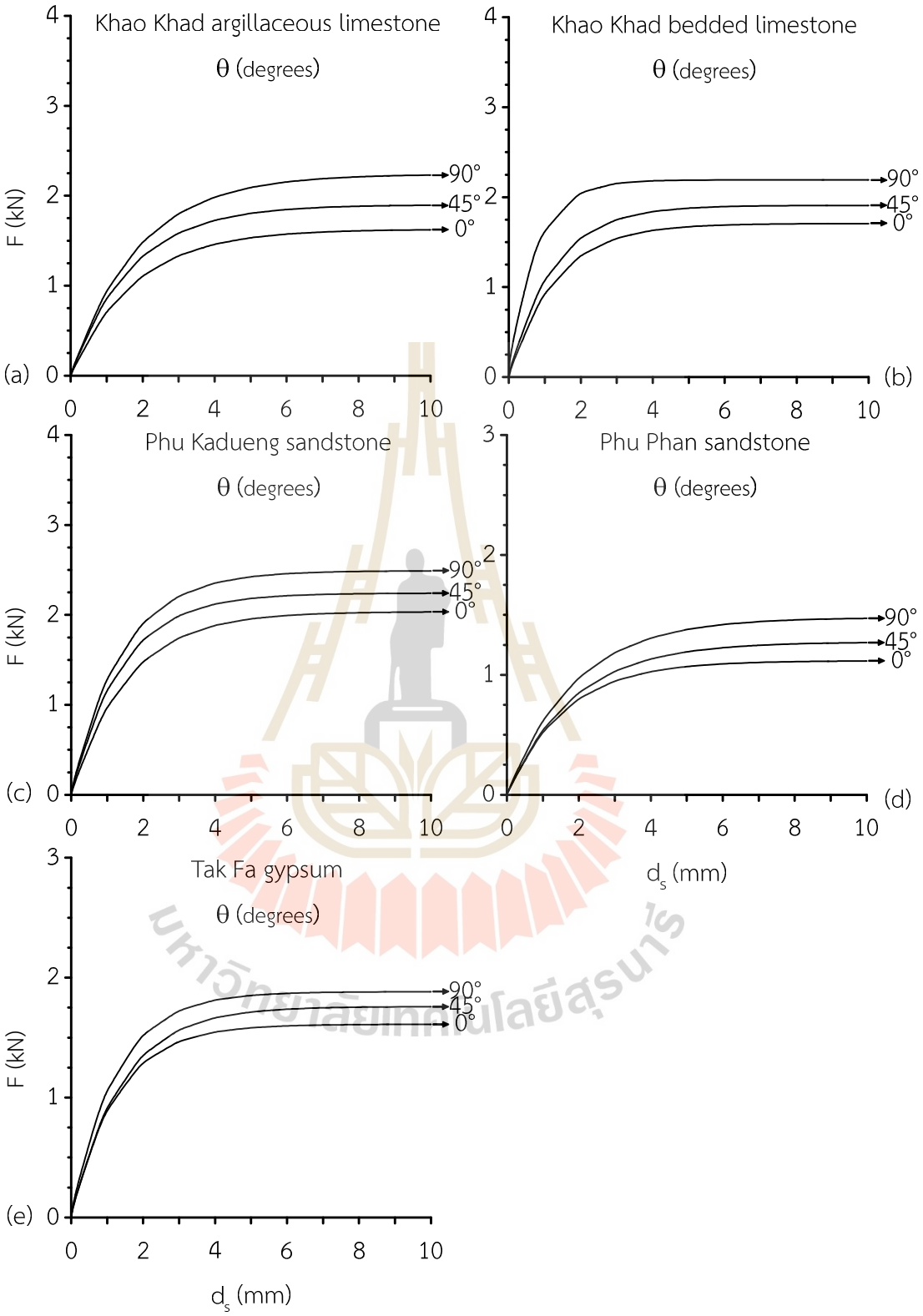

Figure 6.6 Lateral force as a function of scratching directions (θ).

Table 6.5 Empirical constants a and b for F-ds relation and R^2.

Rock type	α (degrees)	θ (degrees)	$F = a \cdot (1 - \exp \cdot (-b \cdot d_s))$		R^2
			a (N)	b (m^{-1})	
Khao Khad argillaceous limestone	0	-	2.789	0.682	0.986
	45	90	2.128	0.654	0.993
	90	0	1.627	0.568	0.950
	90	45	1.899	0.598	0.987
	90	90	2.240	0.541	0.989
	135	90	2.386	0.682	0.977
Khao Khad bedded limestone	0	-	2.012	0.719	0.979
	45	90	2.064	1.062	0.977
	90	0	1.707	0.777	0.990
	90	45	1.909	0.827	0.977
	90	90	2.192	1.339	0.970
	135	90	2.289	1.694	0.970
Phu Kadueng sandstone	0	-	2.759	0.728	0.995
	45	90	2.409	0.728	0.982
	90	0	2.036	0.646	0.989
	90	45	2.242	0.728	0.976
	90	90	2.491	0.724	0.993
	135	90	2.538	0.723	0.995
Phu Phan sandstone	0	-	1.850	0.603	0.978
	45	90	1.411	0.477	0.989
	90	0	1.118	0.626	0.974
	90	45	1.274	0.549	0.967
	90	90	1.478	0.538	0.963
	135	90	1.525	0.477	0.964
Tak Fa gypsum	0	-	1.807	0.912	0.995
	45	90	1.832	0.820	0.982
	90	0	1.611	0.802	0.960
	90	45	1.759	0.730	0.967
	90	90	1.883	0.819	0.983
	135	90	1.925	0.819	0.985

The best-fit equations describing the force-distance relationships while considering the effect of α or θ are presented in Equation (6.6 and 6.7) and summarized in Table 6.6. The force can be expressed as:

$$a\ (\alpha \text{ or } \theta) = m_3 \cdot (\alpha \text{ or } \theta) + \eta_3 \quad (6.6)$$

$$b\ (\alpha \text{ or } \theta) = m_4 \cdot (\alpha \text{ or } \theta) + \eta_4 \quad (6.7)$$

where m_3, η_3, m_4 and η_4 are empirical coefficients determined from experimental data for each rock type. The best-fit values of these parameters, obtained through regression analysis, are presented in Tables 6.6 and 6.7.

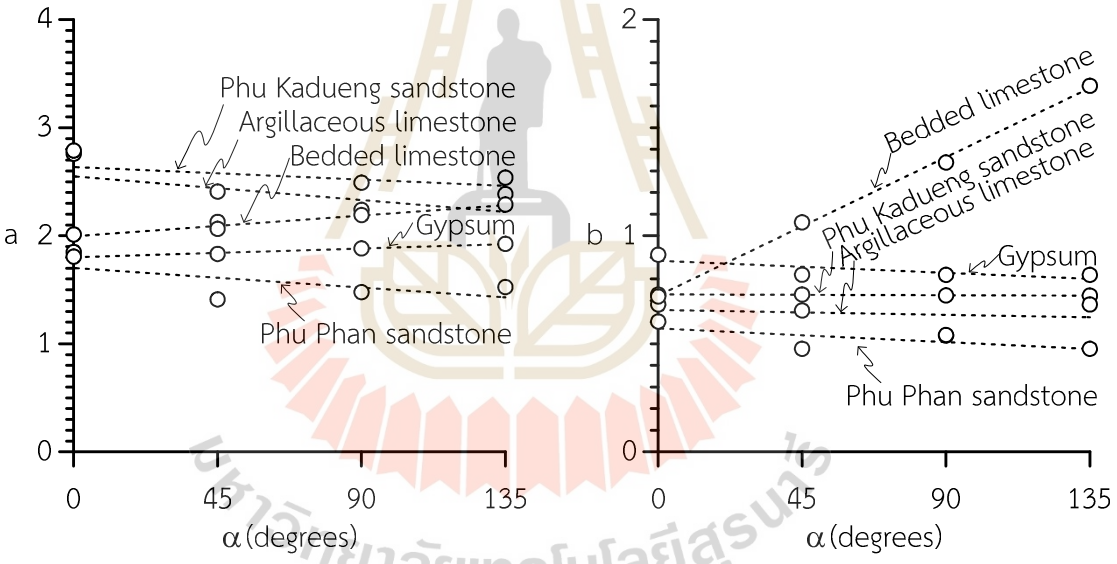

Figure 6.7 Empirical constants a (α) and b (α) for F-d_s with R^2 values by rock type.

Table 6.6 Empirical constants a (α) and b (α) for F-d_s relation and R^2.

Type rock	F = a (α) · (1 - exp · (- b (α) · d_s))	R^2
Khao Khad argillaceous limestone	a (α) = - 0.0024 · α + 2.5503	0.240
	b (α) = - 0.0002 · α + 0.6567	0.047
Khao Khad bedded limestone	a (α) = 0.0021 · α + 1.9954	0.977
	b (α) = 0.0071 · α + 0.7232	0.998
Phu Kadueng sandstone	a (α) = - 0.0013 · α + 2.6364	0.251
	b (α) = - 0.0001 · α + 0.7286	0.870
Phu Phan sandstone	a (α) = - 0.0020 · α + 1.7022	0.361
	b (α) = - 0.0007 · α + 0.5713	0.463
Tak Fa gypsum	a (α) = 0.0009 · α + 1.8010	0.984
	b (α) = - 0.0006 · α + 0.8845	0.689

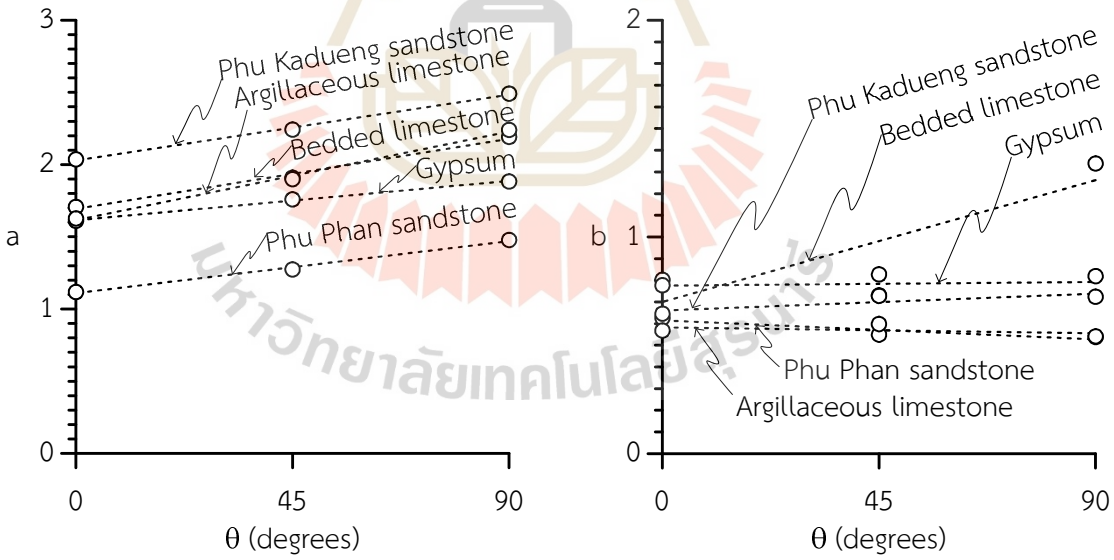

Figure 6.8 Empirical constants a (θ) and b (θ) for F-d_s with R^2 values by rock type.

Table 6.7 Empirical constants a (θ) and b (θ) for F-d_s relation and R^2.

Type rock	$F = a(\theta) \cdot (1 - \exp \cdot(-b(\theta) \cdot d_s))$	R^2
Khao Khad	$a(\theta) = 0.0068 \cdot \theta + 1.6150$	0.996
argillaceous limestone	$b(\theta) = -0.0003 \cdot \theta + 0.5825$	0.224
Khao Khad	$a(\theta) = 0.0054 \cdot \theta + 1.6935$	0.991
bedded limestone	$b(\theta) = 0.0062 \cdot \theta + 0.7000$	0.816
Phu Kadueng	$a(\theta) = 0.0051 \cdot \theta + 2.0288$	0.997
sandstone	$b(\theta) = 0.0009 \cdot \theta + 0.6603$	0.711
Phu Phan	$a(\theta) = 0.0040 \cdot \theta + 1.1100$	0.994
sandstone	$b(\theta) = -0.0009 \cdot \theta + 0.6150$	0.842
Tak Fa	$a(\theta) = 0.0030 \cdot \theta + 1.6150$	0.997
gypsum	$b(\theta) = 0.0002 \cdot \theta + 0.7752$	0.032

6.5 Work and energy

The work done (W) by the stylus during scratching is evaluated to quantify energy expenditure. Figures 6.9 and 6.10 present the work values for all tested rocks as functions of α and θ Among the tested rocks, limestones and Phu Kradueng sandstone require higher scratching energy, whereas Phu Phan sandstone and Tak Fa gypsum require low scratching energy. Table 6.8 The total work done is calculated by integrating force over the scratching path, expressed as:

$$W = \int_{d_s=0}^{10} F \cdot d_S \tag{6.8}$$

where W represents the work done by the stylus pin during the scratching.

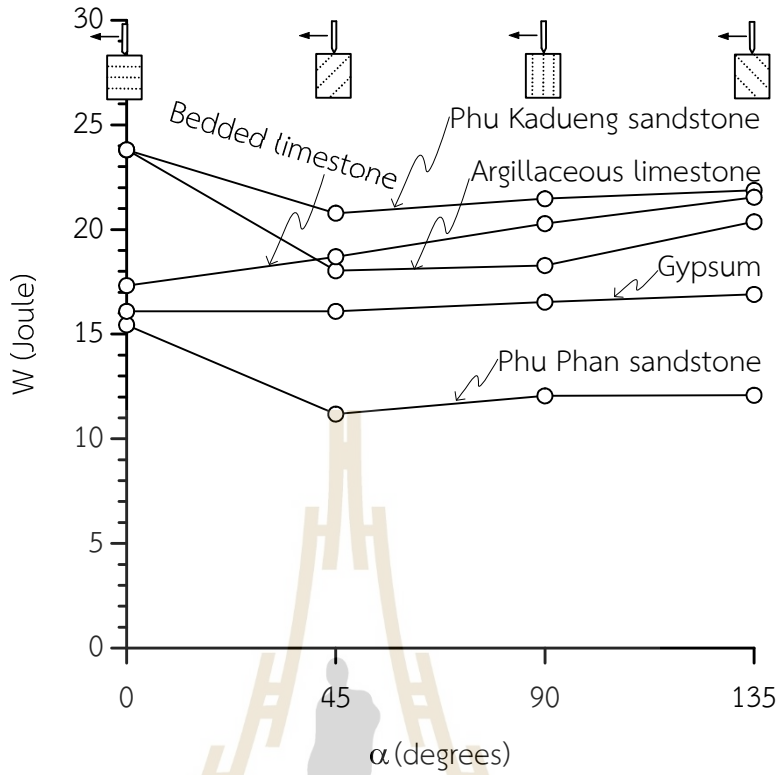

Figure 6.9 Work done as a function of bedding plane orientations (α).

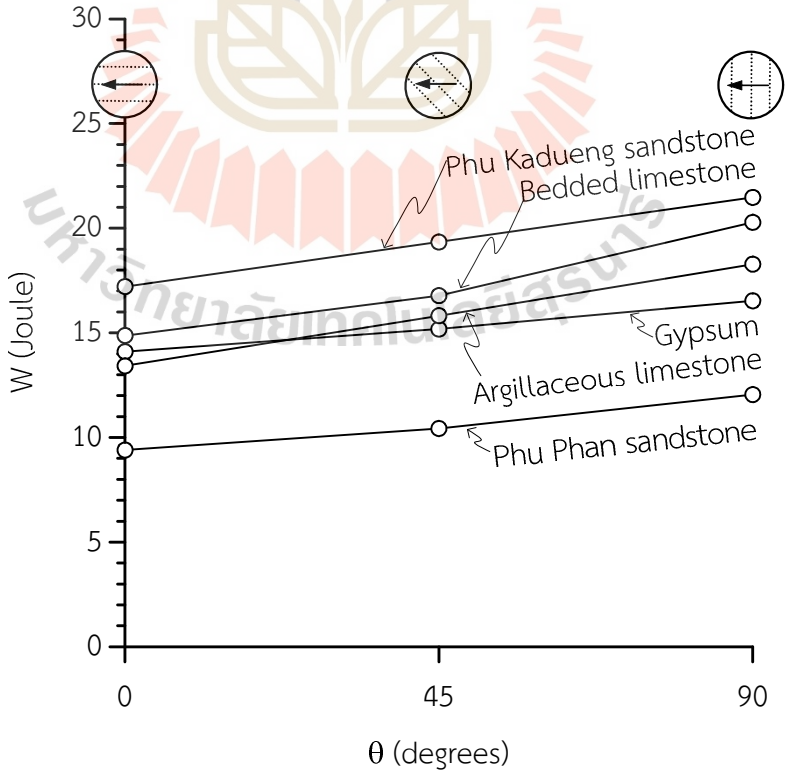

Figure 6.10 Work done as a function of scratching directions (θ).

Table 6.8 Work done for all rock tests.

Rock type	α (degrees)	θ (degrees)	W (J)
Khao Khad argillaceous limestone	0	-	23.81
	45	90	18.03
	90	0	13.42
	90	45	15.82
	90	90	18.28
	135	90	20.37
Khao Khad bedded limestone	0	-	17.32
	45	90	18.70
	90	0	14.87
	90	45	16.78
	90	90	20.28
	135	90	21.54
Phu Kadueng sandstone	0	-	23.80
	45	90	20.78
	90	0	17.21
	90	45	19.34
	90	90	21.47
	135	90	21.87
Phu Phan sandstone	0	-	15.44
	45	90	11.18
	90	0	9.40
	90	45	10.43
	90	90	12.05
	135	90	12.08
Tak Fa gypsum	0	-	16.09
	45	90	16.09
	90	0	14.10
	90	45	15.18
	90	90	16.53
	135	90	16.90

Figure 6.11 plots work energy as functions of α, showing different effects of bedding plane orientations of different rock types. For rocks with strong rocks (e.g. argillaceous limestone and sandstones), work values reach a maximum at α = 90°, where at α = 0° and 135°, work energy is lowest. For rocks with poorly defined bedding structures (e.g. bedded limestone and gypsum), work energy slightly increases from α = 0° to 135°. The relationship is represented by a polynomial equation.

$$W = e_1 \cdot \alpha^2 + e_2 \cdot \alpha + e_3 \quad (6.9)$$

where e_1, e_2 and e_3 are empirical constants. Good correlations are obtained (R^2>0.8) and their numerical values are presented in Table 6.9.

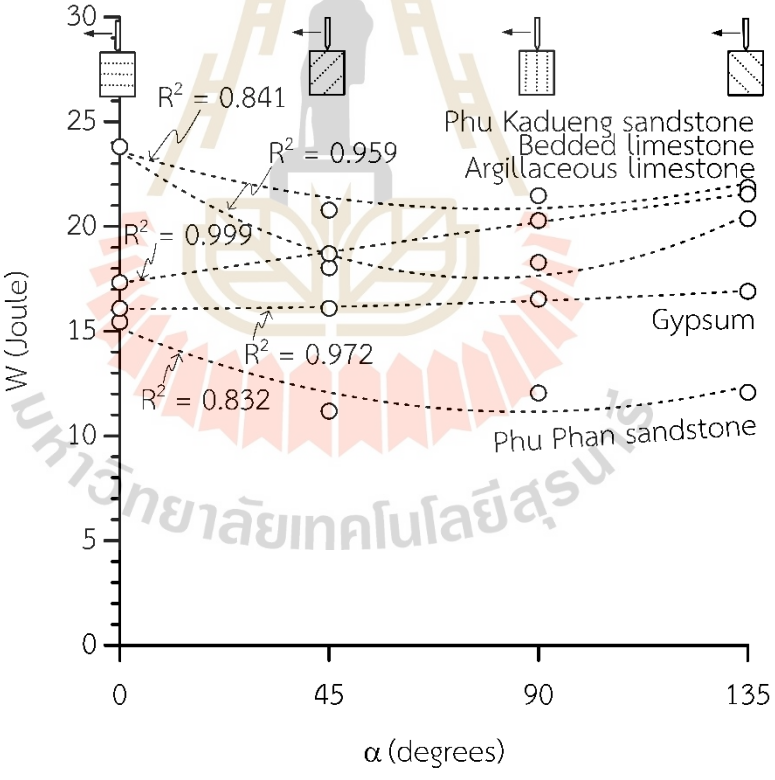

Figure 6.11 Work done as functions of α, with linear equations.

Table 6.9 Numerical values from empirical constants e1, e2 and e3 of equation 6.9.

Type rock	Polynomial regression equations	R^2
Khao Khad argillaceous limestone	$W = 9.7160 \cdot 10^{-4}\alpha^2 - 0.1535\alpha + 23.6005$	0.959
Khao Khad bedded limestone	$W = -1.4815 \cdot 10^{-5}\alpha^2 + 0.0336\alpha + 17.2940$	0.999
Phu Kadueng sandstone	$W = 4.2220 \cdot 10^{-4}\alpha^2 - 0.0683\alpha + 23.6000$	0.841
Phu Phan sandstone	$W = 5.2960 \cdot 10^{-4}\alpha^2 - 0.0920\alpha + 15.1415$	0.832
Tak Fa gypsum	$W = 4.5679 \cdot 10^{-5}\alpha^2 + 0.0002\alpha + 16.0645$	0.972

Figure 6.12 shows work values as a function of θ. The results indicate a slight increase in work with increasing θ across all rock types. which can be represented by a linear equation:

$$W = m_5 \cdot \theta + \eta_5 \qquad (6.10)$$

where m_5 and η_5 are empirical constants. Good correlations are obtained ($R^2>0.9$). Their numerical values are given in Table 6.10.

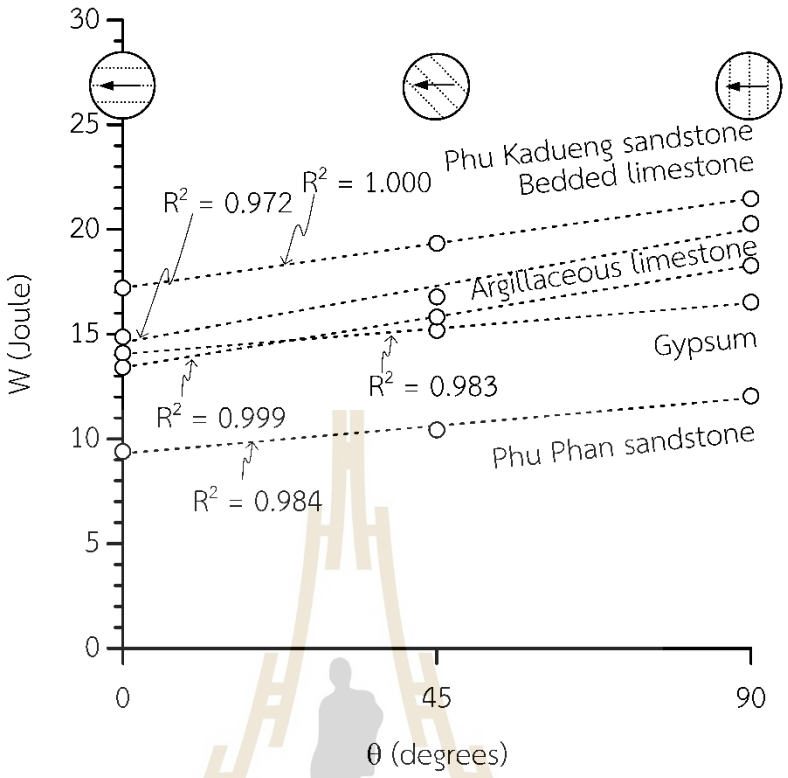

Figure 6.12 Work done as functions of θ, with linear equations.

Table 6.10 Numerical values from empirical constants m_5 and η_5 of equation 6.10.

Type rock	Linear regression equations	R^2
Khao Khad argillaceous limestone	$W = 0.0540 \cdot \theta + 13.4100$	0.999
Khao Khad bedded limestone	$W = 0.0601 \cdot \theta + 14.6050$	0.972
Phu Kadueng sandstone	$W = 0.0473 \cdot \theta + 17.2100$	1.000
Phu Phan sandstone	$W = 0.0294 \cdot \theta + 9.3017$	0.984
Tak Fa gypsum	$W = 0.0270 \cdot \theta + 14.0550$	0.996

6.6 CERCHAR Specific Energy

CERCHAR Specific Energy (CSE), a key parameter derived from the work done during scratching and the groove volume created. The effects of rock type, bedding plane orientation, and scratching direction are evaluated to provide insights into energy dynamics during rock scratching. Figure 6.13 shows CSE as a function of bedding planes and scratching directions, it is calculated by normalizing the work done by the groove volume (V), as expressed in Equation:

$$CSE = \frac{W}{V} = \frac{\int_{d_s=0}^{10} F \cdot d_s}{V} \tag{6.11}$$

where V represents the groove volume created during scratching. By integrating the lateral force over the scratching distance and incorporating the groove volume, CSE provides a quantitative measure of energy expenditure for rock scratching, offering insights into material behavior and tool-rock interactions.

The analysis of CERCHAR Specific Energy (CSE) values, as summarized in Table 6.11, reveals that specific energy of scratching on rock, bedding plane orientations (α) and scratching directions (θ) significantly influence energy expenditure during scratching. Stronger rocks (e.g. Khao Khad argillaceous limestone and Phu Kadueng sandstone), show higher CSE values due to higher lateral forces and smaller groove volumes, whereas softer rocks (e.g. Tak Fa gypsum and Phu Phan sandstone) show lower CSE values, reflecting lower energy consumption per unit material removed. Scratching perpendicular to the bedding plane (θ = 90°) consistently produces the highest CSE values across all rock types, as observed in Khao Khad argillaceous limestone and Phu Kadueng sandstone, owing to increased resistance, while parallel scratching (θ = 0°) results in the lowest CSE values, particularly in Phu Phan sandstone. Bedding plane orientation (α) further amplifies this trend, with CSE values increasing as the angle of the bedding plane changes from 45° to 135°. Groove volume inversely correlates with CSE and lateral force, indicating that energy efficiency improves with increased material removal.

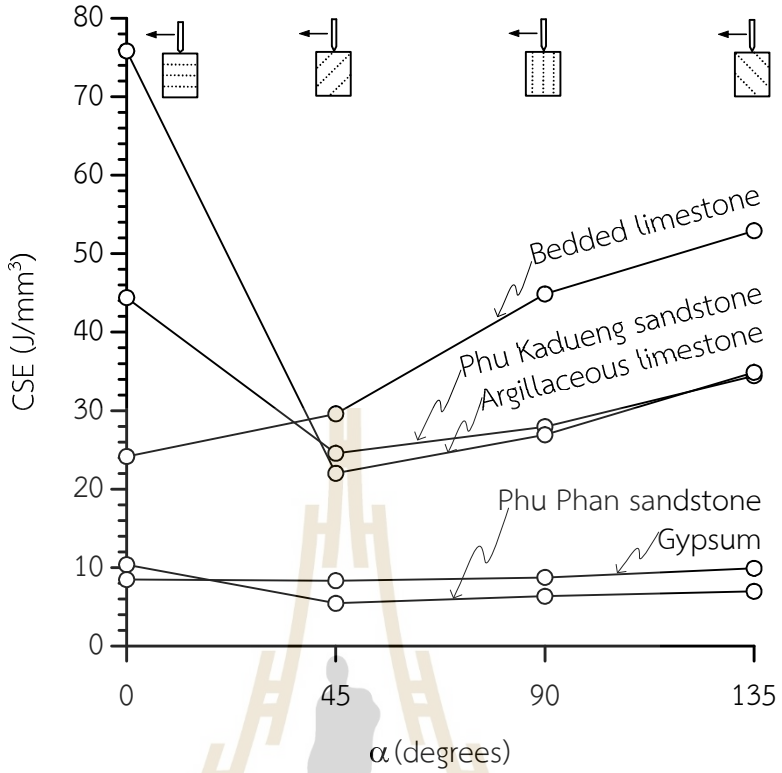

Figure 6.13 CSE as a function of bedding plane orientations (α).

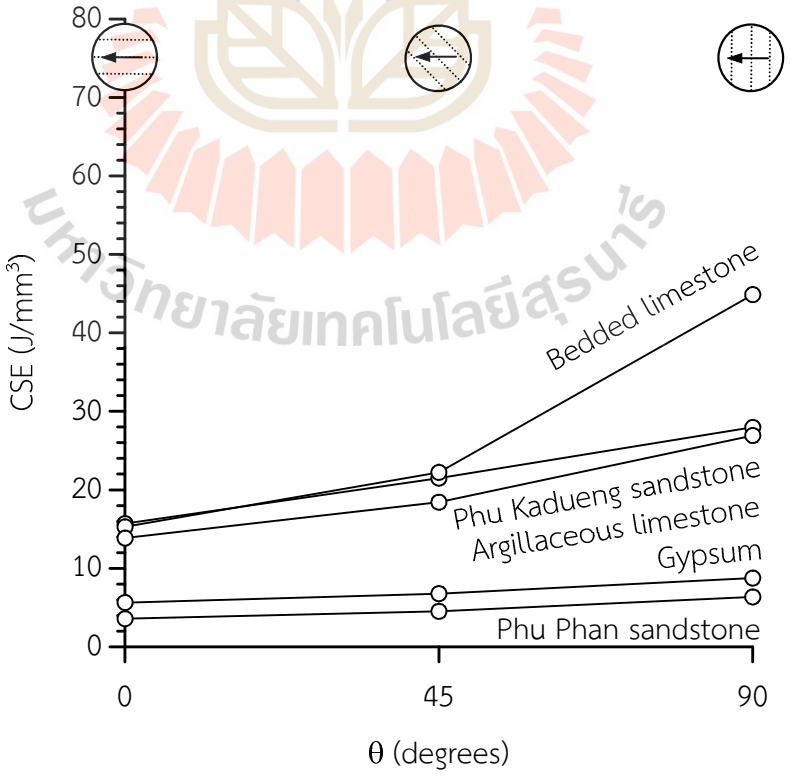

Figure 6.14 CSE as a function of scratching directions (θ).

Table 6.11 CERCHAR specific energy for all rock tests.

Rock type	α (degrees)	θ (degrees)	$F = a \cdot (1 - \exp \cdot (-b \cdot d_s))$		R^2
			a	b	
Khao Khad argillaceous limestone	0	-	2.789	0.682	0.986
	45	90	2.128	0.654	0.993
	90	0	1.627	0.568	0.950
	90	45	1.899	0.598	0.987
	90	90	2.240	0.541	0.989
	135	90	2.386	0.682	0.977
Khao Khad bedded limestone	0	-	2.012	0.719	0.979
	45	90	2.064	1.062	0.977
	90	0	1.707	0.777	0.990
	90	45	1.909	0.827	0.977
	90	90	2.192	1.339	0.970
	135	90	2.289	1.694	0.970
Phu Kadueng Sandstone	0	-	2.759	0.728	0.995
	45	90	2.409	0.728	0.982
	90	0	2.036	0.646	0.989
	90	45	2.242	0.728	0.976
	90	90	2.491	0.724	0.993
	135	90	2.538	0.723	0.995
Phu Phan Sandstone	0	-	1.850	0.603	0.978
	45	90	1.411	0.477	0.989
	90	0	1.118	0.626	0.974
	90	45	1.274	0.549	0.967
	90	90	1.478	0.538	0.963
	135	90	1.525	0.477	0.964
Tak Fa gypsum	0	-	1.807	0.912	0.995
	45	90	1.832	0.820	0.982
	90	0	1.611	0.802	0.960
	90	45	1.759	0.730	0.967
	90	90	1.883	0.819	0.983
	135	90	1.925	0.819	0.985

These relationships can be represented by a polynomial equation:

$$CSE = g_1 \cdot \alpha^2 + g_2 \cdot \alpha + g_3 \qquad (6.12)$$

where g1, g2, and g3 are empirical constants. Good correlations are obtained ($R^2 > 0.9$). Their numerical values are presented in Table 6.12.

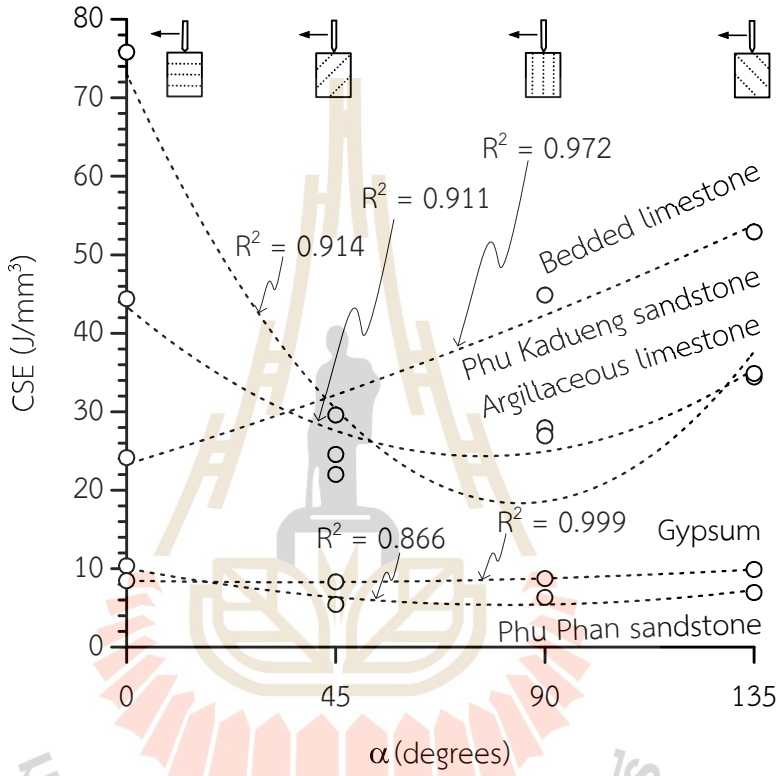

Figure 6.15 CSE as a function of bedding plane orientations (α), with polynomial equations.

Table 6.12 Numerical values from empirical constants g_1, g_2 and g_3 of equation 6.12.

Type rock	Polynomial regression equations	R^2
Khao Khad argillaceous limestone	$CSE = 0.0076\alpha^2 - 1.2916\alpha + 73.0445$	0.914
Khao Khad bedded limestone	$CSE = 0.0032\alpha^2 + 0.1820\alpha + 23.3028$	0.972
Phu Kadueng sandstone	$CSE = 0.0032\alpha^2 - 0.4976\alpha + 43.3959$	0.911
Phu Phan sandstone	$CSE = 0.0007\alpha^2 - 0.1130\alpha + 10.0650$	0.866
Tak Fa gypsum	$CSE = 0.0002\alpha^2 + 0.1111\alpha + 8.4818$	0.999

Figure 6.14 shows CSE as a function of θ. For all rock types, CSE generally increases with θ, where the relationship can be represented by a linear equation:

$$CSE = m_6 \cdot \theta + \eta_6 \quad (6.13)$$

where m_4 and η_4 are empirical constants. Good correlations are obtained (R^2>0.9). Their numerical values are provided in Table 6.13

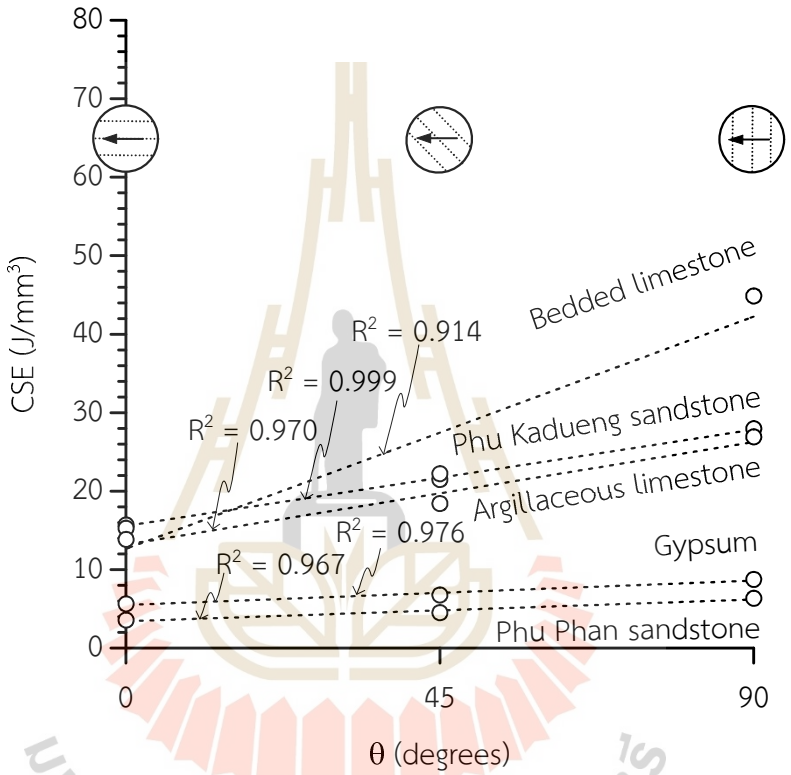

Figure 6.16 CSE as a function of scratching directions (θ), with linear equations.

Table 6.13 Numerical values from empirical constants m_6 and η_6 of equation 6.13.

Type rock	Linear regression equations	R^2
Khao Khad argillaceous limestone	CSE = 0.1452 · θ + 13.1930	0.970
Khao Khad bedded limestone	CSE = 0.3287 · θ + 12.6660	0.914
Phu Kadueng sandstone	CSE = 0.1363 · θ + 15.5772	0.999
Phu Phan sandstone	CSE = 0.0308 · θ + 3.4273	0.967
Tak Fa gypsum	CSE = 0.0346 · θ + 5.4956	0.976

CHAPTER VII

DISCUSSIONS, CONCLUSIONS AND RECOMMENDATIONS

This chapter presents a discussion on the consistency of experimental results obtained from CERCHAR abrasivity testing under varying bedding plane orientations and scratching directions. The influence of different rock types, anisotropic structures, and mechanical responses on the measured parameters, CERCHAR abrasivity index (CAI), ploughing force (F), groove volume (V), work energy (W), and CERCHAR Scratch Energy (CSE) is evaluated. Limitations of the study are also addressed. Conclusions are drawn based on the relationships identified among the test parameters and boundary conditions

7.1 Discussions

The correlations between the CERCHAR Abrasivity Index (CAI), ploughing force (F), groove volume (V), scratch width (W), and CERCHAR Scratch Energy (CSE) across all rock types and boundary conditions suggest that the testing procedure yields consistent and interpretable results. Strong rocks, such as the Khao Khad limestones, tend to produce higher CAI and F values but generate lower groove volumes as compared to softer rocks like Tak Fa gypsum. Work energy (W) shows a direct relationship with F, as it corresponds to the area under the force–distance curves.

The relationship between CSE and CAI, however, is not straightforward. For example, Phu Phan sandstone, which shows a medium CAI, shows a lower CSE than the softer Tak Fa gypsum. This result implies that the specific energy used in scratching (CSE) does not consistently correlate with the stylus tip. This inconsistency may arise from the fact that CSE is derived from energy consumption along the entire scratch path, not solely from the stylus tip response.

In terms of anisotropy, higher CAI values are observed when the scratching direction is opposite to the dip direction of the bedding plane orientation (α) Under this condition, the alternation of soft and hard layers along the scratch path amplifies stylus wear. Conversely, when the scratching direction follows the bedding dip, CAI and F values are reduced, while larger groove volumes are observed. These findings align with the influence of scratching direction (θ), where the highest CAI, F, and V values occur when the stylus moves perpendicular to the bedding trend ($\theta = 90°$).

For clastic rocks, scratching across bedding planes composed of layers with contrasting grain sizes produces greater stylus wear (higher CAI) than scratching along bedding planes composed of homogeneous layers. In crystalline rocks, variations in CAI depend on the hardness contrast among the crystallized layers. If these layers (e.g. calcite) have similar hardness, the bedding plane orientation has little effect on stylus tips.

Rocks with well-defined bedding planes tend to yield stronger correlations among CAI, ploughing force, and groove volume than those with poorly developed structures. However, due to the limited range of bedding thicknesses in the tested specimens (0.5–2 mm), its influence could not be fully assessed in this study. Furthermore, the correlation between CSE and the other parameters remains poor, primarily because CSE does not originate from direct measurement at the stylus tip.

7.2 Conclusions

Results from this study can be concluded as follows.

1) The scratching directions (θ) affect CAI and force than does bedding plane orientations (α).

2) Bedding plane orientation influences the CAI of strong rocks more severely than that of soft rocks.

3) Scratching across bedding planes generally results in higher CAI values than scratching along them.

4) CERCHAR scratch energy (CSE) does not inversely correlate with CAI and may be unreliable as a wear indicator, as it is derived from total energy consumption rather than stylus tip behavior.

5) These findings suggest that in practical applications, particularly in mechanical excavation using roadheaders or cutting tools for mineral extraction, aligning cutting direction parallel to bedding planes can reduce tool wear and improve equipment durability.

7.3 Recommendations for future studies

The suggestions for additional studies are as follows:

1) The range of bedding plane orientations and scratching directions should be expanded to provide more comprehensive coverage and identify critical angular relationships affecting stylus wear.

2) The influence of bedding plane thickness should be studied, which could not be adequately assessed in this study due to the limited range (0.5–2 mm) in the tested specimens.

3) Mineralogical properties that affect rock abrasiveness should be studied, with particular attention to mineral hardness, bonding strength, and distribution within the rock matrix.

4) Environmental factors such as water content, grain or crystal size, and temperature should be intraportal in the future study as they are commonly encountered in in-situ conditions and may influence abrasivity and tool wear.

REFERENCES

Al-Ameen, S. I., & Waller, M. D. (1994). The influence of rock strength and abrasive mineral content on the cerchar abrasive index. *Engineering Geology*, *36*(3), 293-301.

Al-Harthi, A. A. (1998). Effect of planar structures on the anisotropy of ranyah sandstone, saudi arabia. *Engineering Geology*, *50*(1), 49-57.

Alber, M., Yaralı, O., Dahl, F., Bruland, A., Käsling, H., Michalakopoulos, T. N., Cardu, M., Hagan, P., Aydın, H., & Özarslan, A. (2014). ISRM suggested method for determining the abrasivity of rock by the cerchar abrasivity test. *Rock Mechanics and Rock Engineering*, *47*(1), 261-266.

Atkinson, T., Cassapi, V. B., & Singh, R. N. (1986). Assessment of abrasive wear resistance potential in rock excavation machinery. *International Journal of Mining and Geological Engineering*, *4*(2), 151-163.

American Society for Testing and Materials. (2022). *Annual Book of ASTM Standards: Standard test method for laboratory determination of abrasiveness of rock using the cerchar method (vol. 04.09).* West Conshohocken, PA: ASTM International.

Aydın, H. (2019). Investigating the effects of various testing parameters on cerchar abrasivity index and its repeatability. *Wear*, *418-419*, 61-74.

Aydın, H., Yaralı, O., & Duru, H. (2016). The effects of specimen surface conditions and type of test apparatus on cerchar abrasivity index. *Karaelmas Fen ve Mühendislik Dergisi*, *6*(2), 293-298.

Chenevert, M. E., & Gatlin, C. (1965). Mechanical anisotropies of laminated sedimentary rocks. *Society of Petroleum Engineers Journal*, *5*(1), 67-77.

Comakli, R. & Aldalahali, A. M. J. (2024). Effect of water saturation on cerchar abrasivity index (cai) of clay-rich rocks at different scratch lengths. *Wear*, 538-539, 205187.

Er, S., & Tuğrul, A. (2016). Correlation of physico-mechanical properties of granitic rocks with cerchar abrasivity index in turkey. *Measurement*, *91*, 114-123.

Fuenkajorn, K., & Singkhiaw, P. (2022). Effect of transverse isotropy on mechanical properties of phu phan sandstone. *Proceedings of Academicsera international conference* (pp. 6-11). China.

Hamzaban, M. T., Karami, B., & Rostami, J. (2019). Effect of pin speed on cerchar abrasion test results. *Journal of Testing and Evaluation*, *47*(1), 121-139.

Hamzaban, M. T., Memarian, H., & Rostami, J. (2018). Determination of scratching energy index for CERCHAR abrasion test. *Journal of Mining and Environment*, *9*(1), 73-89.

Hamzaban, M. T., Rostami, J., Dahl, F., Macias, F. J., & Jakobsen, P. D. (2022). Wear of cutting tools in hard rock excavation process: A critical review of rock abrasiveness testing methods. *Rock Mechanics and Rock Engineering*, *56*, 1843-1882.

Horino, F. G., & Ellickson, M. L. (1970). *A method for estimating strength of rock containing planes of weakness* (Vol. 7449). US Department of Interior, Bureau of Mines.

Janc, B., Jovicic, V., & Vukelić, Ž. (2020). Laboratory test methods for assessing the abrasivity of rocks and soils in geotechnology and mining applications. *Materials and Geoenvironment*, *67*(3), 103-118.

Ji, Y., Wang, L., Zheng, Y., & Wu, W. (2021). Temperature-dependent abrasivity of bukit timah granite and implications for drill bit wear in thermo-mechanical drilling. *Acta Geotechnica*, *16*(3), 885-893.

Jin, Z., Li, W., Jin, C., Hambleton, J., & Cusatis, G. (2018). Anisotropic elastic, strength, and fracture properties of marcellus shale. *International Journal of Rock Mechanics and Mining Sciences*, *109*, 124-137.

Käsling, H. & Thuro, K. (2010). Determining rock abrasivity in the laboratory. In ISRM International Symposium - EUROCK 2010, *Lausanne*, 425-428.

Kathancharoen, N., & Fuenkajorn, K. (2023). Effects of mechanical and mineralogical properties on cerchar abrasivity index and specific energy of some thai rocks. *Engineering & Applied Science Research*, *50*(5), 478–489.

Ko, T. Y., Kim, T. K., Son, Y., & Jeon, S. (2016). Effect of geomechanical properties on cerchar abrasivity index (CAI) and its application to TBM tunnelling. *Tunnelling and Underground Space Technology*, *57*, 99-111.

Kotsombat, T., Thongprapha, T., & Fuenkajorn, K. (2020). Scratching rate effects on cerchar abrasiveness index of sandstones. *Proceedings of Academicsera International Conference* (pp. 6-9). Thailand.

Lassnig, K., Latal, C., & Klima, K. (2008). Impact of grain size on the cerchar abrasiveness test. *Geomechanics and Tunnelling*, *1*(1), 71-76.

Lee, S., Jeong, H., & Jeon, S. (2013). Assessment of TBM cutter wear using cerchar abrasiveness test. *Proceedings of world tunneling conference* (pp. 1209-1216). Switzerland.

Li, M., Zhou, F., Yuan, L., Chen, L., Hu, X., Huang, G., & Han, S. (2021). Numerical modeling of multiple fractures competition propagation in the heterogeneous layered formation. *Energy Reports*, *7*, 3737-3749.

Mucha, K. (2023). Application of rock abrasiveness and rock abrasivity test methods. *Sustainability*, *15*, 11243.

Plinninger, R., Käsling, H., Thuro, K., & Spaun, G. (2003). Testing conditions and geomechanical properties influencing the cerchar abrasiveness index (CAI) value. *International Journal of Rock Mechanics and Mining Sciences*, *40*(2), 259-263.

Ramamurthy, T. (1993). Strength and modulus responses of anisotropic rocks. *Comprehensive rock engineering*, *1*(13), 313-329.

Rostami, J., Ghasemi, A., Alavi Gharahbagh, E., Dogruoz, C., & Dahl, F. (2014). Study of dominant factors affecting cerchar abrasivity index. *Rock Mechanics and Rock Engineering*, *47*(5), 1905-1919.

Rossi, E., Saar, M. O., & Rudolf von Rohr, P. (2020). The influence of thermal treatment on rock–bit interaction: A study of a combined thermo–mechanical drilling (ctmd) concept. *Geothermal Energy*, *8*(1), 16.

Sanford, J. & Hagan, P. (2009). An assessment of the impact of stylus metallurgy on the cerchar abrasiveness index value. *Coal operators*, University of Wollongong, pp. 13.

Sukjaroen, N., Thongprapha, T., Liabkrathok, P., & Fuenkajorn, K. (2021). Effects of loading rate on transverse isotropic responses of bedded gypsum. *Arabian Journal of Geosciences*, *14*(22), 2442

Teymen, A. (2020). The usability of cerchar abrasivity index for the estimation of mechanical rock properties. *International Journal of Rock Mechanics and Mining Sciences*, *128*, 104258.

Torrijo, F. J., Garzón-Roca, J., Company, J., & Cobos, G. (2019). Estimation of cerchar abrasivity index of andesitic rocks in ecuador from chemical compounds and petrographical properties using regression analyses. *Bulletin of Engineering Geology and the Environment*, *78*(4), 2331-2344.

Wang, L., Guo, K., & Wu, W. (2023). Abrasivity measurement of brittle rock after thermal treatment. *Measurement*, *212*, 112710.

West, G. (1989). Rock abrasiveness testing for tunnelling. *International Journal of Rock Mechanics and Mining Sciences & Geomechanics Abstracts*, *26*(2), 151-160.

Yaralı, O., & Duru, H. (2016). Investigation into effect of scratch length and surface condition on cerchar abrasivity index. *Tunnelling and Underground Space Technology*, *60*, 111-120.

Yaralı, O., Yaşar, E., Bacak, G., & Ranjith, P. G. (2008). A study of rock abrasivity and tool wear in coal measures rocks. *International Journal of Coal Geology*, *74*(1), 53-66.

Zhang, G., Konietzky, H., Song, Z., & Zhang, M. (2020). Study of cerchar abrasive parameters and their relations to intrinsic properties of rocks for construction. *Construction and Building Materials*, *244*, 118327.

Zhang, G., Konietzky, H., & Frühwirt, T. (2020). Investigation of scratching specific energy in the cerchar abrasivity test and its application for evaluating rock-tool interaction and efficiency of rock cutting. *Wear*, 448-449, 203218.

Zhang, G., Konietzky, H., Song, Z., & Huang, S. (2020). Study of some testing condition-based factors affecting the cerchar abrasivity index (CAI). *Arabian Journal of Geosciences*, *13*(23), 1254.

Zhang, S.-R., She, L., Wang, C., Wang, Y.-J., Cao, R.-L., Li, Y.-L., & Cao, K.-L. (2021). Investigation on the relationship among the cerchar abrasivity index, drilling parameters and physical and mechanical properties of the rock. *Tunnelling and Underground Space Technology*, *112*, 103907

APPENDIX A

IMAGES OF CERCHAR STYLUS TIPS AND THEIR CORRESPONDING GROOVES

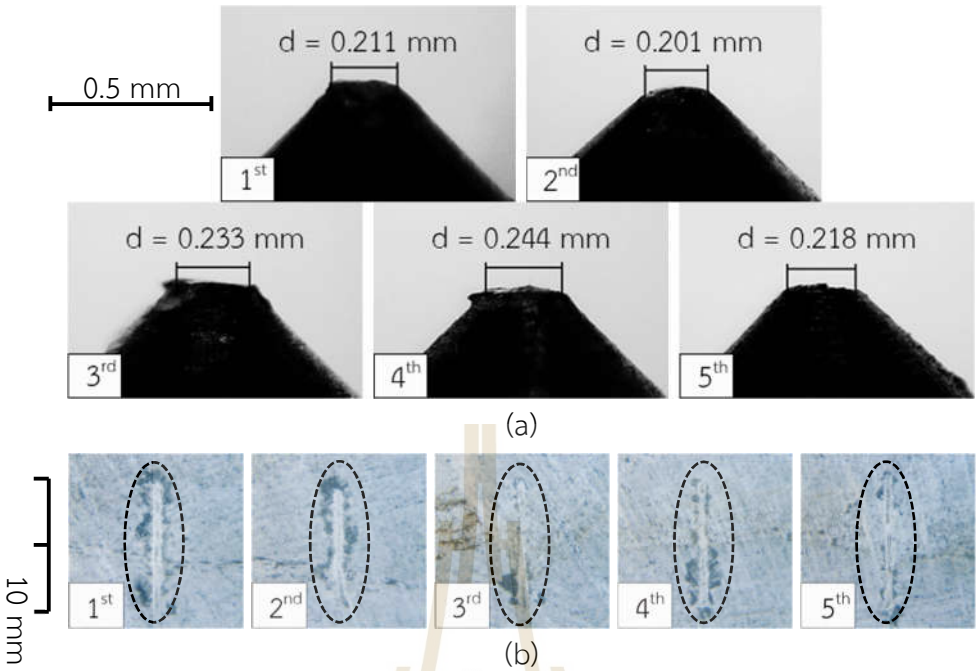

Figure A.1 Close-up images of stylus tip after scratching on Khao Khad argillaceous limestone with α = 0° (a) and their corresponding groove images (b).

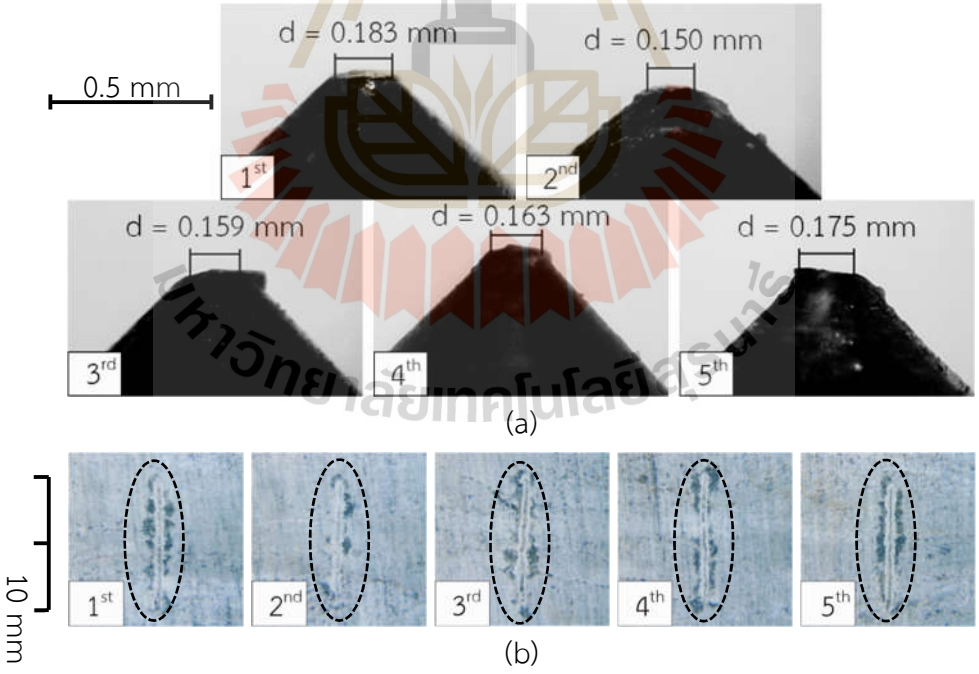

Figure A.2 Close-up images of stylus tip after scratching on Khao Khad argillaceous limestone with α = 45°, θ = 90° (a) and their corresponding groove images (b).

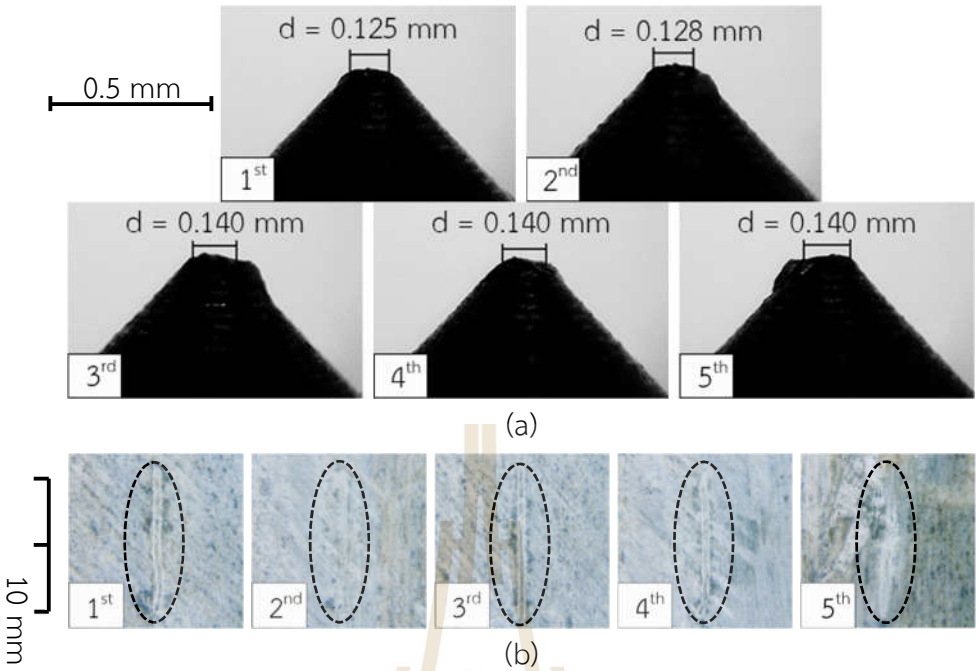

Figure A.3 Close-up images of stylus tip after scratching on Khao Khad argillaceous limestone with α = 90°, θ = 0° (a) and their corresponding groove images (b).

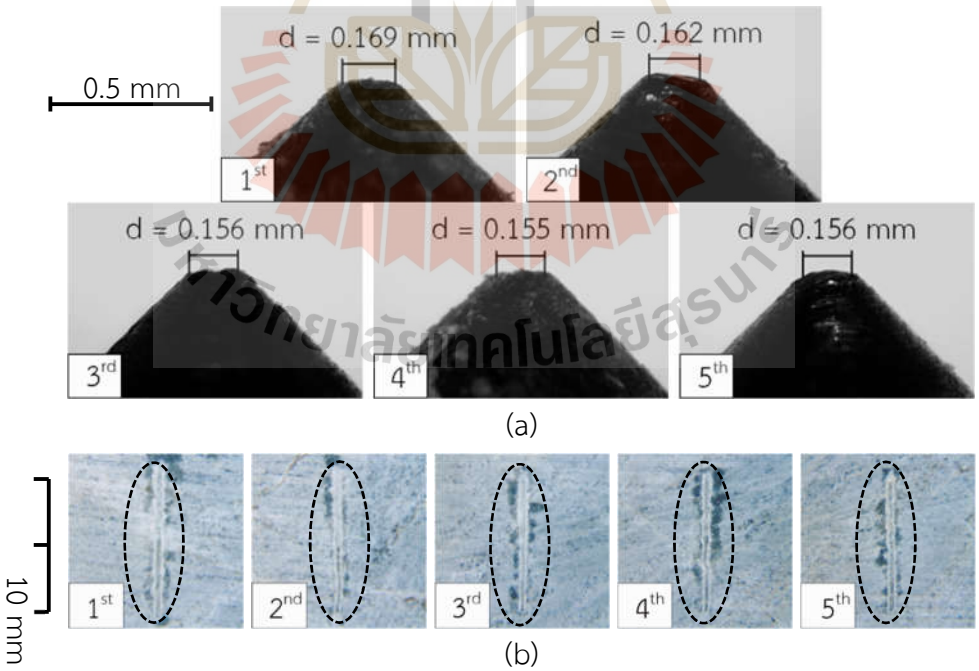

Figure A.4 Close-up images of stylus tip after scratching on Khao Khad argillaceous limestone with α = 90°, θ = 45° (a) and their corresponding groove images (b).

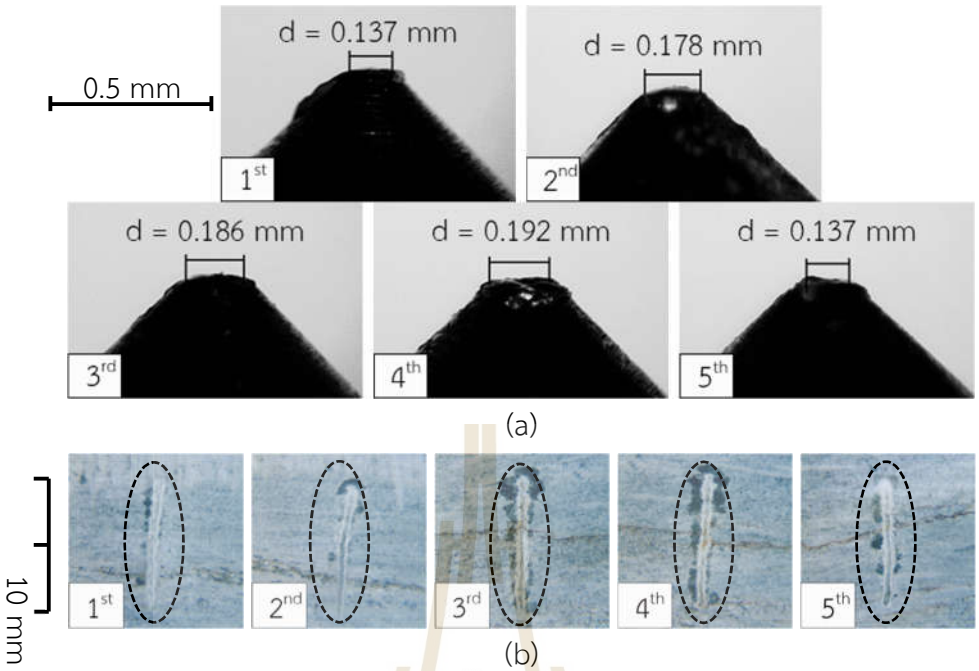

Figure A.5 Close-up images of stylus tip after scratching on Khao Khad argillaceous limestone with α = 90°, θ = 90° (a) and their corresponding groove images (b).

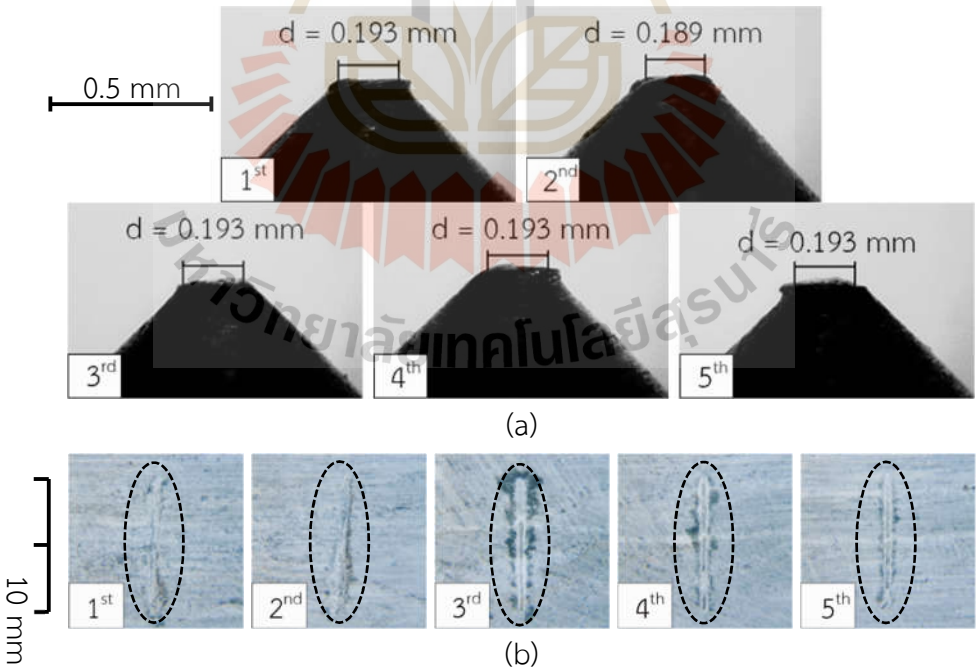

Figure A.6 Close-up images of stylus tip after scratching on Khao Khad argillaceous limestone with α = 135°, θ = 90° (a) and their corresponding groove images (b).

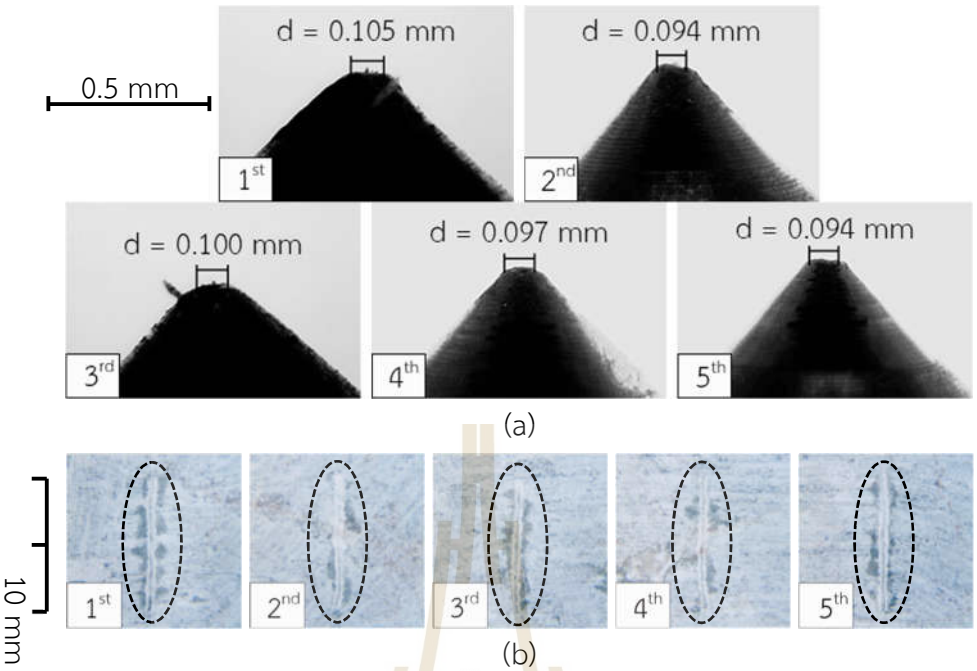

Figure A.7 Close-up images of stylus tip after scratching on Khao Khad bedded limestone with α = 0° (a) and their corresponding groove images (b).

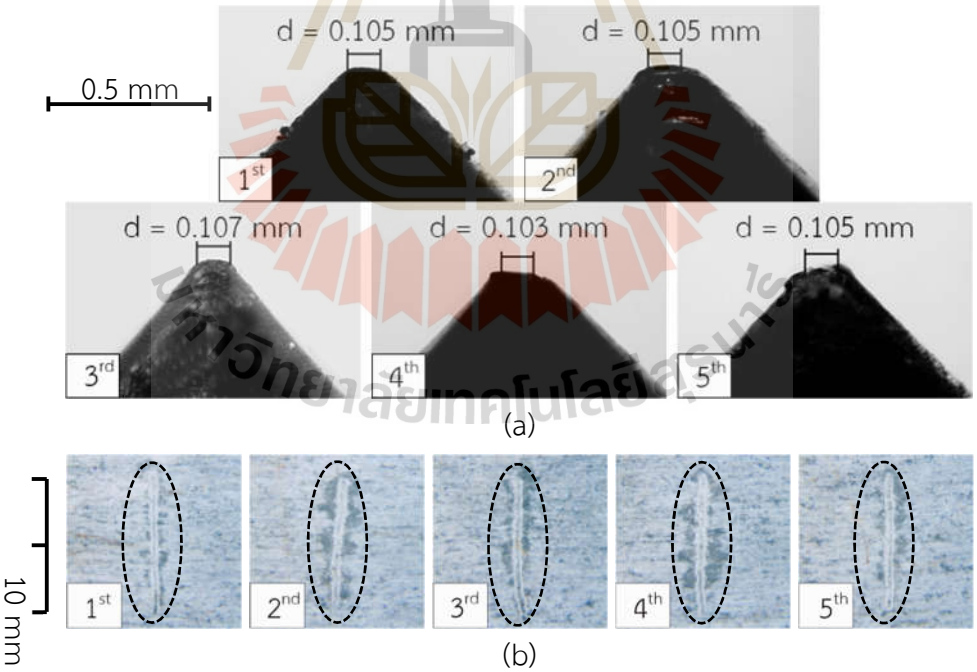

Figure A.8 Close-up images of stylus tip after scratching on Khao Khad bedded limestone with α = 45°, θ = 90° (a) and their corresponding groove images (b).

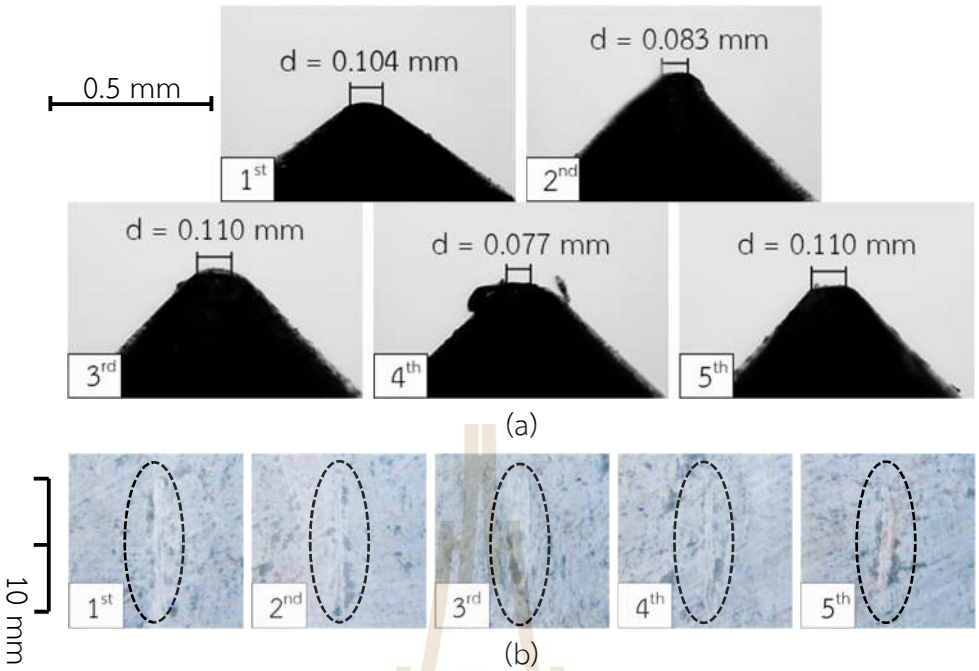

Figure A.9 Close-up images of stylus tip after scratching on Khao Khad bedded limestone with α = 90°, θ = 0° (a) and their corresponding groove images (b).

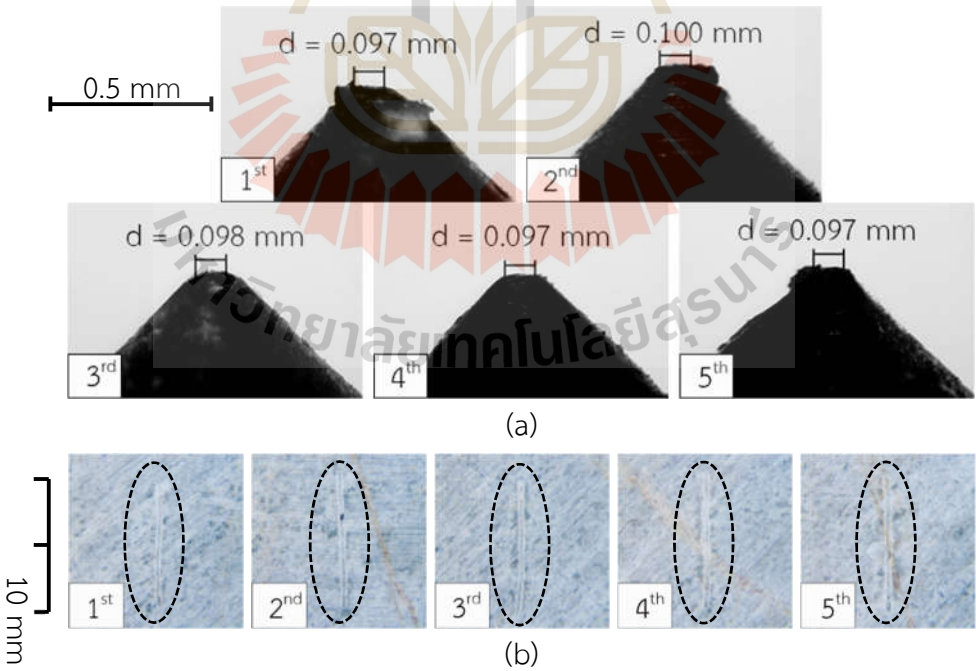

Figure A.10 Close-up images of stylus tip after scratching on Khao Khad bedded limestone with α = 90°, θ = 45° (a) and their corresponding groove images (b).

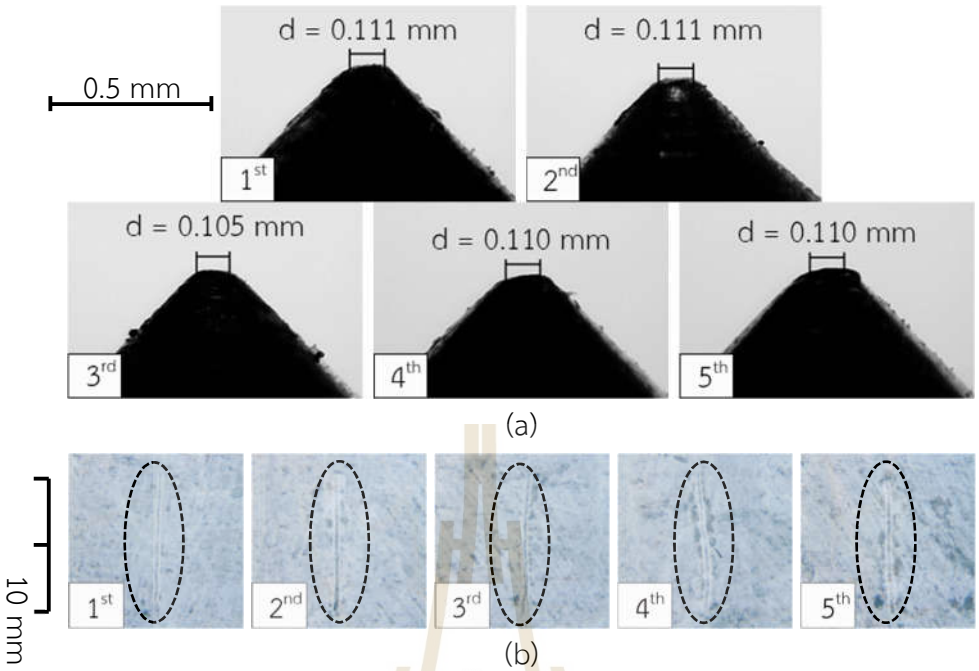

Figure A.11 Close-up images of stylus tip after scratching on Khao Khad bedded limestone with α = 90°, θ = 90° (a) and their corresponding groove images (b).

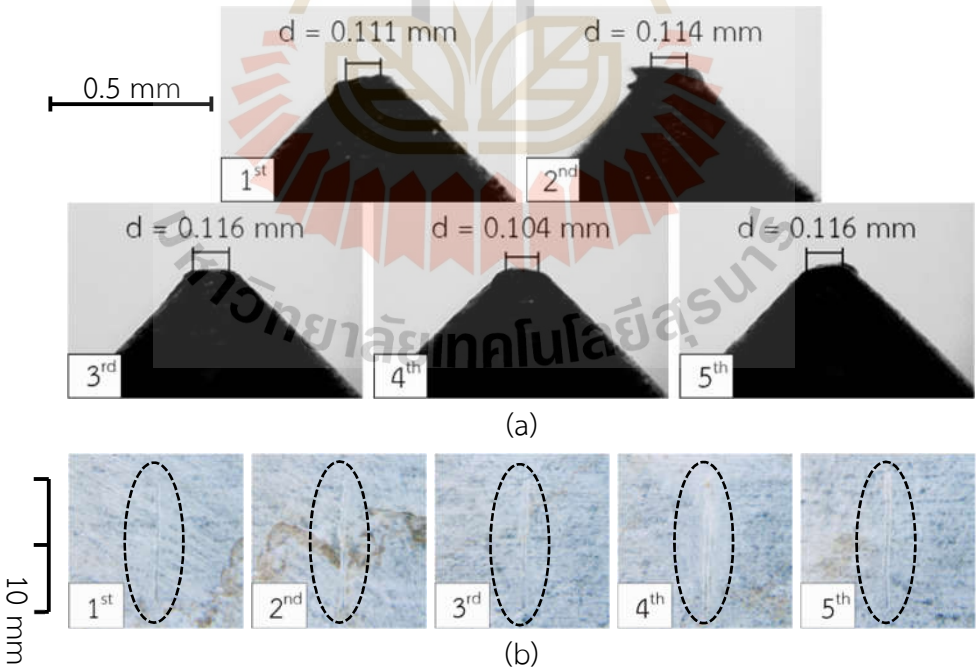

Figure A.12 Close-up images of stylus tip after scratching on Khao Khad bedded limestone with α = 135°, θ = 90° (a) and their corresponding groove images (b).

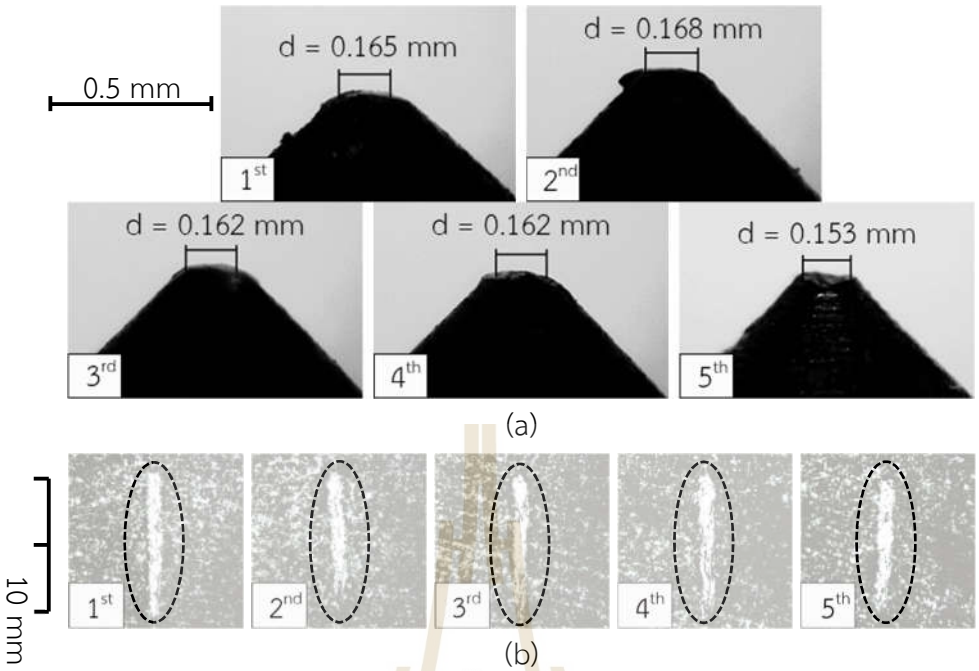

Figure A.13 Close-up images of stylus tip after scratching on Phu Kadueng sandstone with α = 0° (a) and their corresponding groove images (b).

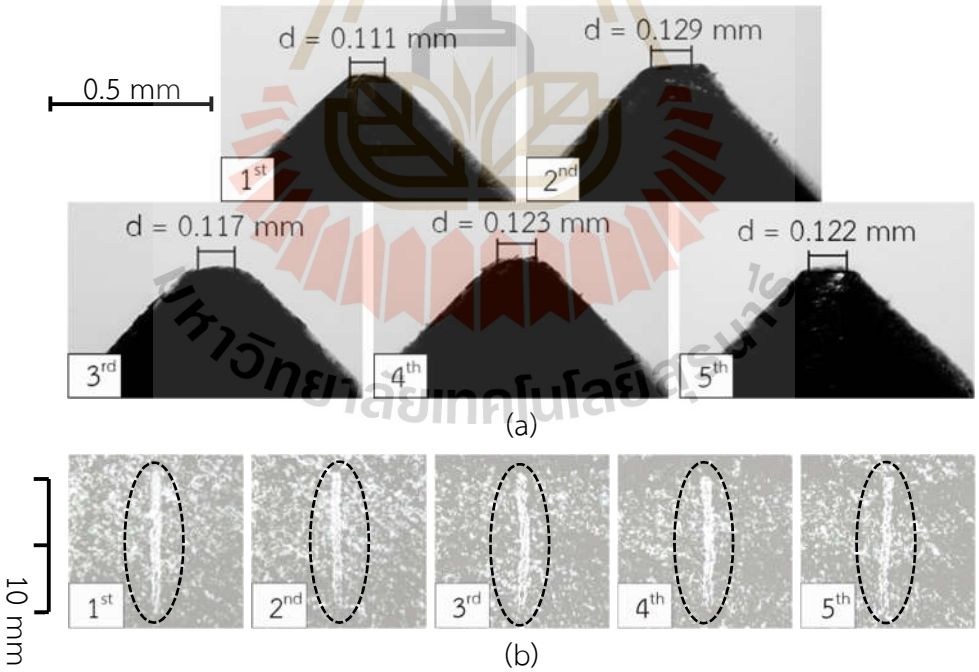

Figure A.14 Close-up images of stylus tip after scratching on Phu Kadueng sandstone with α = 45°, θ = 90° (a) and their corresponding groove images (b).

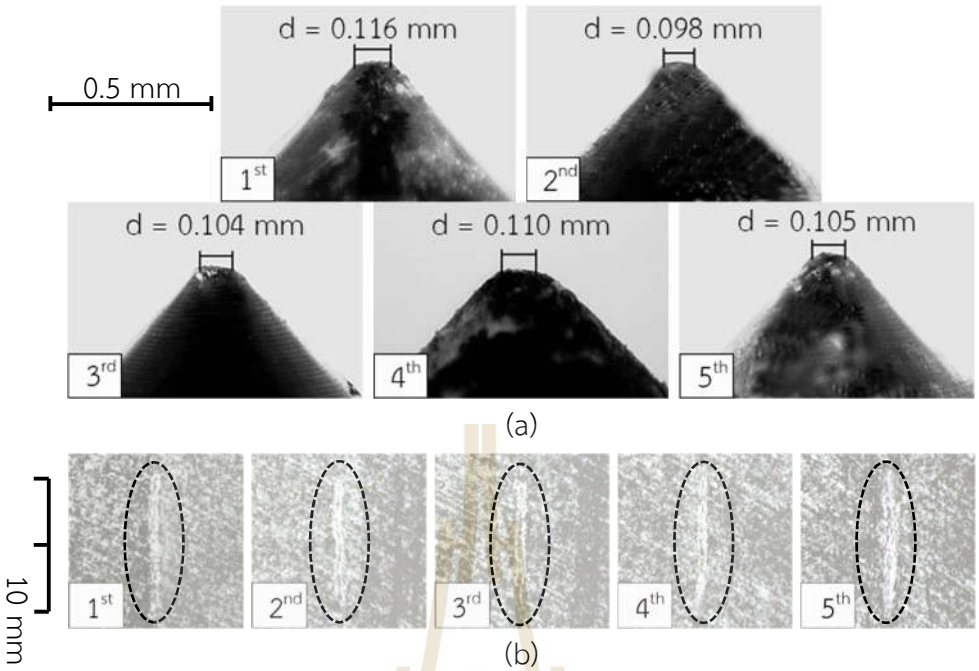

Figure A.15 Close-up images of stylus tip after scratching on Phu Kadueng sandstone with α = 90°, θ = 0° (a) and their corresponding groove images (b).

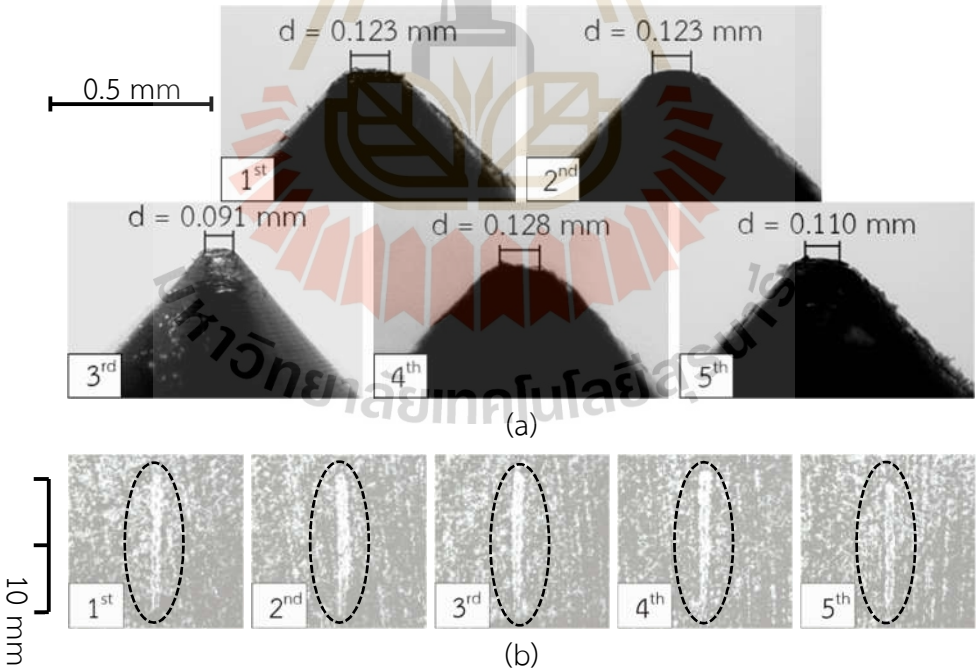

Figure A.16 Close-up images of stylus tip after scratching on Phu Kadueng sandstone with α = 90°, θ = 45° (a) and their corresponding groove images (b).

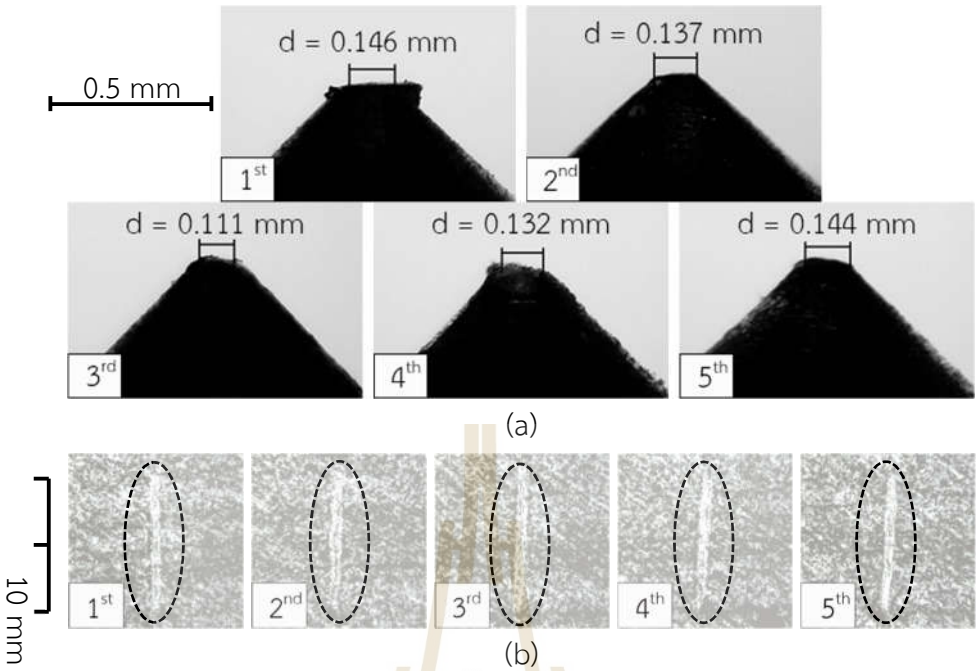

Figure A.17 Close-up images of stylus tip after scratching on Phu Kadueng sandstone with α = 90°, θ = 90° (a) and their corresponding groove images (b).

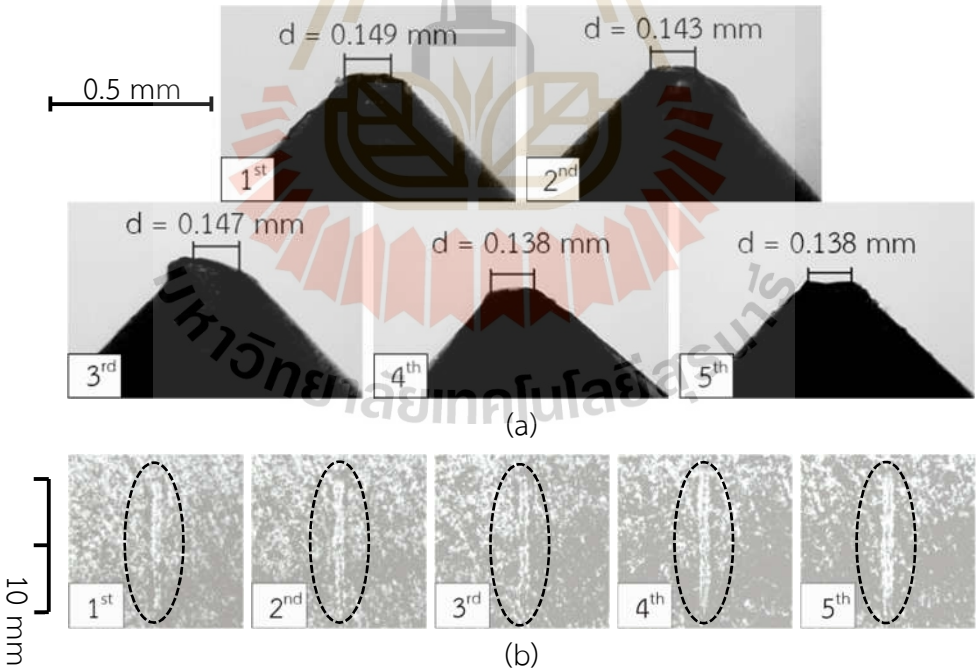

Figure A.18 Close-up images of stylus tip after scratching on Phu Kadueng sandstone with α = 135°, θ = 90° (a) and their corresponding groove images (b).

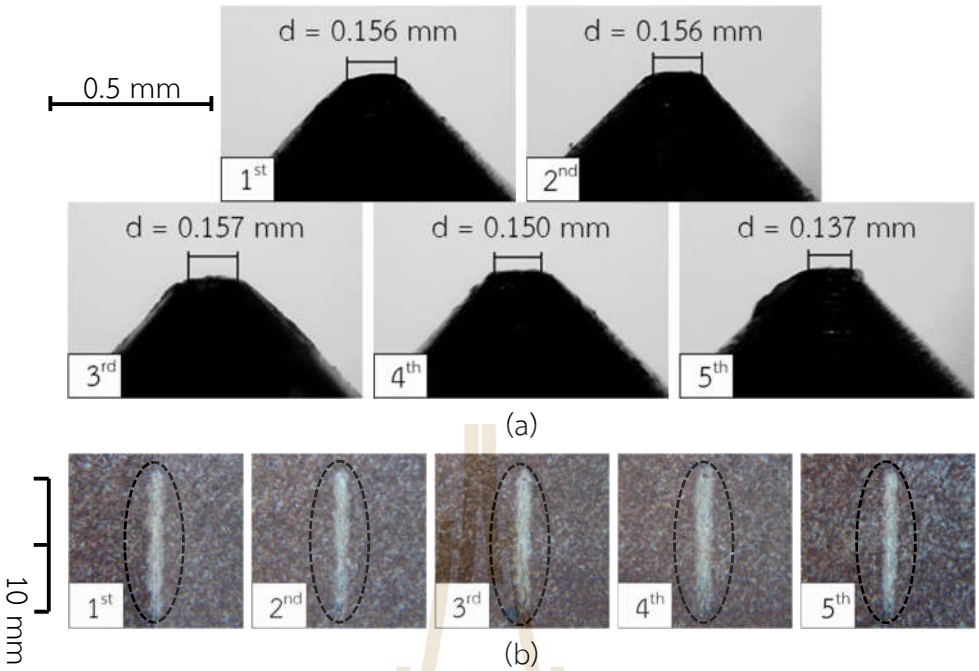

Figure A.19 Close-up images of stylus tip after scratching on Phu Phan sandstone with α = 0° (a) and their corresponding groove images (b).

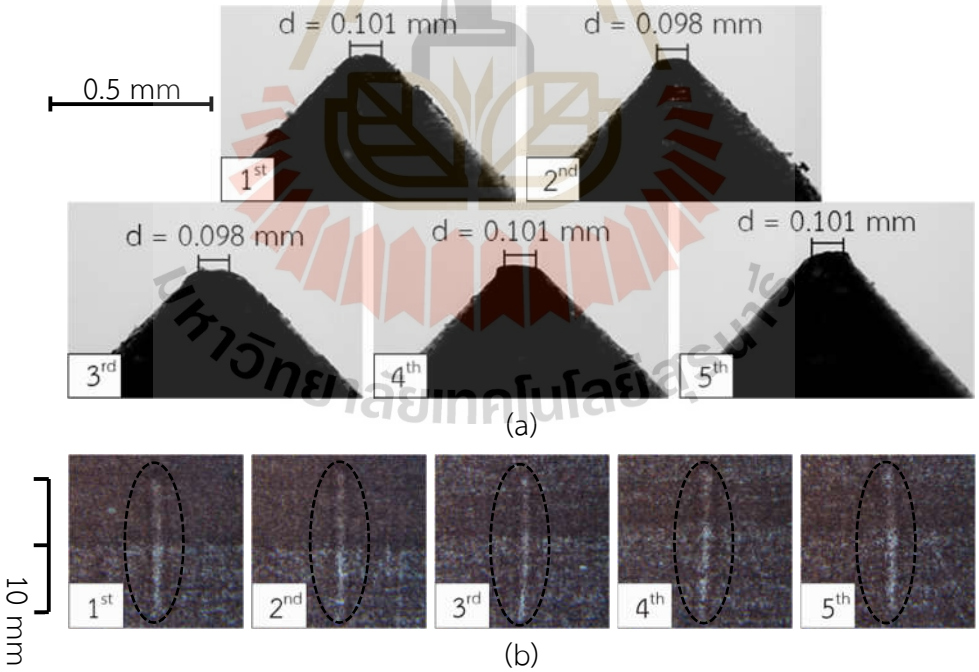

Figure A.20 Close-up images of stylus tip after scratching on Phu Phan sandstone with α = 45°, θ = 90° (a) and their corresponding groove images (b).

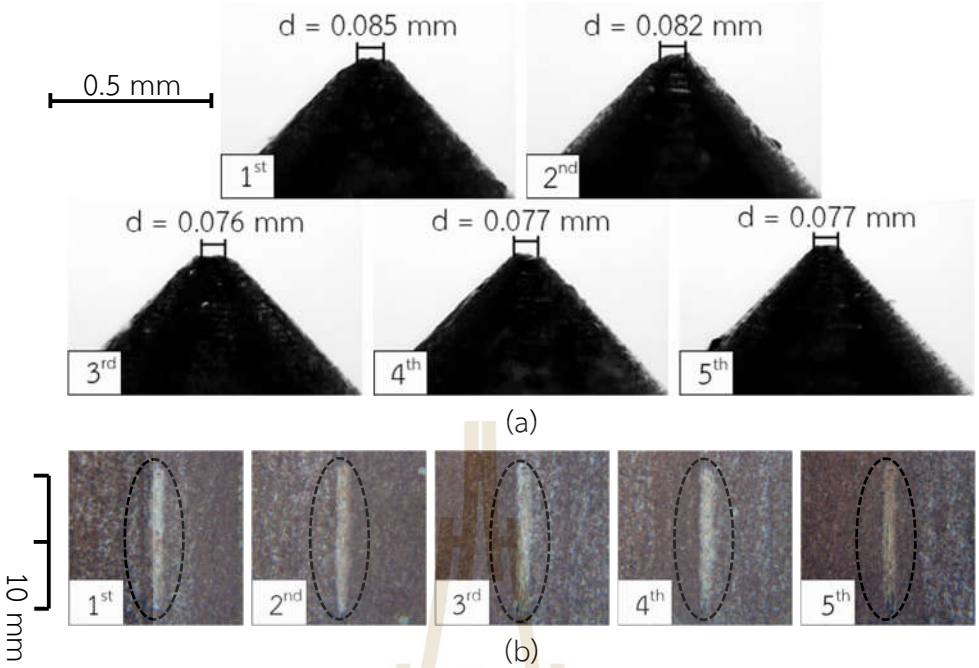

Figure A.21 Close-up images of stylus tip after scratching on Phu Phan sandstone with α = 90°, θ = 0° (a) and their corresponding groove images (b).

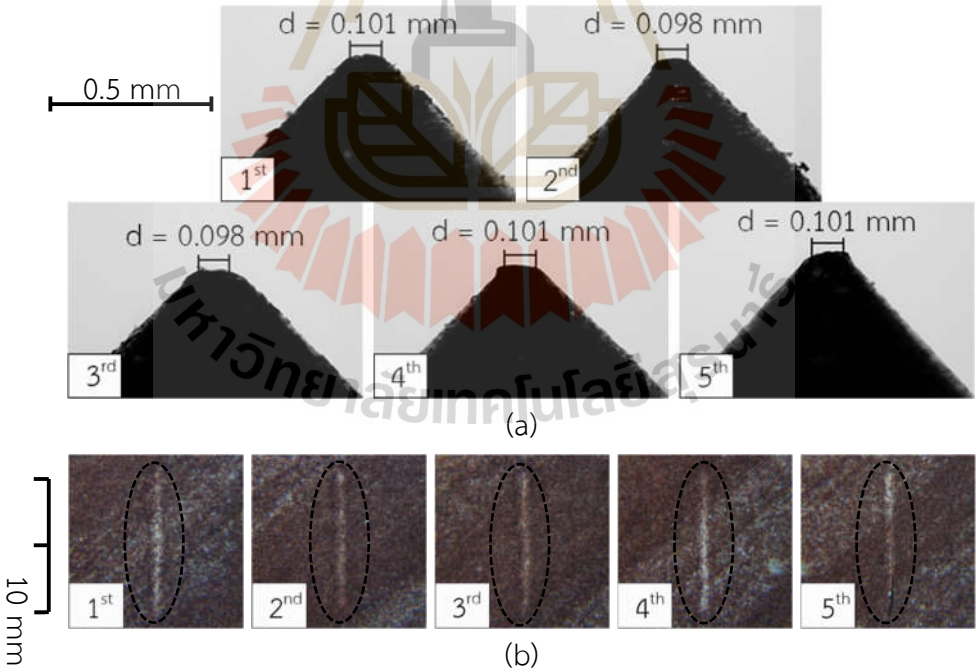

Figure A.22 Close-up images of stylus tip after scratching on Phu Phan sandstone with α = 90°, θ = 45° (a) and their corresponding groove images (b).

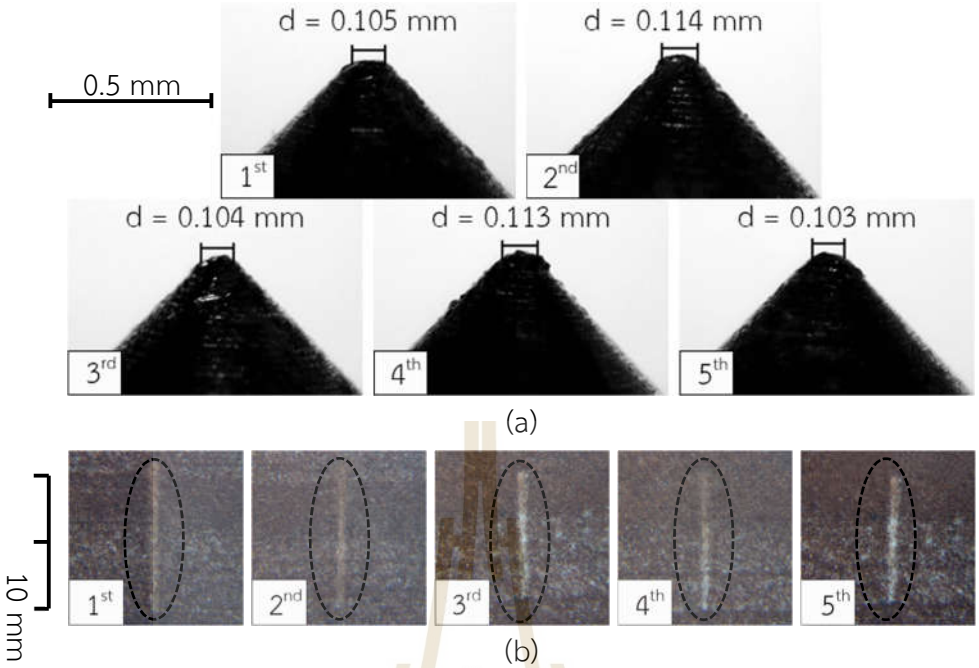

Figure A.23 Close-up images of stylus tip after scratching on Phu Phan sandstone with α = 90°, θ = 90° (a) and their corresponding groove images (b).

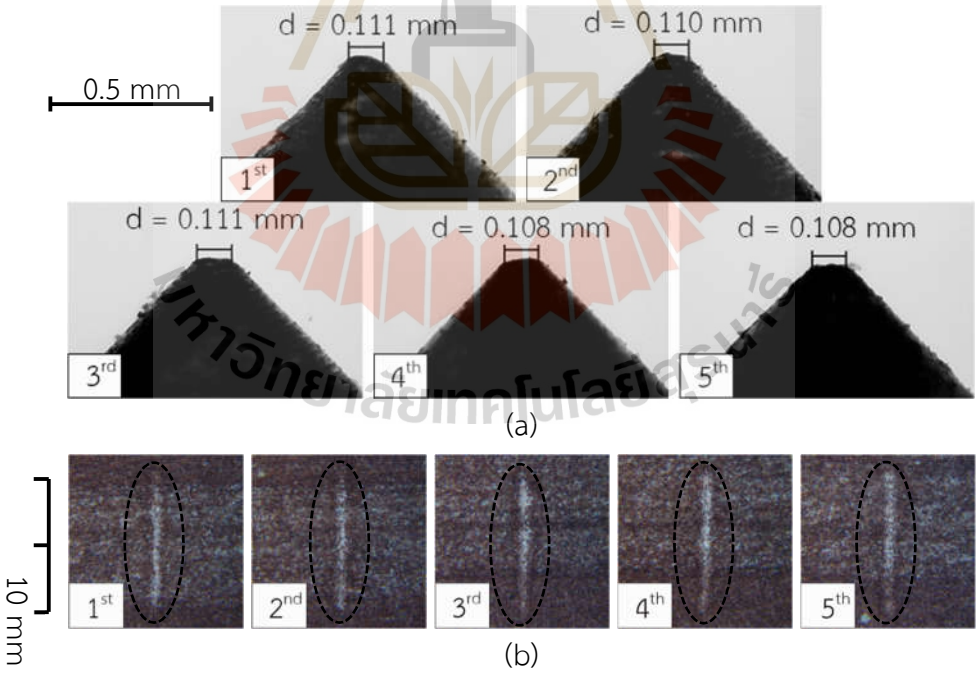

Figure A.24 Close-up images of stylus tip after scratching on Phu Phan sandstone with α = 135°, θ = 90° (a) and their corresponding groove images (b).

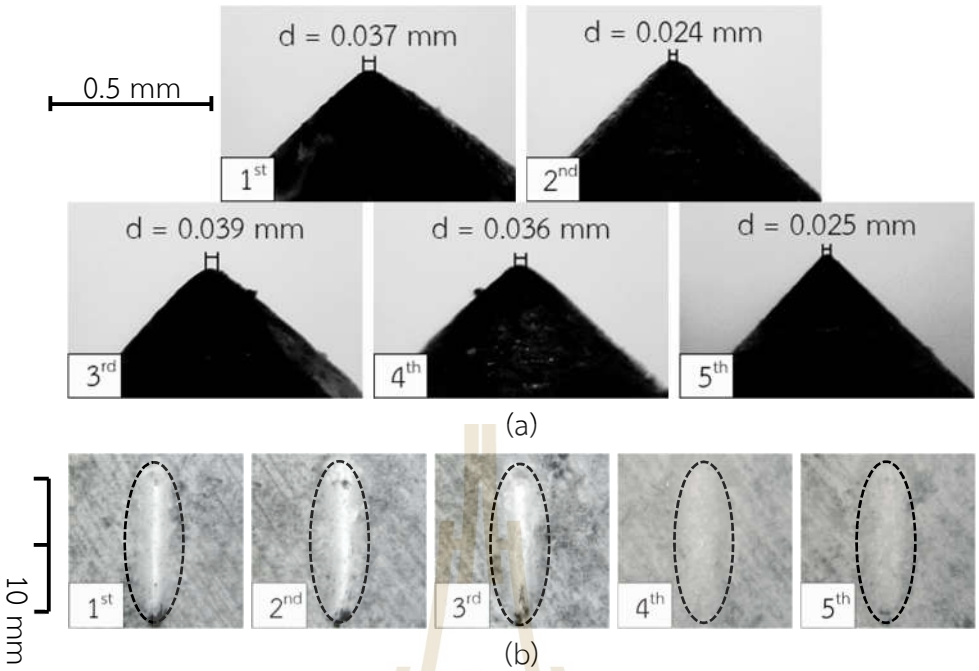

Figure A.25 Close-up images of stylus tip after scratching on Tak Fa gypsum with α = 0° (a) and their corresponding groove images (b).

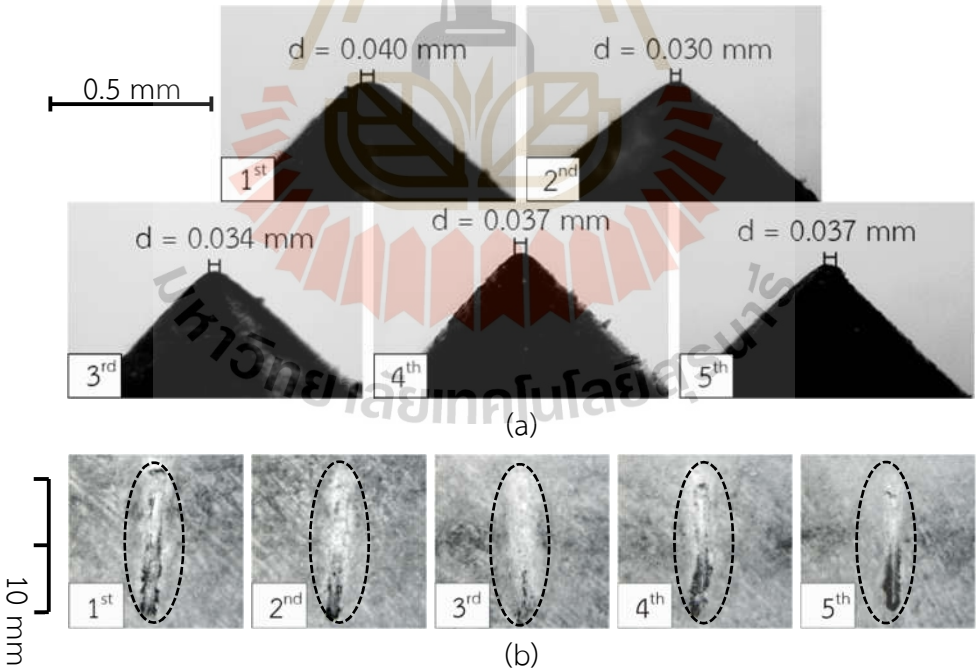

Figure A.26 Close-up images of stylus tip after scratching on Tak Fa gypsum with α = 45°, θ = 90° (a) and their corresponding groove images (b).

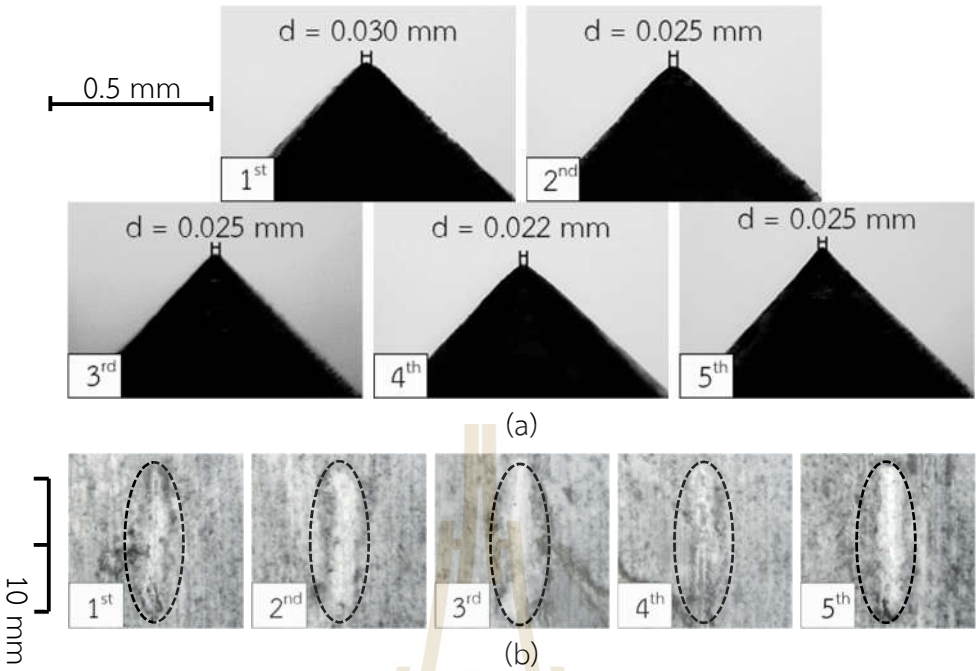

Figure A.27 Close-up images of stylus tip after scratching on Tak Fa gypsum with α = 90°, θ = 0° (a) and their corresponding groove images (b).

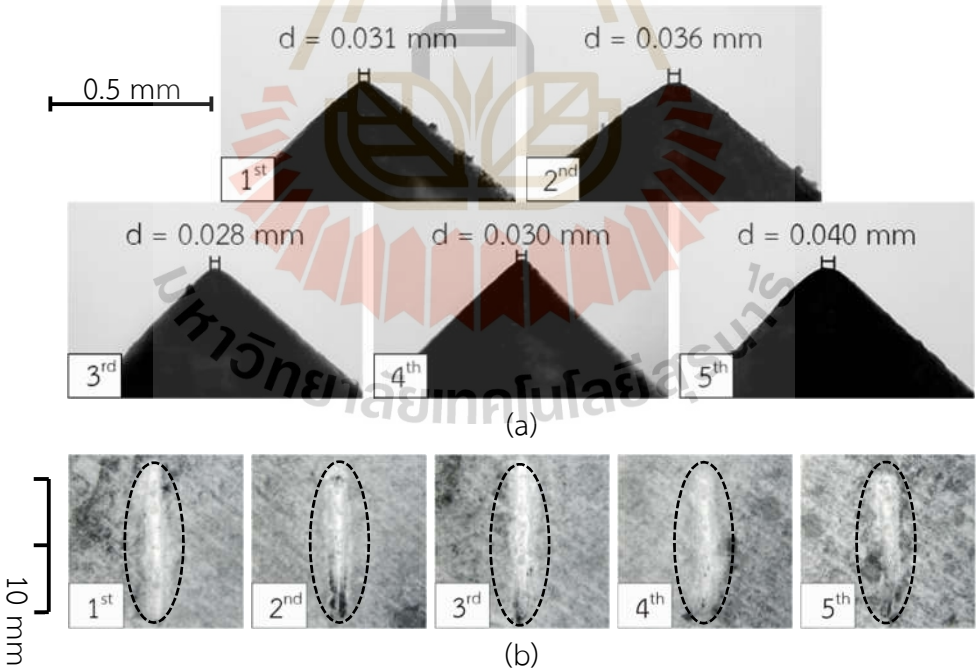

Figure A.28 Close-up images of stylus tip after scratching on Tak Fa gypsum with α = 90°, θ = 45° (a) and their corresponding groove images (b).

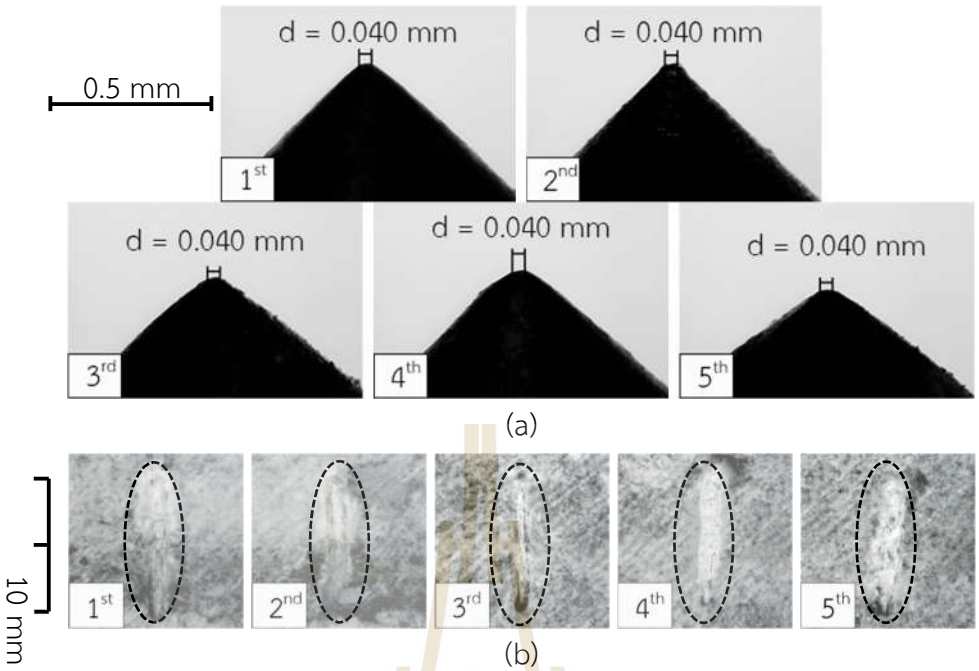

Figure A.29 Close-up images of stylus tip after scratching on Tak Fa gypsum with α = 90°, θ = 90° (a) and their corresponding groove images (b).

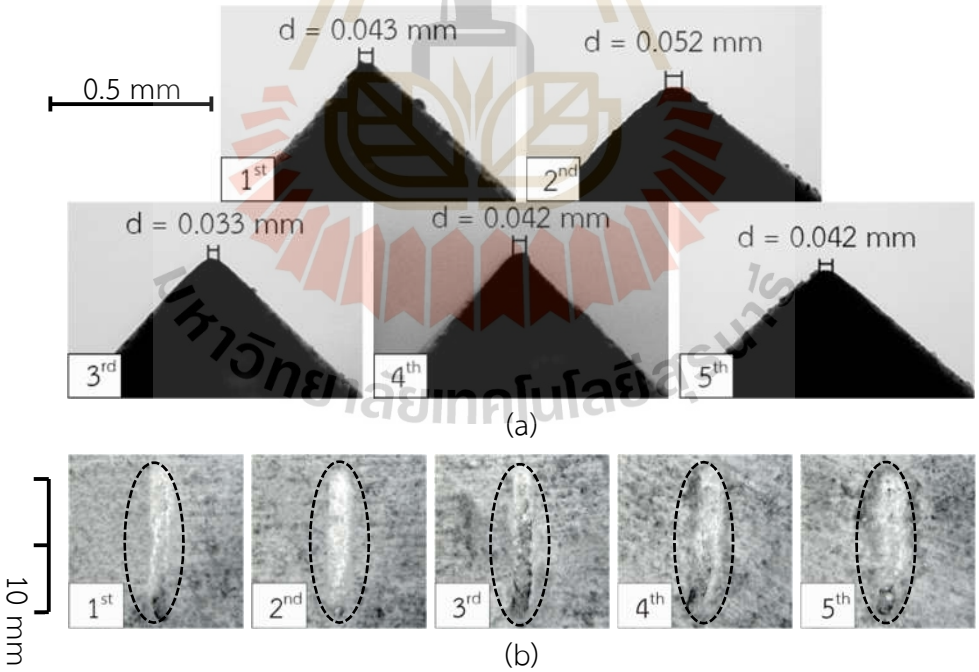

Figure A.30 Close-up images of stylus tip after scratching on Tak Fa gypsum with α = 135°, θ = 90° (a) and their corresponding groove images (b).

APPENDIX B

CERCHAR TEST RESULTS

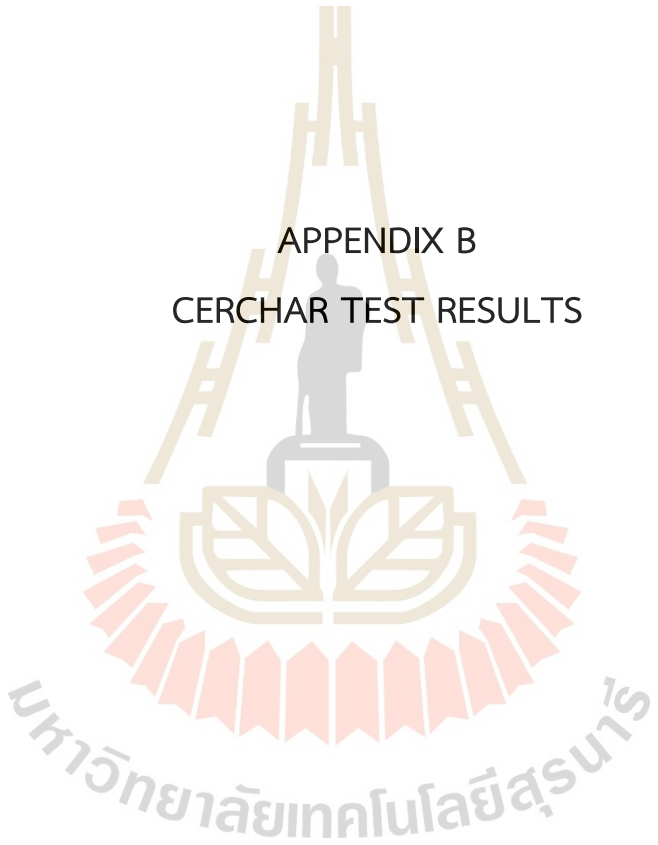

Table B.1 Measurement results of stylus tip wear at four directions on Khao Khad argillaceous limestone.

α (degrees)	θ (degrees)	Lines	d (mm)					
			Front	Left	Right	Back	Average	SD
0	-	1st	0.211	0.211	0.211	0.211	0.211	0.000
		2nd	0.233	0.201	0.195	0.230	0.215	0.017
		3rd	0.244	0.229	0.233	0.244	0.238	0.007
		4th	0.257	0.193	0.227	0.244	0.230	0.024
		5th	0.218	0.218	0.218	0.218	0.218	0.000
45	90	1st	0.183	0.150	0.150	0.180	0.166	0.016
		2nd	0.175	0.150	0.152	0.165	0.161	0.010
		3rd	0.168	0.162	0.159	0.162	0.163	0.003
		4th	0.171	0.163	0.149	0.169	0.163	0.009
		5th	0.175	0.155	0.152	0.171	0.163	0.010
90	0	1st	0.149	0.125	0.135	0.148	0.139	0.010
		2nd	0.148	0.128	0.135	0.148	0.140	0.009
		3rd	0.142	0.142	0.140	0.142	0.142	0.001
		4th	0.143	0.141	0.140	0.142	0.142	0.001
		5th	0.149	0.138	0.136	0.145	0.142	0.005
90	45	1st	0.169	0.146	0.146	0.160	0.155	0.010
		2nd	0.162	0.160	0.141	0.162	0.156	0.009
		3rd	0.156	0.141	0.156	0.156	0.152	0.006
		4th	0.162	0.149	0.155	0.155	0.155	0.005
		5th	0.163	0.149	0.149	0.156	0.154	0.006
90	90	1st	0.186	0.175	0.163	0.181	0.176	0.009
		2nd	0.183	0.166	0.144	0.178	0.168	0.015
		3rd	0.186	0.165	0.169	0.180	0.175	0.008
		4th	0.193	0.143	0.181	0.192	0.177	0.020
		5th	0.201	0.180	0.137	0.189	0.177	0.024
135	90	1st	0.193	0.193	0.193	0.193	0.193	0.000
		2nd	0.212	0.189	0.163	0.204	0.192	0.019
		3rd	0.194	0.193	0.192	0.194	0.193	0.001
		4th	0.195	0.192	0.191	0.192	0.193	0.002
		5th	0.194	0.192	0.192	0.194	0.193	0.001

Table B.2 Measurement results of stylus tip wear at four directions on Khao Khad bedded limestone.

α (degrees)	θ (degrees)	Lines	d (mm)					
			Front	Left	Right	Back	Average	SD
0	-	1st	0.105	0.102	0.103	0.103	0.103	0.001
		2nd	0.107	0.105	0.094	0.106	0.103	0.005
		3rd	0.105	0.096	0.100	0.105	0.102	0.004
		4th	0.106	0.097	0.099	0.105	0.102	0.004
		5th	0.105	0.102	0.094	0.105	0.102	0.005
45	90	1st	0.108	0.104	0.104	0.105	0.105	0.002
		2nd	0.105	0.105	0.105	0.105	0.105	0.000
		3rd	0.108	0.106	0.105	0.107	0.107	0.001
		4th	0.106	0.103	0.103	0.105	0.104	0.001
		5th	0.105	0.105	0.105	0.105	0.105	0.000
90	0	1st	0.104	0.080	0.095	0.095	0.094	0.009
		2nd	0.110	0.091	0.083	0.095	0.095	0.010
		3rd	0.110	0.086	0.079	0.095	0.093	0.012
		4th	0.105	0.095	0.077	0.100	0.094	0.011
		5th	0.110	0.071	0.086	0.107	0.094	0.016
90	45	1st	0.100	0.086	0.097	0.100	0.096	0.006
		2nd	0.100	0.092	0.094	0.100	0.097	0.004
		3rd	0.101	0.092	0.097	0.098	0.097	0.003
		4th	0.097	0.097	0.097	0.097	0.097	0.000
		5th	0.097	0.097	0.097	0.097	0.097	0.000
90	90	1st	0.111	0.111	0.111	0.111	0.111	0.000
		2nd	0.111	0.111	0.111	0.111	0.111	0.000
		3rd	0.111	0.105	0.111	0.111	0.110	0.003
		4th	0.110	0.110	0.110	0.110	0.110	0.000
		5th	0.112	0.109	0.109	0.110	0.110	0.001
135	90	1st	0.119	0.111	0.111	0.111	0.113	0.003
		2nd	0.114	0.105	0.110	0.111	0.110	0.003
		3rd	0.116	0.104	0.116	0.116	0.113	0.005
		4th	0.117	0.104	0.115	0.115	0.113	0.005
		5th	0.116	0.105	0.102	0.116	0.110	0.006

Table B.3 Measurement results of stylus tip wear at four directions on Phu Kadueng sandstone.

α (degrees)	θ (degrees)	Lines	d (mm)					
			Front	Left	Right	Back	Average	SD
0	-	1st	0.168	0.162	0.165	0.165	0.165	0.002
		2nd	0.170	0.166	0.166	0.168	0.168	0.002
		3rd	0.170	0.162	0.160	0.170	0.166	0.005
		4th	0.172	0.165	0.162	0.170	0.167	0.004
		5th	0.172	0.153	0.168	0.170	0.166	0.007
45	90	1st	0.138	0.111	0.122	0.122	0.123	0.010
		2nd	0.134	0.120	0.110	0.129	0.123	0.009
		3rd	0.129	0.114	0.117	0.125	0.121	0.006
		4th	0.123	0.120	0.118	0.123	0.121	0.002
		5th	0.123	0.122	0.120	0.123	0.122	0.001
90	0	1st	0.125	0.082	0.082	0.116	0.101	0.020
		2nd	0.105	0.098	0.097	0.103	0.101	0.003
		3rd	0.116	0.094	0.092	0.104	0.102	0.010
		4th	0.110	0.092	0.100	0.110	0.103	0.008
		5th	0.105	0.098	0.105	0.103	0.103	0.003
90	45	1st	0.123	0.110	0.110	0.123	0.117	0.007
		2nd	0.129	0.113	0.103	0.123	0.117	0.010
		3rd	0.128	0.091	0.107	0.128	0.114	0.016
		4th	0.128	0.110	0.107	0.110	0.114	0.008
		5th	0.134	0.110	0.110	0.110	0.116	0.010
90	90	1st	0.149	0.108	0.146	0.147	0.138	0.017
		2nd	0.137	0.137	0.137	0.137	0.137	0.000
		3rd	0.147	0.137	0.111	0.143	0.135	0.014
		4th	0.147	0.125	0.132	0.135	0.135	0.008
		5th	0.144	0.132	0.122	0.141	0.135	0.009
135	90	1st	0.149	0.140	0.138	0.142	0.142	0.004
		2nd	0.145	0.139	0.140	0.143	0.142	0.002
		3rd	0.147	0.143	0.142	0.145	0.144	0.002
		4th	0.145	0.138	0.142	0.145	0.143	0.003
		5th	0.145	0.140	0.138	0.143	0.142	0.003

Table B.4 Measurement results of stylus tip wear at four directions on Phu Phan sandstone.

α (degrees)	θ (degrees)	Lines	d (mm)					
			Front	Left	Right	Back	Average	SD
0	-	1st	0.159	0.105	0.156	0.150	0.143	0.022
		2nd	0.156	0.143	0.126	0.152	0.144	0.012
		3rd	0.169	0.110	0.131	0.157	0.142	0.023
		4th	0.150	0.129	0.138	0.150	0.142	0.009
		5th	0.152	0.137	0.128	0.149	0.142	0.010
45	90	1st	0.101	0.101	0.097	0.101	0.100	0.002
		2nd	0.101	0.098	0.097	0.100	0.099	0.002
		3rd	0.101	0.098	0.101	0.101	0.100	0.001
		4th	0.101	0.098	0.097	0.101	0.099	0.002
		5th	0.101	0.101	0.101	0.101	0.101	0.000
90	0	1st	0.085	0.082	0.082	0.082	0.083	0.001
		2nd	0.082	0.082	0.082	0.082	0.082	0.000
		3rd	0.088	0.077	0.076	0.088	0.082	0.006
		4th	0.086	0.077	0.077	0.086	0.082	0.005
		5th	0.086	0.077	0.077	0.077	0.079	0.004
90	45	1st	0.092	0.089	0.089	0.092	0.091	0.002
		2nd	0.096	0.084	0.084	0.096	0.090	0.006
		3rd	0.091	0.091	0.088	0.091	0.090	0.001
		4th	0.094	0.094	0.091	0.091	0.093	0.002
		5th	0.094	0.091	0.080	0.091	0.089	0.005
90	90	1st	0.108	0.105	0.098	0.105	0.104	0.004
		2nd	0.114	0.091	0.108	0.108	0.105	0.009
		3rd	0.107	0.098	0.104	0.107	0.104	0.004
		4th	0.113	0.098	0.095	0.113	0.105	0.008
		5th	0.108	0.103	0.103	0.108	0.106	0.003
135	90	1st	0.111	0.101	0.111	0.111	0.109	0.004
		2nd	0.110	0.106	0.107	0.108	0.108	0.001
		3rd	0.111	0.106	0.111	0.111	0.110	0.002
		4th	0.113	0.100	0.108	0.111	0.108	0.005
		5th	0.110	0.100	0.108	0.108	0.107	0.004

Table B.5 Measurement results of stylus tip wear at four directions on Tak Fa gypsum.

α (degrees)	θ (degrees)	Lines	d (mm)					
			Front	Left	Right	Back	Average	SD
0	-	1st	0.037	0.032	0.034	0.036	0.035	0.002
		2nd	0.040	0.036	0.024	0.038	0.035	0.006
		3rd	0.039	0.030	0.030	0.039	0.035	0.005
		4th	0.040	0.030	0.032	0.036	0.035	0.004
		5th	0.039	0.025	0.035	0.038	0.034	0.006
45	90	1st	0.040	0.040	0.033	0.040	0.038	0.003
		2nd	0.040	0.030	0.040	0.040	0.038	0.004
		3rd	0.039	0.034	0.033	0.036	0.036	0.002
		4th	0.040	0.033	0.036	0.037	0.037	0.003
		5th	0.040	0.039	0.037	0.039	0.039	0.001
90	0	1st	0.030	0.025	0.024	0.025	0.026	0.002
		2nd	0.035	0.025	0.024	0.025	0.027	0.004
		3rd	0.025	0.025	0.021	0.025	0.024	0.002
		4th	0.025	0.022	0.022	0.025	0.024	0.002
		5th	0.025	0.025	0.025	0.025	0.025	0.000
90	45	1st	0.033	0.031	0.031	0.031	0.032	0.001
		2nd	0.037	0.031	0.030	0.036	0.034	0.003
		3rd	0.028	0.028	0.028	0.028	0.028	0.000
		4th	0.033	0.028	0.030	0.033	0.031	0.002
		5th	0.040	0.025	0.028	0.033	0.032	0.006
90	90	1st	0.040	0.040	0.040	0.040	0.040	0.000
		2nd	0.040	0.040	0.040	0.040	0.040	0.000
		3rd	0.040	0.040	0.040	0.040	0.040	0.000
		4th	0.040	0.040	0.040	0.040	0.040	0.000
		5th	0.040	0.037	0.039	0.040	0.039	0.001
135	90	1st	0.051	0.045	0.043	0.046	0.046	0.003
		2nd	0.062	0.037	0.042	0.052	0.048	0.010
		3rd	0.046	0.033	0.042	0.042	0.041	0.005
		4th	0.042	0.040	0.040	0.042	0.041	0.001
		5th	0.042	0.041	0.041	0.042	0.042	0.001

APPENDIX C

SCRATCHING FORCES

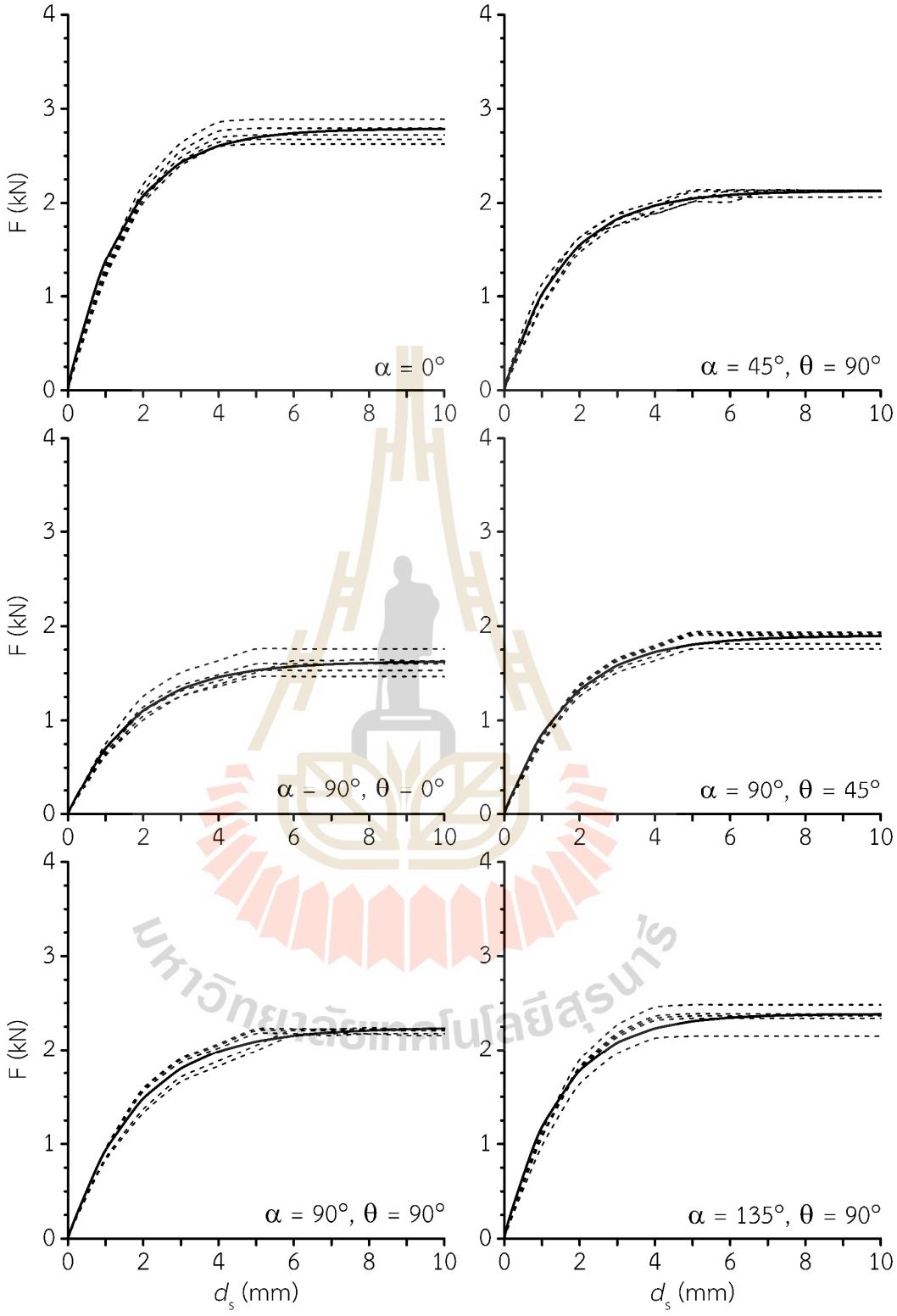

Figure C.1 Scratching forces (F) as a function of scratching displacement (d_s) for Khao Khad argillaceous limestone. Dash line represents each groove. Solid lines are their average.

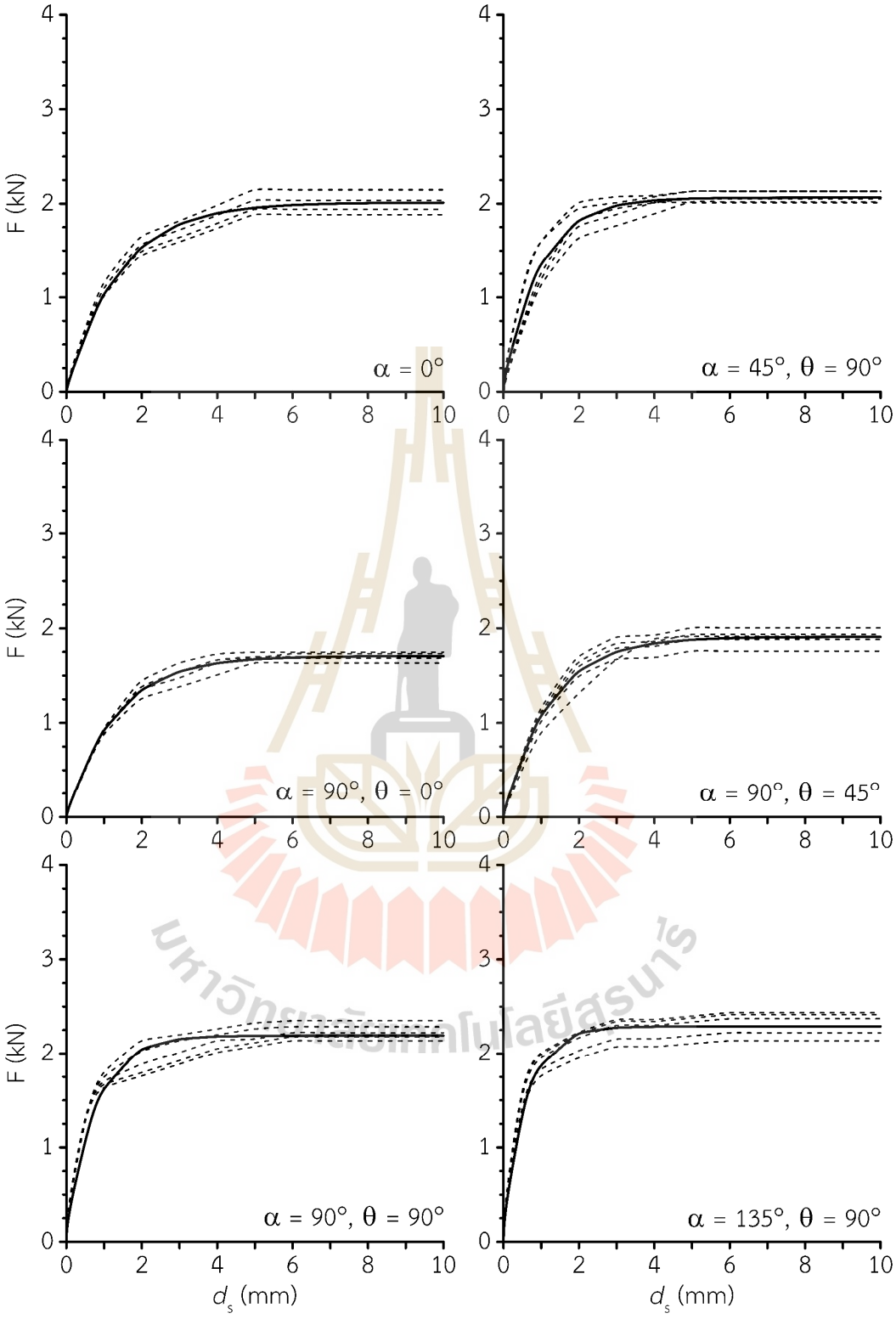

Figure C.2 Scratching forces (F) as a function of scratching displacement (d_s) for Khao Khad bedded limestone. Dash line represents each groove. Solid lines are their average.

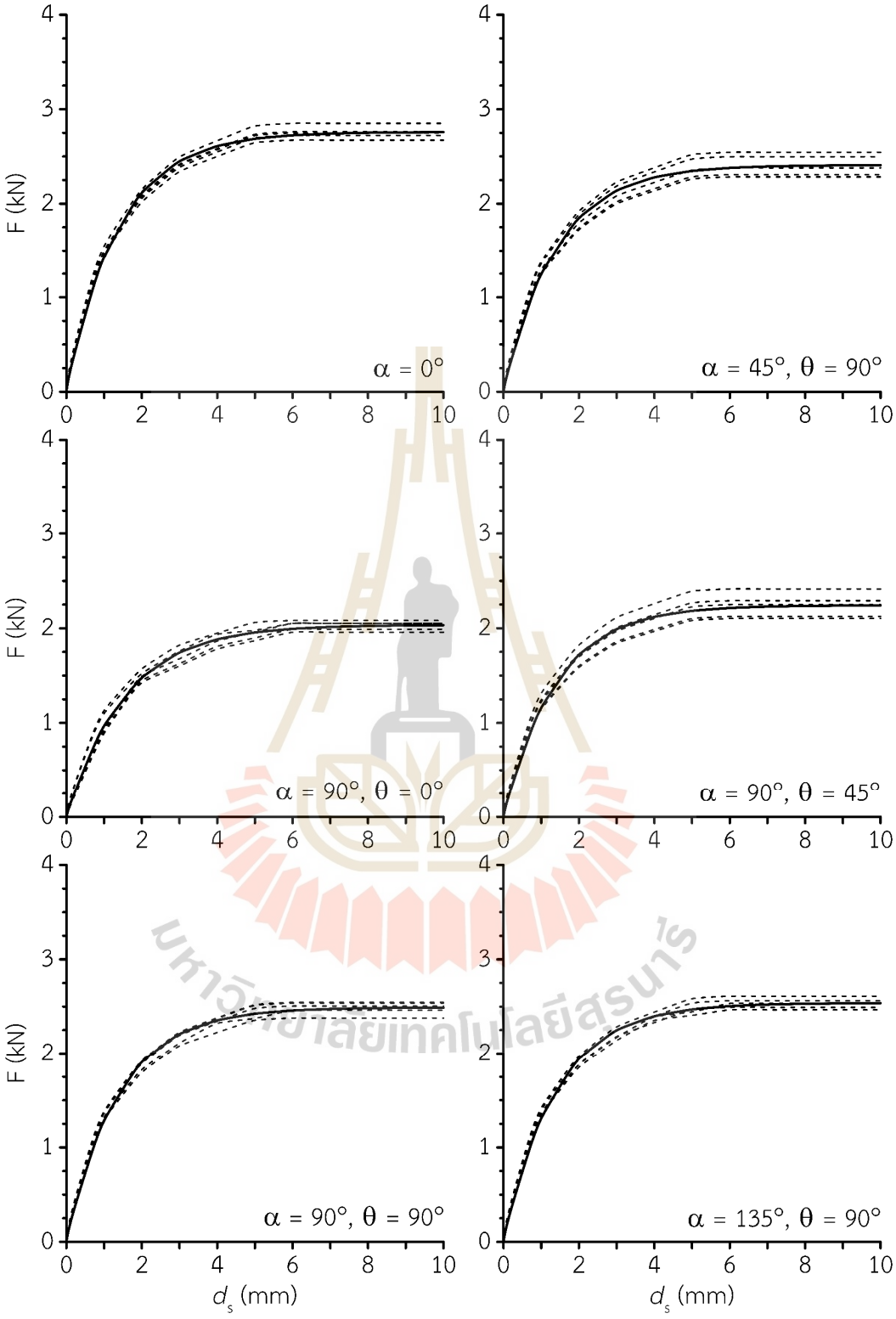

Figure C.3 Scratching forces (F) as a function of scratching displacement (d_s) for Phu Kadueng sandstone. Dash line represents each groove. Solid lines are their average.

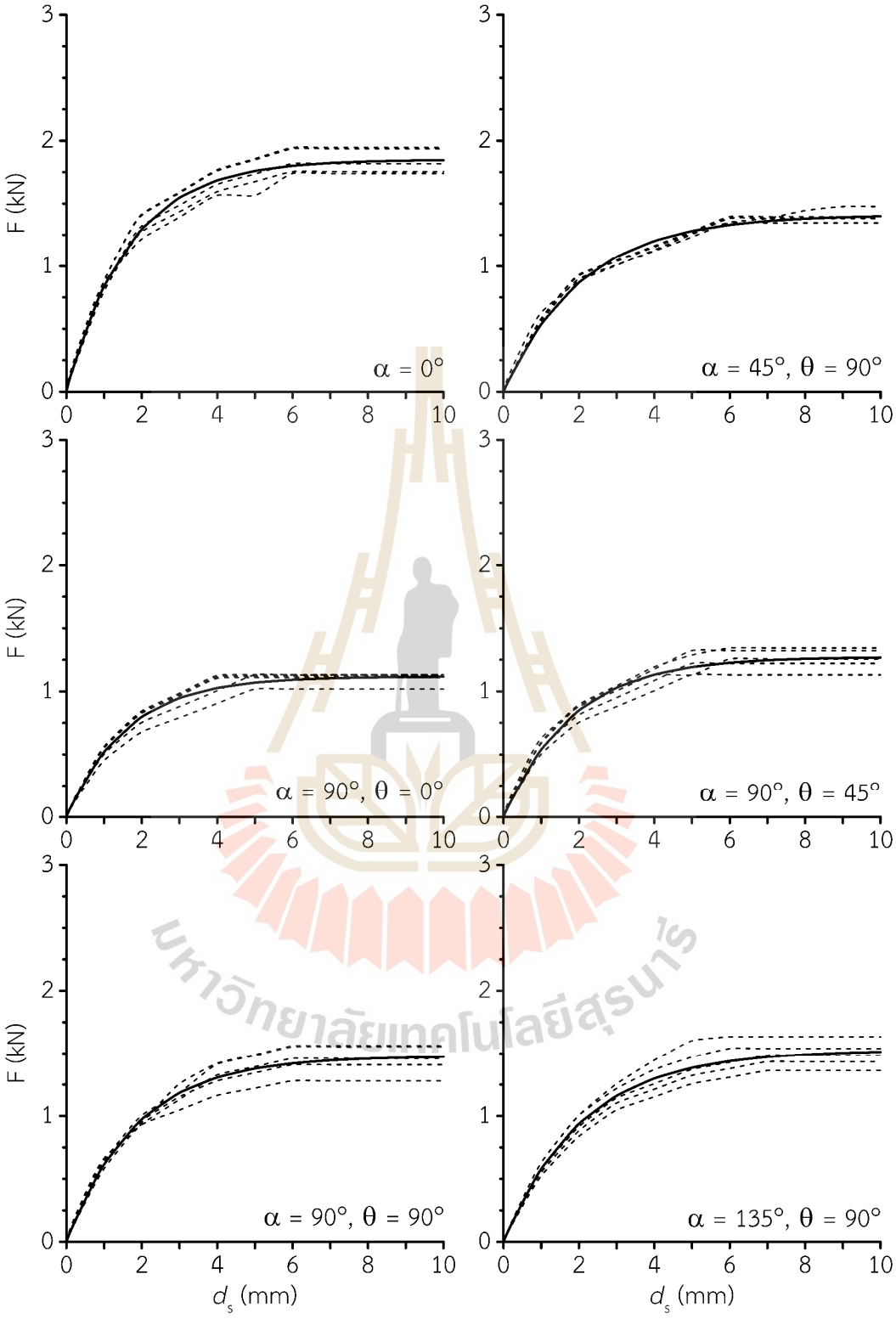

Figure C.4 Scratching forces (F) as a function of scratching displacement (d_s) for Phu Phan sandstone. Dash line represents each groove. Solid lines are their average.

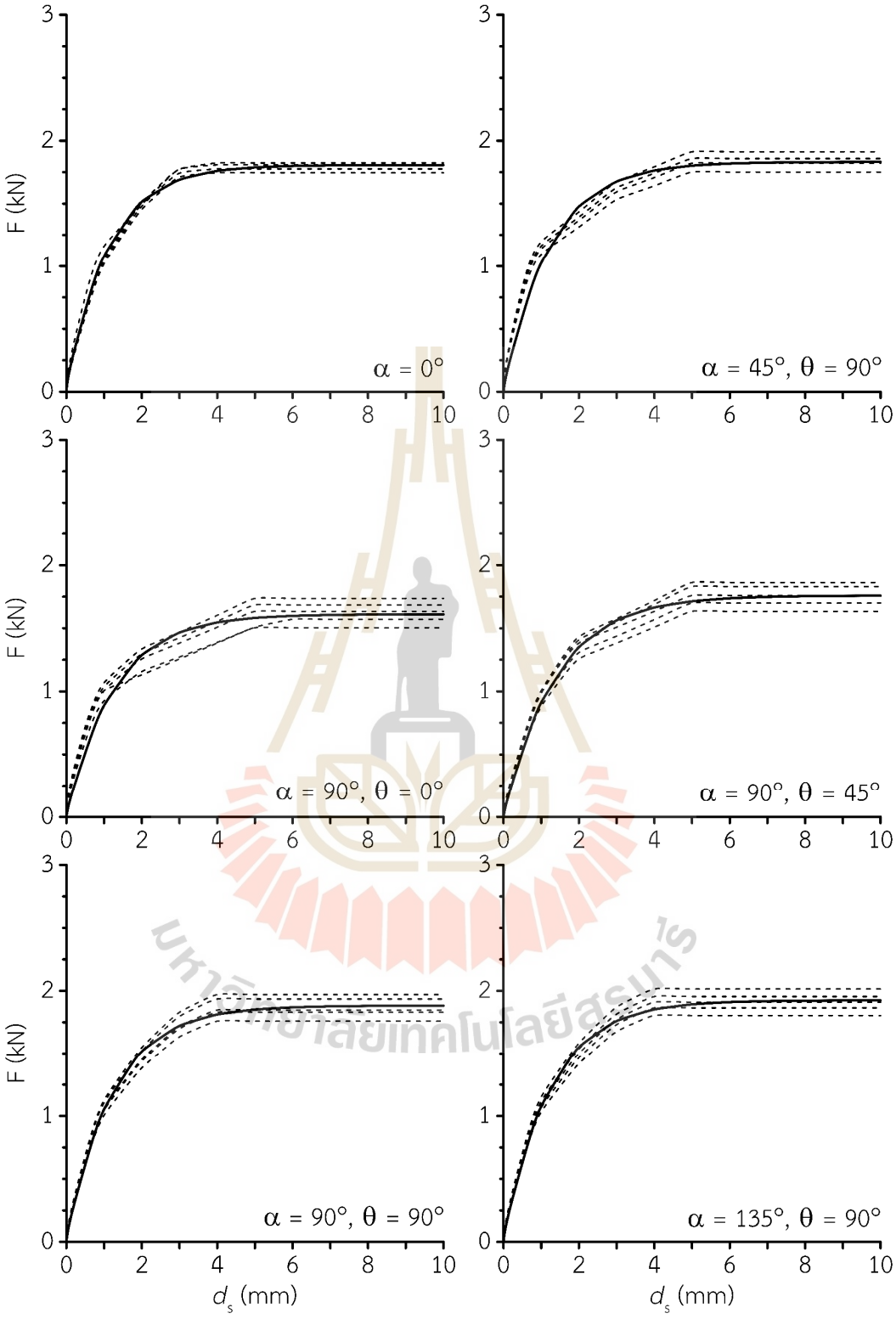

Figure C.5 Scratching forces (F) as a function of scratching displacement (d_s) for Tak Fa gypsum. Dash line represents each groove. Solid lines are their average.

APPENDIX D

LASER - SCANNED IMAGES

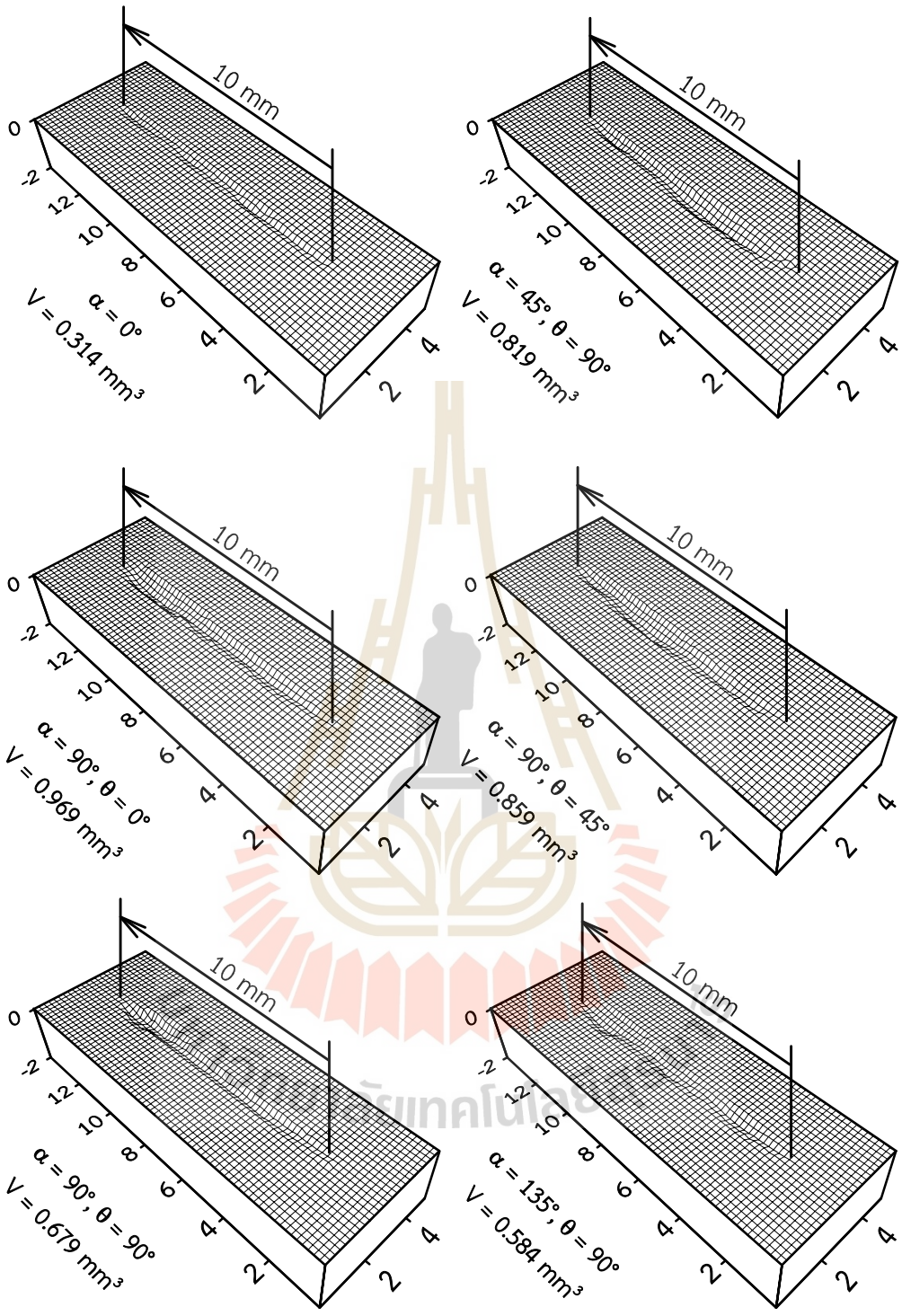

Figure D.1 Groove volume after CERCHAR testing on Khao Khad argillaceous limestone specimens vary bedding plane orientations and scratching directions.

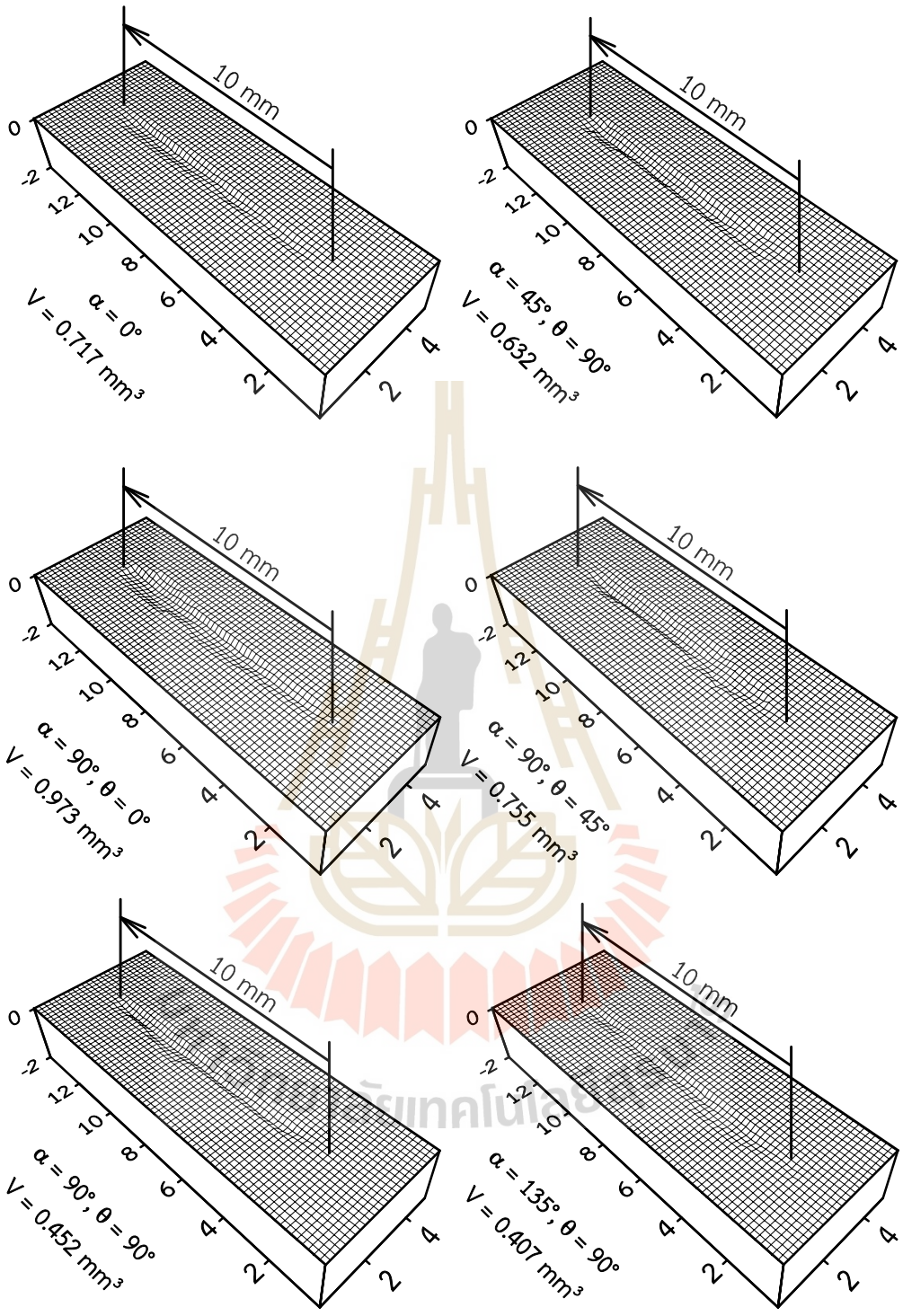

Figure D.2 Groove volume after CERCHAR testing on Khao Khad bedded limestone specimens vary bedding plane orientations and scratching directions.

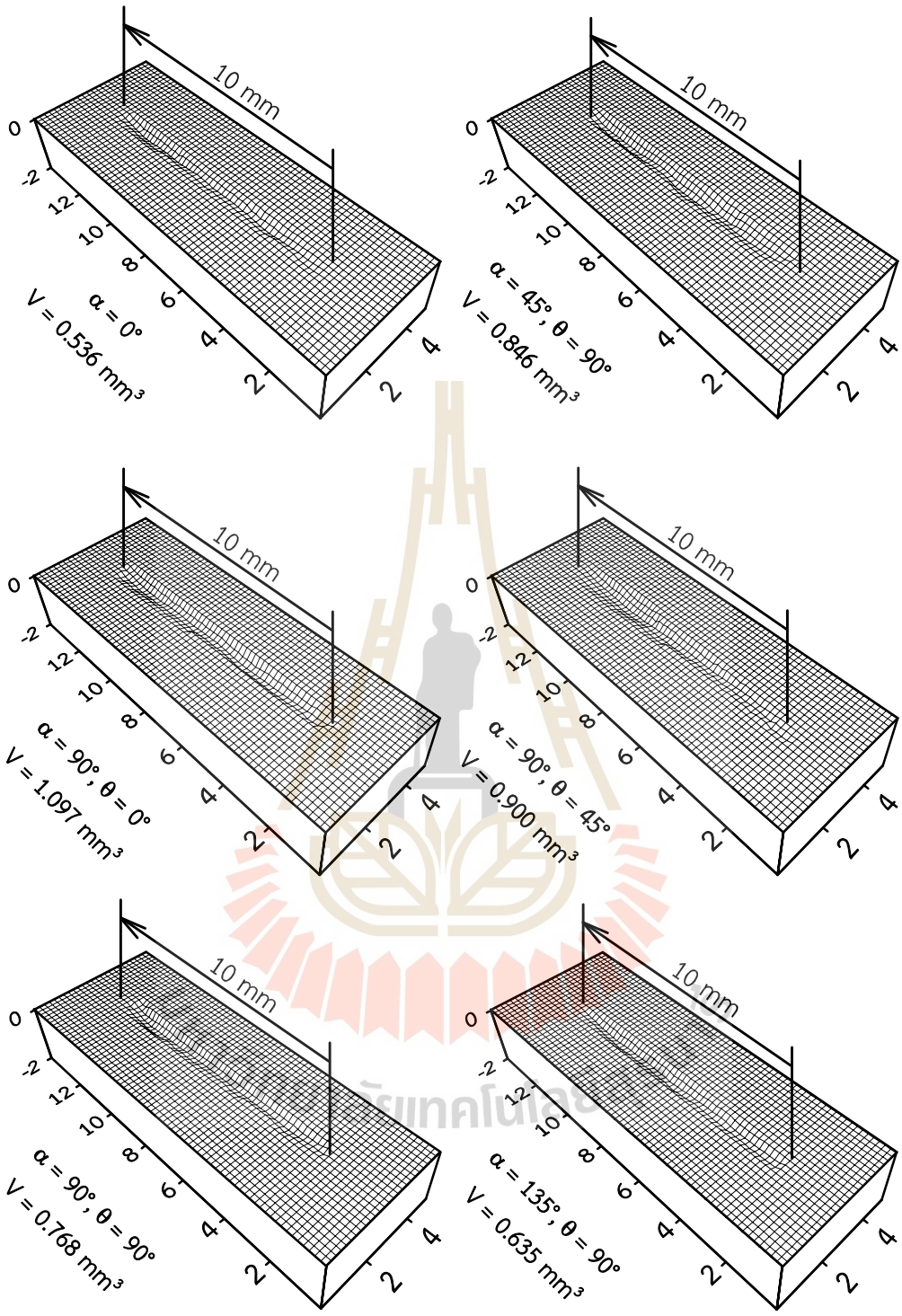

Figure D.3 Groove volume after CERCHAR testing on Phu Kadueng sandstone specimens vary bedding plane orientations and scratching directions.

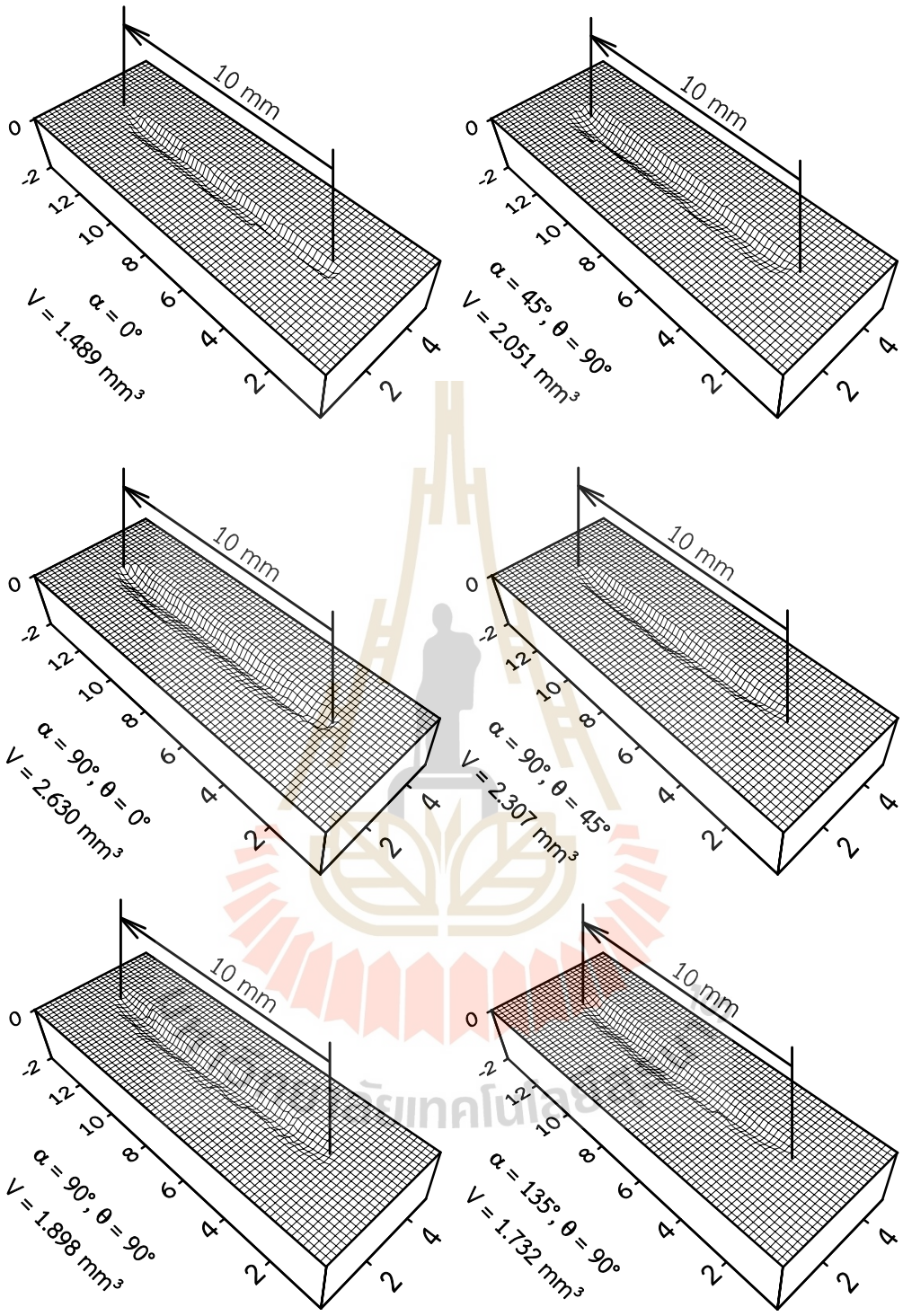

Figure D.4 Groove volume after CERCHAR testing on Phu Phan sandstone specimens vary bedding plane orientations and scratching directions.

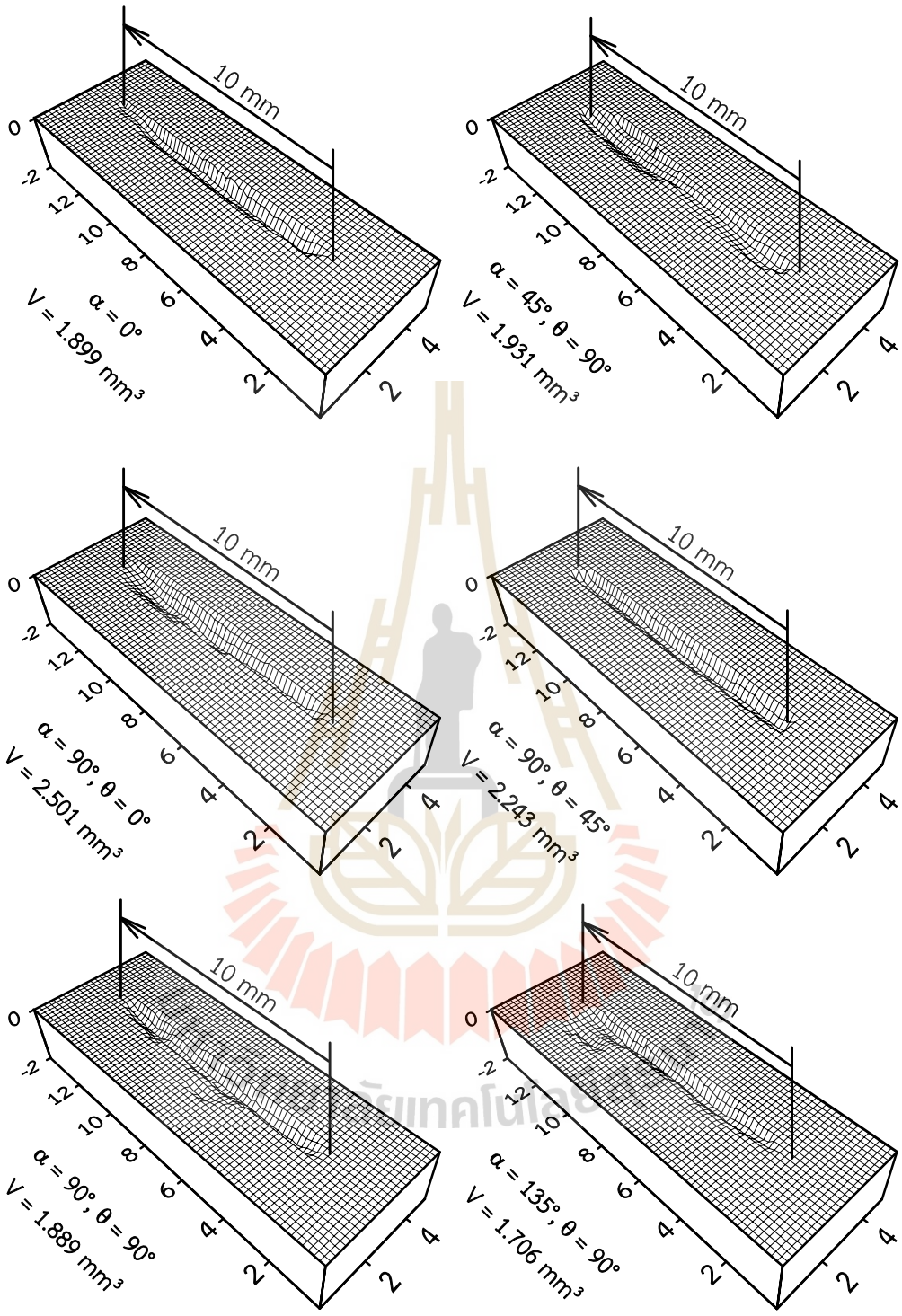

Figure D.5 Groove volume after CERCHAR testing on Tak Fa gypsum specimens vary bedding plane orientations and scratching directions.

APPENDIX E

LIST OF PUBLICATION

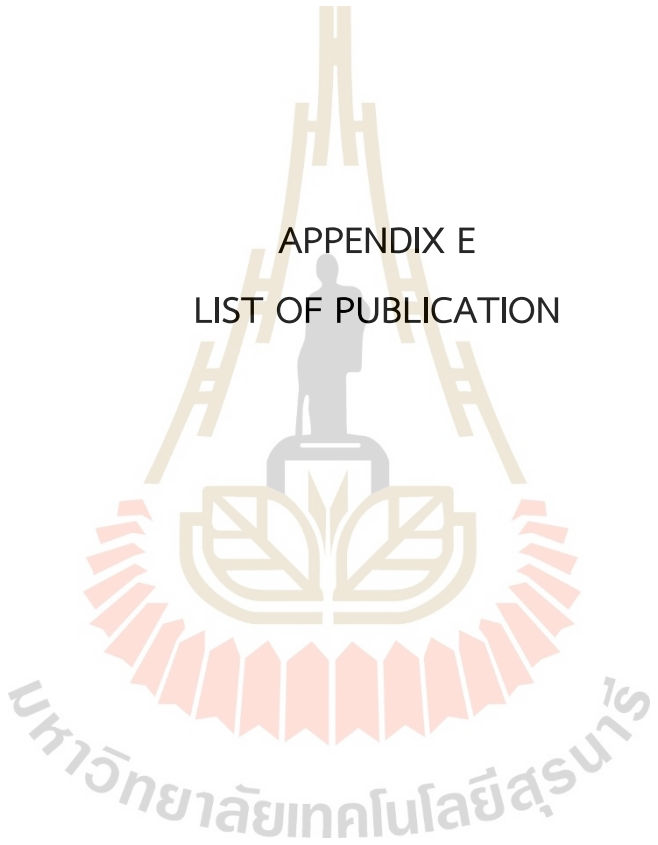

Effect of Bedding Plane Orientations and Scratching Directions on CERCHAR Abrasivity Index of Soft to Medium-hard Rocks

Thiti Patcharaarpakul(✉), Laksikar Sitthimongkol, Kittitep Fuenkajorn, and Thanittha Thongprapha

Geomechanics Research Unit, Suranaree University of Technology, Nakhon Ratchasima 30000, Thailand
thiti.b6110819@gmail.com

Abstract. The objective of this study is to determine the effects of bedding plane orientations and scratching directions on the CERCHAR Abrasivity Index (*CAI*) of various rock types, including Khao Khad argillaceous limestone, Khao Khad bedded limestone, Phu Kadueng sandstone, Phu Phan sandstone and Tak Fa gypsum. The ploughing forces and groove volumes are also investigated. The results indicate that higher *CAI* values and ploughing forces are observed in stronger rocks (limestones and sandstones) compared to softer rocks (gypsum). The groove volume increases as the *CAI* value decreases for all tested specimens. Higher *CAI* values are obtained for hard rocks when the scratching direction is opposite to the dip direction of the bedding planes. The highest *CAI* values are observed when the stylus pin moves perpendicular to the bedding trend, rather than along the bedding planes. The effect of bedding plane orientation on *CAI* is more pronounced in strong rocks than in soft ones. These findings will play an important role in maintaining drill bit lifetime, especially within rock types with varying bedding planes.

Keywords: Stylus pin · Abrasiveness · Ploughing force · Groove volume

1 Introduction

Assessing rock properties and steel durability is important for determining the lifespan of cutting tools in construction and excavation industries [1]. Abrasivity testing evaluates tool durability against wear from rock surfaces. CERCHAR abrasivity index (*CAI*) is one of the methods that have been widely used. Several researchers have identified various factors affecting the *CAI*, such as stylus hardness [2, 3], scratching rate [4, 5], scratching distance [6–8], surface condition [6, 9, 10], moisture content [4, 7, 8], temperature [4, 7, 8, 11–13], and rock properties [3, 14, 15]. Bedding planes, which are inherent stratifications within sedimentary rocks, may also considerably affect their abrasivity [16, 17]. Numerous tests on anisotropic rock properties have demonstrated that anisotropic characteristics significantly affecting rock strength results, with maximum rock strengths typically observed at bedding plane orientations of 0° and 90°, and minimum values

T. Kang and Y. Lee (Eds.): ICCEA 2024, LNCE 640, pp. 338–347, 2025.
https://doi.org/10.1007/978-981-96-6115-2_28

between 45° and 60° [17–19]. The effect of bedding planes and their orientations on the abrasiveness of cutting tools has rarely been investigated.

The objective of this study is to determine the effects of bedding plane orientations and scratching directions on the abrasivity of some sedimentary rocks. Crystalline and clastic rocks in Thailand are used as rock samples. The *CAI* test method follows the ASTM D7625-22 standard practice [20].

2 Samples Preparation

Rock samples used in this study are Khao Khad argillaceous limestone, Khao Khad bedded limestone, Phu Kadueng sandstone, Phu Phan sandstone, and Tak Fa gypsum. These rocks are subjected to various excavation tools in mining and construction industry. The test surfaces are cut flat with length-to-diameter (*L*/*D*) ratio of 1. The nominal angles (α) between the test surface and bedding plane vary from 0°, 45°, 90° to 135°. The scratching directions of the stylus pin with respect to the bedding trends vary from 0° to 90°. The specimens are oven-dried before testing. Table 1 shows bedding plane characteristics of the test samples.

Table 1. Bedding plane characteristics.

Rock type	Bedding plane characteristics
Khao Khad argillaceous limestone	Bedding planes can be observed by the alternation of gray limestone and pale brown clay bands, with average thickness of 1 mm.
Khao Khad bedded limestone	Bedding planes can be observed by the alternation of gray limestone and white calcite bands, with average thickness of 0.5 mm.
Phu Kadueng sandstone	Bedding planes can be observed by the alternation of pale green quartz and black biotite bands, with average thickness of 1.5 mm.
Phu Phan sandstone	Bedding planes can be observed by the alternation of pale red quartz and red microcline bands, with average thickness of 1 mm.
Tak Fa gypsum	Bedding planes can be observed by the alternation of white gypsum and gray anhydrite bands, with average thickness of 2 mm.

3 Test Method

The test method and calculation follow ASTM D7625-22 standard practice [20]. Two test series are performed to determine the effects of bedding plane orientation (α) and scratching direction (θ), as shown in Fig. 1. CERCHAR testing is conducted on saw-cut

surfaces with varying bedding plane angles using a device based on the West apparatus, as shown in Fig. 2. The wear on the stylus tip is measured under a microscope with 50 times magnification. Five pins are used per bedding plane angle. Ploughing force on the stylus is calculated from the torque applied to the hand crank as follows (Eq. 1):

$$F = 2\pi T/P \tag{1}$$

where F represents ploughing force (N), T denotes torque (N·m) applied on the crank, and P is screw pitch (0.001 mm). Groove volume produced by scratching on specimen surface are measured by laser-scanning with a 0.1 mm line scan interval and vertical precision of ± 1 micron. The results are used to calculate the groove volume by using SURFER software.

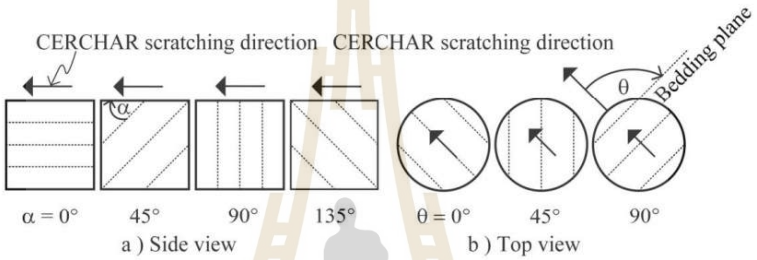

Fig. 1. Scratching direction as compound to bedding plane angles (a), and as compared to trends of bedding planes (b).

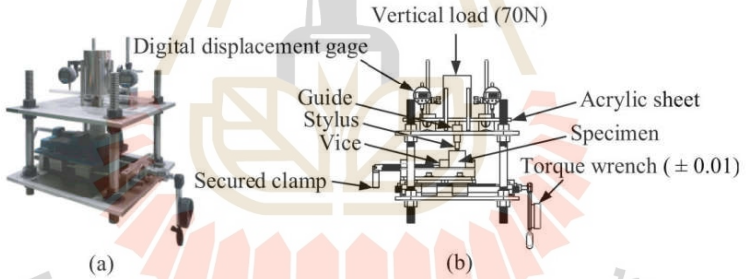

Fig. 2. Device based on West CERCHAR apparatus with additional torque measurements (a) schematic drawing of CERCHAR device (b) [15].

4 Results

4.1 CERCHAR Abrasivity Index

Bedding plane angle (α) and scratching direction (θ) do affect the wear of stylus pins. Table 2 presents *CAI* results for all boundary conditions. Based on ASTM D7625-22 [20] these rocks are classified as medium to high abrasiveness, except for Tak Fa

gypsum where it is classified as very low abrasiveness regarding of scratching direction and bedding plane angle. For all bedding plane orientations, Khao Khad argillaceous limestone has the highest *CAI*, while Tak Fa gypsum has the lowest *CAI* values.

The *CAI* varies with α angle, as shown in Fig. 3a. For the argillaceous limestone, the *CAI* is highest at $\alpha = 0°$ and lowest at $\alpha = 45°$. Similar trends are observed for Phu Kadueng and Phu Phan sandstones. The bedded limestone and Tak Fa gypsum show the highest *CAI* at $\alpha = 135°$ and the lowest at $\alpha = 0°$. The *CAI* increases slightly with θ angle, peaking at $\theta = 90°$ and reaching its lowest value at $\theta = 0°$ for all tested rocks (Fig. 3b).

4.2 Groove Volume

The groove volume obtained from laser 2-D scanner is consistent with the *CAI* values. It increases as the *CAI* value decreases. Table 2 gives groove volumes for all boundary conditions. Largest volumes are obtained for $\alpha = 45°$. This is true for all tested specimens. For $\alpha = 90°$, largest groove volume can be observed when the pin direction is parallel to the bedding trends ($\theta = 0°$). Soft rocks (e.g. gypsum) show largest groove volume, as

Table 2. CERCHAR abrasivity index and groove volume with different bedding plane orientations.

Rock type	α (degrees)	θ (degrees)	*CAI*	Abrasiveness index	Volume (mm^3)
Khao Khad argillaceous limestone	0	–	2.54 ± 0.11	High	0.314 ± 0.03
	45	90	1.86 ± 0.02	Medium	0.819 ± 0.06
	90	0	1.61 ± 0.01	Medium	0.969 ± 0.04
	90	45	1.76 ± 0.01	Medium	0.859 ± 0.05
	90	90	1.99 ± 0.04	Medium	0.679 ± 0.05
	135	90	2.20 ± 0.00	High	0.584 ± 0.04
Khao Khad bedded limestone	0	–	1.17 ± 0.00	Medium	0.717 ± 0.02
	45	90	1.20 ± 0.01	Medium	0.632 ± 0.04
	90	0	1.07 ± 0.01	Medium	0.973 ± 0.06
	90	45	1.10 ± 0.00	Medium	0.755 ± 0.03
	90	90	1.26 ± 0.00	Medium	0.452 ± 0.02
	135	90	1.28 ± 0.01	Medium	0.407 ± 0.07
Phu Kadueng sandstone	0	–	1.90 ± 0.01	Medium	0.536 ± 0.03
	45	90	1.39 ± 0.01	Medium	0.846 ± 0.10
	90	0	1.16 ± 0.01	Medium	1.097 ± 0.05
	90	45	1.32 ± 0.01	Medium	0.900 ± 0.05

(*continued*)

Table 2. (*continued*)

Rock type	α (degrees)	θ (degrees)	*CAI*	Abrasiveness index	Volume (mm^3)
	90	90	1.55 ± 0.01	Medium	0.768 ± 0.08
	135	90	1.63 ± 0.01	Medium	0.635 ± 0.04
Phu Phan sandstone	0	–	1.63 ± 0.01	Medium	1.489 ± 0.10
	45	90	1.13 ± 0.00	Medium	2.051 ± 0.04
	90	0	0.93 ± 0.00	Low	2.630 ± 0.12
	90	45	1.03 ± 0.01	Medium	2.307 ± 0.05
	90	90	1.19 ± 0.00	Medium	1.898 ± 0.03
	135	90	1.24 ± 0.01	Medium	1.732 ± 0.08
Tak Fa gypsum	0	–	0.40 ± 0.00	Very low	1.899 ± 0.06
	45	90	0.43 ± 0.01	Very low	1.931 ± 0.05
	90	0	0.29 ± 0.01	Very low	2.501 ± 0.04
	90	45	0.36 ± 0.02	Very low	2.243 ± 0.03
	90	90	0.45 ± 0.00	Very low	1.889 ± 0.07
	135	90	0.50 ± 0.03	Very low	1.706 ± 0.06

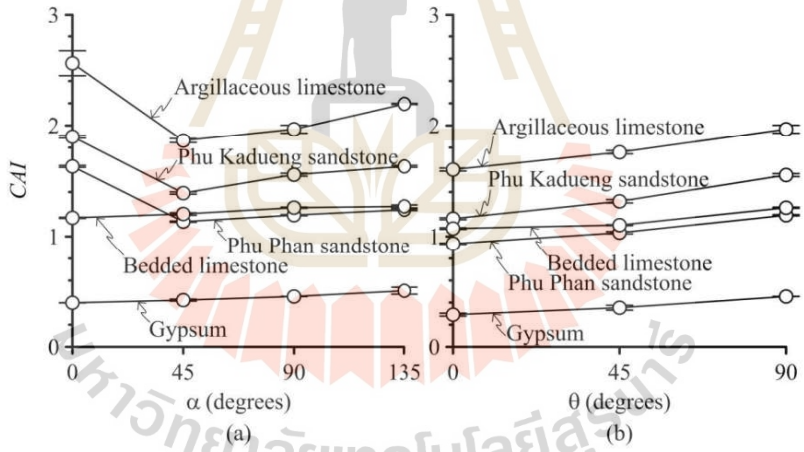

Fig. 3. *CAI* as a function of bedding plane angle (a), and scratching direction (b).

compared to the stronger ones (e.g. limestones), as shown in Fig. 4. Similar trends are observed for Phu Kadueng and Phu Phan sandstone. Gypsum and bedded limestone have the highest groove volume at $\alpha = 0°$ and the lowest at $\alpha = 135°$. As shown in Fig. 4b,

groove volume increases with the θ angle, peaking at $\theta = 90°$ and reaching its lowest at $\theta = 0°$ for all tested rocks. Phu Phan sandstone and Tak Fa gypsum show similar groove volume despite their different levels of abrasiveness.

4.3 Ploughing Force

An empirical equation is proposed to represent F as a function of d_s:

$$F = a \cdot (1 - exp \cdot (-b \cdot d_s)) \tag{2}$$

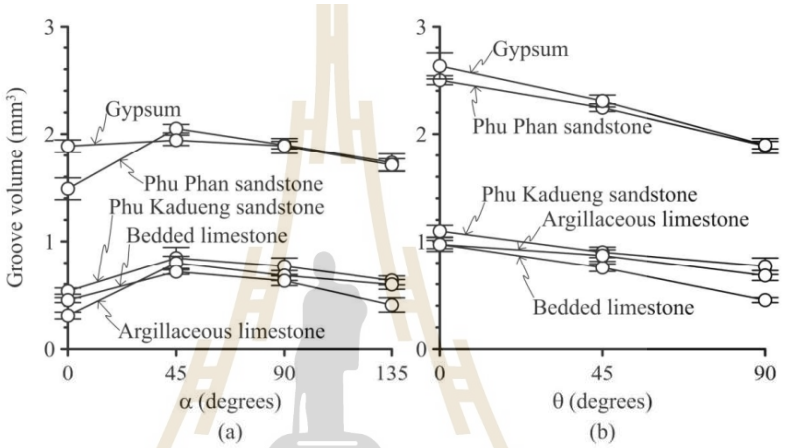

Fig. 4. Groove volume as a function of bedding plane angle (a), and scratching direction (b).

where a and b are empirical constants depending on rock types, as shown in Table 3. Good correlations are obtained for all boundary conditions ($R^2 > 0.9$). Figs. 5 and 6 shows examples of ploughing force as a function of scratching distance for different α and θ angles, respectively. They increase rapidly within the first 2-4 mm and then trend to approach constant magnitudes. Stronger rocks (limestones) show higher ploughing forces than the soft ones (gypsum), regarding of α and θ angles. Highest force is observed from $\alpha = 0°$ with the lowest at 45° and 90°. The differences vary from 5% (soft rocks) to 15% (strong rocks). For scratching direction with $\theta = 0°$, larger difference is observed from strong rocks, as compared to those of soft rocks. This implies that the effects of bedding plane orientations and scratching directions are pronounced more in strong rocks than in soft rocks.

5 Discussions

The agreements between *CAI*, *F* and *V* for all rocks and boundary conditions confirm that the results of testing are correct. The higher *CAI* and *F* with lower groove volume are observed for strong rocks as compared to soft rocks.

Higher *CAI* values are obtained for both crystalline and clastic rocks when the scratching direction is opposite to the dip direction (α) of bedding plane. Under this condition, the alternation of soft and hard layers show the largest effect on the stylus wear. On the contrary, if the scratching direction is the same with bedding plane dip angle, the wear of stylus pins (*CAI*) becomes lower. This also results in a lower *CAI* and ploughing force, F, with higher scratching volume. This also agrees with the results obtained from the effects of scratching direction that largest *CAI*, *F* and *V* values are observed when the stylus pin moves perpendicular to the bedding trend ($\theta = 90°$).

Table 3. Empirical constants *a* and *b* for F-d_s relation and R^2.

Rock type	α (degrees)	θ (degrees)	$F = a \cdot (1 - exp \cdot (-b \cdot d_s))$		R^2
			a (N)	*b* (m^{-1})	
Khao Khad argillaceous limestone	0	–	2.789	0.682	0.986
	45	90	2.128	0.654	0.993
	90	0	1.627	0.568	0.950
	90	45	1.899	0.598	0.987
	90	90	2.240	0.541	0.989
	135	90	2.386	0.682	0.977
Khao Khad bedded limestone	0	–	2.012	0.719	0.979
	45	90	2.064	1.062	0.977
	90	0	1.707	0.777	0.990
	90	45	1.909	0.827	0.977
	90	90	2.192	1.339	0.970
	135	90	2.289	1.694	0.970
Phu Kadueng sandstone	0	–	2.759	0.728	0.995
	45	90	2.409	0.728	0.982
	90	0	2.036	0.646	0.989
	90	45	2.242	0.728	0.976
	90	90	2.491	0.724	0.993
	135	90	2.538	0.723	0.995
Phu Phan sandstone	0	–	1.850	0.603	0.978
	45	90	1.411	0.477	0.989
	90	0	1.118	0.626	0.974
	90	45	1.274	0.549	0.967
	90	90	1.478	0.538	0.963
	135	90	1.525	0.477	0.964

(*continued*)

Table 3. (*continued*)

Rock type	α (degrees)	θ (degrees)	$F = a \cdot (1 - exp \cdot (-b \cdot d_s))$		R^2
			a (N)	b (m^{-1})	
Tak Fa gypsum	0	–	1.807	0.912	0.995
	45	90	1.832	0.820	0.982
	90	0	1.611	0.802	0.960
	90	45	1.759	0.730	0.967
	90	90	1.883	0.819	0.983
	135	90	1.925	0.819	0.985

For clastic rocks, the results also imply that scratching across bedding planes through layers with different grain sizes would cause more wear to the stylus pin (higher *CAI*), as compared to that along bedding plans through the same layers of the similar grain size.

For crystalline rocks, the variation of *CAI* would depend on the hardness of the crystallization layers (in this case, calcite). If the hardness of different crystallized layers is the same, the effect of bedding plane would be minimal.

The bedding plane thickness of all rocks tested here is similar (0.5-2 mm). The ef-fect of bedding plane thickness cannot be assessed.

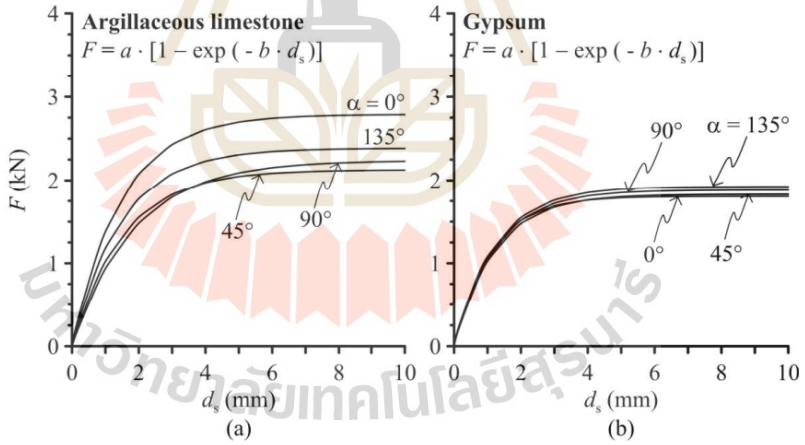

Fig. 5. Scratching force as a function of direction under different bedding plane angles for Khao Khad argillaceous limestone (a), and Tak fa gypsum (b).

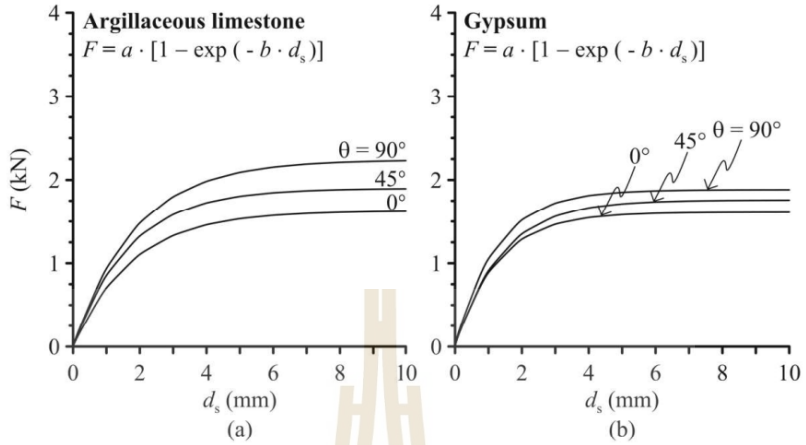

Fig. 6. Scratching force as a function of direction under different scratching directions for Khao Khad argillaceous limestone (a), and Tak fa gypsum (b).

6 Concussion

Results from this study can be concluded, as follows:

- The scratching directions (θ) affect *CAI* and force that does bedding plane orientations (α).
- Bedding plane orientations affect *CAI* of strong rocks more than soft rocks.
- Scratching of stylus pin across bedding planes show larger *CAI* than along bedding planes.

References

1. Rajati, M.H., Rostami, J., Memarian, H., Hamzaban, M.T.: A study on predicting the wear of TBM disc cutters using Cerchar testing. Tunn. Undergr. Space Technol. **140**, 105290 (2023)
2. Yaralı, O., Duru, H.: Investigation into effect of scratch length and surface condition on Cerchar abrasivity index. Tunn. Undergr. Space Technol. **60**, 111–120 (2016)
3. Teymen, A.: The usability of Cerchar abrasivity index for the estimation of mechanical rock properties. Int. J. Rock Mech. Min. Sci. **128**, 104258 (2020)
4. Aydın, H.: Investigating the effects of various testing parameters on Cerchar abrasivity index and its repeatability. Wear **418–419**, 61–74 (2019)
5. Hamzaban, M.T., Karami, B., Rostami, J.: Effect of pin speed on Cerchar abrasion test results. J. Test. Eval. **47**(1), 121–139 (2019)
6. Al Ameen, S.I., Waller, M.D.: The influence of rock strength and abrasive mineral content on the Cerchar Abrasive Index. Eng. Geol. **36**(3), 293–301 (1994)
7. Plinninger, R., Käsling, H., Thuro, K., Spaun, G.: Testing conditions and geomechanical properties influencing the CERCHAR abrasiveness index (CAI) value. Int. J. Rock Mech. Min. Sci. **40**(2), 259–263 (2003)

8. Zhang, G., Konietzky, H., Song, Z., Huang, S.: Study of some testing condition-based factors affecting the Cerchar abrasivity index (CAI). Arab. J. Geosci. **13**(23), 1254 (2020)
9. Aydın, H., Yaralı, O., Duru, H.: The effects of specimen surface conditions and type of test apparatus on Cerchar Abrasivity index. Karaelmas Fen ve Mühendislik Dergisi **6**(2), 293–298 (2016)
10. Hamzaban, M.T., Rostami, J., Dahl, F., Macias, F.J., Jakobsen, P.D.: Wear of cutting tools in hard rock excavation process: a critical review of rock abrasiveness testing methods. Rock Mech. Rock Eng. **56**, 1843–1882 (2022)
11. Rossi, E., Saar, M.O., Rudolf von Rohr, P.: The influence of thermal treatment on rock–bit interaction: a study of a combined thermo–mechanical drilling (CTMD) concept. Geothermal Energy **8**(1), 16 (2020)
12. Ji, Y., Wang, L., Zheng, Y., Wu, W.: Temperature-dependent abrasivity of Bukit Timah granite and implications for drill bit wear in thermo-mechanical drilling. Acta Geotech. **16**(3), 885–893 (2021)
13. Wang, L., Guo, K., Wu, W.: Abrasivity measurement of brittle rock after thermal treatment. Measurement **212**, 112710 (2023)
14. Alber, M.: Stress dependency of the Cerchar abrasivity index (CAI) and its effects on wear of selected rock cutting tools. Tunn. Undergr. Space Technol. **23**(4), 351–359 (2008)
15. Kathancharoen, N., Fuenkajorn, K.: Effects of mechanical and mineralogical properties on CERCHAR abrasivity index and specific energy of some Thai rocks. Eng. Appl. Sci. Res. **50**(5), 478–489 (2023)
16. Ramamurthy, T.: Strength and Modulus Responses of Anisotropic Rocks. Pergamon, Oxford (1993)
17. Gholami, R., Rasouli, V.: Mechanical and elastic properties of transversely isotropic slate. Rock Mech. Rock Eng. **47**, 1763–1773 (2014)
18. Al-Harthi, A.A.: Effect of planar structures on the anisotropy of Ranyah sandstone. Saudi Arabia. Eng. Geol. **50**(1), 49–57 (1998)
19. Sukjaroen, N., Thongprapha, T., Liabkrathok, P., Fuenkajorn, K.: Effects of loading rate on transverse isotropic responses of bedded gypsum. Arab. J. Geosci.Geosci. **14**(22), 2442 (2021)
20. ASTM D7625-22.: Standard Test Method for Laboratory Determination of Abrasiveness of Rock Using the CERCHAR Abrasiveness Index Method. West Conshohocken, PA (2022)

BIOGRAPHY

Mr. Thiti Patcharaarpakul was born on April 30, 2000 in Nakhon Ratchasima, Thailand. He received his Bachelor's Degree in Engineering (Geological Engineering) from Suranaree University of Technology in 2022. After graduation, he continued to study with Master's degree in school of Geological Engineering, Institute of Engineering, Suranaree University of Technology. During graduation, 2022-2025, he was a part time worker in position of research associate at the Geomechanics Research Unit, Institute of Engineering, Suranaree University of Technology.